2022

Transcriptomic and Proteomic Studies of Intercellular Communication Between Melanocytes and Keratinocytes in Human Skin

Gabriella Stephanne Spitz-Becker

TRANSCRIPTOMIC AND PROTEOMIC STUDIES OF INTERCELLULAR COMMUNICATION BETWEEN MELANOCYTES AND KERATINOCYTES IN HUMAN SKIN

A Thesis Presented to the Faculty of

The Rockefeller University

in Partial Fulfillment of the Requirements for

the degree of Doctor of Philosophy

by

Gabriella Stephanne Spitz-Becker

June 2022

TRANSCRIPTOMIC AND PROTEOMIC STUDIES OF INTERCELLULAR COMMUNICATION BETWEEN MELANOCYTES AND KERATINOCYTES IN HUMAN SKIN

Gabriella Stephanne Spitz-Becker, Ph.D.
The Rockefeller University 2022

The epidermis is a stratified epithelium composed of multiple cell types. Keratinocytes are the most prevalent cells in the epidermis and provide the barrier function of the skin. Interspersed amongst the keratinocytes in the basal layer of the epidermis are melanocytes, the pigment producing cells of the epidermis. Melanocytes produce melanin pigment which resides in melanosomes, organelles that are transferred to keratinocytes. In my thesis work, I focused on identifying downstream results of intercellular communication between melanocytes and keratinocytes for each of these cell types.

I characterized the transcriptomes of human melanocytes and keratinocytes that were freshly derived from human tissue in Chapter 2. These data served as a reference for comparison and validation for the work that followed. In Chapter 3, I studied the effect of the presence of melanocytes on keratinocyte gene expression. I identified Neuronal Cell Adhesion Molecule (NRCAM) as being upregulated in keratinocytes in the presence of melanocytes, which is the first suggestion of a role for NRCAM in melanocyte-keratinocyte interactions. In Chapter 4, I studied the effects of endothelin-1 (ET-1), a signaling molecule produced by keratinocytes, on melanocyte gene expression. I found that genes involved in cell morphology, neurite growth, and cytoskeletal organization were upregulated in melanocytes in response

to ET-1. I specifically identified microtubule associated protein 2 (MAP2) as being upregulated in response to ET-1, which suggests a mechanism for how ET-1 induces changes in melanocyte morphology. I also found that the nerve growth factor receptor (NGFR) is upregulated in melanocytes in response to ET-1. This reveals a new locus of interaction between two cell-cell signaling pathways in melanocytes and keratinocytes.

In Chapter 5, I used a proteomic approach to study keratinocyte phagosomes. This is the first such proteomic characterization of phagosomes from an epithelial cell. In the final chapter of my thesis, I outlined the immediate future directions of this work, and discussed how these basic biological findings may be applied to our understanding of disease states.

To Bernie and Marcia

ACKNOWLEDGEMENTS

I would first like to thank my advisor, Sandy Simon, whose scientific curiosity, enthusiasm and rigor are unparalleled. I am deeply grateful for his mentorship, support, guidance and inspiration during my PhD work. He has created a very unusual laboratory environment that fosters independence, self-reliance, and comradeship. I am also indebted to my wonderful thesis committee, Shai Shaham and Elaine Fuchs. My committee meetings yielded many of the ideas that are contained within this thesis, and I am extremely appreciative of their intellectual contributions to this work.

I also thank the Rockefeller University Dean's Office (Sid Strickland, Emily Harms, Andre Morris, Marta Delgado, Kristin Cullen, Cris Rosario and Stephanie Fernandez), who have created a truly remarkable doctoral program that allows the students to truly focus on the science. The advertising of the graduate program is accurate.

I have many lab mates to thank for their contributions to this work. David Requena was a true collaborator in every RNA sequencing experiment described in the following thesis (and there are many!). He is both a veritable bioinformatics wiz and a great colleague, and he deserves full credit for the computational analyses described in Chapters 2-4. Rachel Belote was a delight to work with and sparked my interest in melanocytes and keratinocytes. She established the cell culture system that I used throughout this thesis and was essential to the early stages of this work. Rachel and I collaborated on the experiments in Chapter 2. Marina Bleck and Bassem Shebl have been two postdoctoral rocks during various years of my PhD.

Marina taught me everything I know about biochemistry, and Bassem is the only person I know who will bring me both anti-GFP resin and cookies when I need them most.

Xiao Wang, Kate Bredbenner and Joan Pulupa provided moral, emotional and technical support and companionship at all stages of this work. They also serve the distinct honor of being the only people I have ever gotten stuck in a literal elevator with (in addition to the metaphorical elevator of graduate school). They also served as an extra six eyes on this thesis, which was invaluable. Tova Finkelstein, Harriet Prior and James Knox also provided an extra six hands in the final weeks of this work, and I am appreciative of their helpfulness and talent. Harriet also saved the day last year when my left arm was incapacitated due to shoulder surgery, and I could not perform any experiments unaided. I also thank Daniel Firester for years of close friendship and scientific conversations.

Many thanks are due to several Rockefeller University resource centers. The Proteomics, Flow Cytometry and Genomics Resource Centers were absolutely critical to every chapter of this thesis. The skill and kindness of Svetlana Mazel, Henrik Molina and Connie Zhao is remarkable, and I am so lucky to have done my work at an institution that has such fantastic scientists to turn to.

Finally, I thank the non-scientists in my life, who provided the groundwork upon which my research career was possible. My parents, Jonathan, Erica and Susannah are all classical musicians, and I learned through observation the importance of hard work, preparation and patience. My younger brothers Sebastian and Lukas are truly the best in every way. My grandparents Marcia, Bernard and

Stephanne, none of whom were able to see me complete this work, were eternally supportive of whatever whim I was currently pursuing, including science. My dear friend Elizabeth has been so patient throughout this seven-year process, and I relied upon her for a greater perspective. Finally, my wife Rachel is the best partner a person could imagine and has facilitated and supported my scientific career in innumerable ways. Thank you to everyone!

TABLE OF CONTENTS

ACKNOWLEDGEMENTS iv

TABLE OF CONTENTS vii

LIST OF ABBREVIATIONS xv

CHAPTER 1: INTRODUCTION 1

1.1 THE EPIDERMIS 2

1.2 MELANOSOMES 5

1.3 MELANOSOME TRANSFER 9

1.3.1 Cytophagocytosis: 10

1.3.2 Shedding phagocytosis: 10

1.3.3 Exocytosis-Phagocytosis: 12

1.3.4 Tunneling nanotubule: 13

1.4 THE FATE OF THE MELANOSOME WITHIN KERATINOCYTES 14

1.5 PHAGOCYTOSIS 16

1.6 STEPS OF PHAGOCYTOSIS 17

1.6.1 Recognition and Internalization 17

1.6.2 Maturation 19

1.7 EPITHELIAL CELLS AS PHAGOCYTES 21

1.8 KERATINOCYTES AS PHAGOCYTIC CELLS 22

1.9 UNRESOLVED QUESTIONS IN MELANOSOME TRANSFER 23

1.10 SIGNALING BETWEEN KERATINOCYTES AND MELANOCYTES 24

1.10.1 NGF *25*

1.10.2 PAR-2 ..... *25*

1.10.3 Keratinocyte Growth Factor *28*

1.10.4 Endothelin *28*

1.11 SUMMARY 29

CHAPTER 2: TRANSCRIPTOMIC ANALYSIS OF MELANOCYTES AND KERATINOCYTES FROM INTACT SKIN 31

2.1 PREPARATION OF EPIDERMAL CELLS FOR FACS SORT 32

2.2 BUILDING A PRIMARY CELL TRANSCRIPTOME 35

2.3 EXPRESSION PROFILE OF BASAL KERATINOCYTES 37

2.4 EXPRESSION PROFILE OF SUPRABASAL KERATINOCYTES 38

2.5 EXPRESSION PROFILE OF MELANOCYTES 40

2.6 DISCUSSION AND CONSIDERATIONS 41

CHAPTER 3: THE EFFECTS OF MELANOCYTES ON KERATINOCYTE GENE EXPRESSION 43

3.1 CHARACTERIZING CHANGES IN KERATINOCYTES DUE TO THE PRESENCE OF MELANOCYTES USING FLOW CYTOMETRY 43

3.2 ANALYZING CHANGES IN THE KERATINOCYTE TRANSCRIPTOME 47

3.3 TRAP-SEQ OF KERATINOCYTES GROWN WITH AND WITHOUT MELANOCYTES 55

3.4 CONCLUSIONS 56

CHAPTER 4: THE EFFECTS OF ENDOTHELIN ON MELANOCYTE GENE EXPRESSION 59

4.1 TRAP-SEQ OF MELANOCYTES GROWN WITH AND WITHOUT KERATINOCYTES 60

4.2 CHARACTERIZING CHANGES IN MELANOCYTES DUE TO THE PRESENCE OF MELANOCYTES USING FLOW CYTOMETRY 62

4.3 CHARACTERIZING CHANGES IN MELANOCYTES DUE TO ENDOTHELIN SIGNALING 63

4.4 VALIDATING GENES IDENTIFIED IN ET-1 DIFFERENTIAL EXPRESSION 77

4.4.1 NGFR 78

4.4.2 MAP2 81

4.4.3 Actin Structure 84

4.5 CONCLUSIONS 89

CHAPTER 5: CHARACTERIZATION OF PRIMARY KERATINOCYTE PHAGOSOMES 90

5.1 PHAGOCYTOSIS OF MICROSPHERES 91

5.2 ESTABLISHING BEAD PHAGOCYTOSIS IN KERATINOCYTES 92

5.3 FRACTIONATION OF BEAD PHAGOSOMES IN KERATINOCYTES. 95

5.4 VALIDATION OF FRACTIONATION BY COMPARISON TO SODIUM AZIDE TREATMENT .. 97

5.5 ANALYSIS OF KERATINOCYTE PHAGOSOME PROTEOME 100

5.6 PROXIMITY LABELING AS A METHOD OF STUDYING PHAGOSOMES 104

5.7 CONCLUSIONS 105

CHAPTER 6: FUTURE DIRECTIONS AND IMPLICATIONS 106

6.1 KERATINOCYTE AND MELANOCYTE TRANSCRIPTOMICS 107

6.2 STUDIES OF THE KERATINOCYTE PHAGOSOME 111

6.3 CONCLUSIONS 112

CHAPTER 7: MATERIALS AND METHODS 114

Isolation of Melanocytes and Keratinocytes 114

Culturing of Melanocytes and Keratinocytes 114

Proteomics of Isolated Keratinocyte Phagosomes 115

Mass Spectrometry 117

Preparation of Tissue for Flow Cytometry 117

Flow Cytometry Sample Preparation 117

RNA Sequencing 118

Preparation of Tissue for Immunofluorescence 119

Immunofluorescence of Cells 119

Confocal Microscopy 120

Epifluorescence Microscopy 120

Quantification of Bead Internalization 120

Immunofluorescence of Tissue Cryosections 121

Virus Production 122

Lentiviral Transduction 122

Translating Ribosome Affinity Purification 122

Construction of pGS28, BioID-M-Ink Expression Plasmid 124

Purification of M-Ink-BioID 125

Streptavidin Blot 126

Melanocore Preparation and Labeling 127

BioID Melanocore Treatment 128

APPENDIX I: DESCRIPTION OF BIOID BASED KERATINOCYTE PHAGOCYTOSIS EXPERIMENTS 130

REFERENCES 135

LIST OF FIGURES

Figure 1 Structure of the Epidermis 4
Figure 2 Steps of Melanosome Biogenesis 6
Figure 3 Models of Melanosome Transfer 9
Figure 4 Schematic of Phagosome Maturation 21
Figure 5 Schematic of Par-2 Activation 27
Figure 6 Flow Cytometry of Keratinocytes and Melanocytes Derived from Human Tissue 34
Figure 7 Quality of RNA from FACS Sorted Cells 35
Figure 8 Quality Control Analyses of RNA Sequencing Data for FACS Sorted Samples 36
Figure 9 Schematic of Experimental Workflow Used to Study Keratinocyte RNA from Keratinocytes Grown in Monoculture and Co-Culture 45
Figure 10 FACS Plots for Keratinocyte Co-Culture and Monoculture 46
Figure 11 Quality Control Analyses of RNA Sequencing Data for FACS Sorted Keratinocytes 47
Figure 12 Principal Component Analysis and Hierarchical Clustering of Keratinocytes Grown Alone and with Melanocytes 49
Figure 13 Expression Levels of Upregulated Genes in Basal Keratinocyte, Suprabasal Keratinocyte and Melanocyte Transcriptomes from *In Situ* Cells 52
Figure 14 Human Keratinocytes Express NRCAM *In Situ* 54
Figure 15 Schematic of TRAP-Seq Experiment 58
Figure 16 Schematic of Melanocyte Endothelin-1 Treatment 65
Figure 17 Quality Control Data of ET-1 Treated Melanocytes 67
Figure 18 Principal Component Analysis and Hierarchical Clustering of ET-1 Treated Melanocytes 68
Figure 19 Immunofluorescence of NGFR and MAP2 *In Situ* 82
Figure 20 Immunofluorescence of NGFR in Melanocyte Monoculture and Melanocyte-Keratinocyte Co-Culture 80

Figure 21 Immunofluorescence of MAP-2 in Melanocytes 83
Figure 22 Phalloidin Staining of melanocytes in monoculture and co-culture 88
Figure 23 Primary Keratinocytes Internalize Microspheres. 93
Figure 24. Number of Beads Internalized by Primary Keratinocytes Under Different Conditions. 95
Figure 25 Schematic of Phagosome Fractionation and Mass Spectrometry 97
Figure 26 Venn Diagram of Proteins Present in Phagocytosis Sample Compared to Non-Internalization Control 98
Figure 27 Comparison of Specific Proteins in Phagocytosis Sample and Non-Internalization Control 100
Figure 28 String Plot of Endosomal and Phagosomal Proteins Present in Keratinocyte Phagosomes. 102
Figure 29 String Plot of Lysosomal Proteins Present in Keratinocyte Phagosomes. 103
Figure 30 Coomassie-Stained Gel of Purification of BioID-M-Ink 126
Figure 31 Testing the Biotinylation Efficacy and Binding Ability of BioID-M-Ink 132

LIST OF TABLES

Table 1 Top 15 Most Expressed Genes in Basal Keratinocytes 38
Table 2 Top 15 Most Expressed Genes in Suprabasal Keratinocytes 39
Table 3 Top 15 Most Expressed Genes in Melanocytes 41
Table 4 Differentially Expressed Genes (Upregulated) in Keratinocytes Cultured with Melanocytes 50
Table 5 Differentially Expressed Genes (Downregulated) 51
Table 6 Top Differentially Expressed Genes in Pull-Down of Keratinocyte Ribosomes from Keratinocyte-Melanocyte Co-Culture Compared to Keratinocyte Monoculture 58
Table 7 Top 15 Differentially expressed genes in melanocytes cultured with keratinocytes compared to melanocytes cultured with HeLa cells 62
Table 8 Genes Upregulated After 5 and 24 Hour Treatments with Endothelin-1 70
Table 9 Molecular Functions of Genes Upregulated in Melanocytes after ET-1 Treatment 71
Table 10 Subset of Biological Pathways of Genes Upregulated in Melanocytes after ET-1 Treatment 77
Table 11 Validation of *In-Situ* Expression of Subset of Genes Identified in ET-1 Differential Expression 78
Table 12 FACS Antibodies 118
Table 13 Immunofluorescence Antibodies 122
Table 14 GO Analysis of BioID-M-Ink Pulldown 133

List of Abbreviations

ACTH	Adrenocorticotropic hormone
bFGF	Basic Fibroblast Growth Factor
DCT	DOPAchrome Tautomerase
DHPC	1,2-dihexanoyl-sn-glycero-3-phosphocholine
DMSO	Dimethyl Sulfoxide
ECM	Extra Cellular Matrix
ET	Endothelin
FACS	Fluorescence activated cell sorting
FBS	Fetal Bovine Serum
GPCR	G-protein coupled receptor
HaCaT	A spontaneously transformed, aneuploid human keratinocyte cell
Hap1	A haploid human cell line
HBSS	Hank's Balanced Salt Solution
HKGS	Human Keratinocyte Growth Serum
HMGS-2	Human Melanocyte Growth Serum 2
IPD	Immediate Pigment Darkening
lncRNA	Long Noncoding RNA
NRCAM	Neuronal Cell Adhesion Molecule
KGF	Keratinocyte Growth Factor
KGFR	Keratinocyte Growth Factor Receptor
LDS	Lithium Dodecyl Sulfate
MOPS	3-(N-morpholino)propanesulfonic acid
NGF	Nerve Growth Factor
OA1	Ocular Albinism Type 1
PAR-2	Protease-Activated Receptor 2
PBS	Phosphate buffered Saline
PMEL17	Premelanosome Protein Gene
PNS	post-nuclear supernatant
POS	Photoreceptor Outer Segment
RIN	RNA integrity number

RNA	Ribonucleic acid
STI	Soybean Trypsin Inhibitor
TRAP-seq	Translating Ribosome Affinity Purification Sequencing
TRP1	Tyrosinase Related Protein 1
TYR	Tyrosinase
UV	Ultraviolet
UVB	Ultraviolet B

CHAPTER 1: INTRODUCTION

This thesis is focused on identifying genes involved in communication between melanocytes and keratinocytes, as well as on identifying proteins involved in melanosome transfer, a process by which melanosomes are delivered from melanocytes to keratinocytes. The introductory chapter describes melanocytes and keratinocytes and the environment they inhabit in the body. In sections 1.2-1.8, I will provide a summary of existing research surrounding the process of melanosome transfer, particularly focusing on the role of keratinocytes as phagocytic cells, which pertains to the experiments described in Chapter 6. In section 1.9, I will then discuss what is known about how melanocytes and keratinocytes communicate with each other in the epidermis, which pertains to work described in Chapter 3 and 4.

When moving through the world, our bodies are exposed to numerous environmental assaults, including pathogens, ultraviolet (UV) radiation and mechanical injury. We rely on the epidermis to provide protection from these external threats. The epidermis is a stratified epithelium composed of several cell types that work in concert to provide this protection. In addition to protecting the organism from hazards from without, the epidermis also prevents moisture and nutrient loss from within the organism (Fuchs, 2016). Keratinocytes compose the majority of cells in the epidermis, and are the cells primarily responsible for the barrier function of the skin (Madison, 2003).

Melanocytes are the pigment producing cells of the body. Approximately 1 in every 10 cells of basal layer of the epidermis is a melanocyte (Hoath and Leahy, 2003). They have a complexly branched morphology, and their dendritic projections

contact approximately thirty-six keratinocytes per melanocyte *in situ* (Fitzpatrick and Breathnach, 1963). Melanocytes contain specialized, membrane-bound, lysosome-related organelles called melanosomes, in which melanin pigment is synthesized and stored. As a mechanism of protection from UV-induced damage, melanosomes are transferred to keratinocytes, where they tend to reside on the apical side of the keratinocyte's nucleus, shielding the DNA from ultraviolet radiation (Wu and Hammer, 2014). The exact mechanism by which these organelles are transferred from melanocyte to keratinocyte has not been resolved, and evidence exists for several modes of transfer, which will be discussed later in this introduction.

1.1 The Epidermis

This skin is composed of two layers. The inner layer of the skin is the dermis, a connective tissue matrix containing fibroblasts, immune cells, nerve fibers and blood vessels. The dermal fibroblasts produce an extracellular matrix (ECM) primarily composed of type I and type III collagen fibrils, and also containing elastin and proteoglycans (Frantz et al., 2010). Above the dermis is the epidermis, which resides at the interface between the organism and the environment. The epidermis serves as a bi-directional barrier, preventing loss of fluids from within the organism, while protecting from physical, microbial and chemical assaults (Proksch et al., 2008). The epidermis also helps to regulate body temperature through its hair and sweat gland appendages. The epidermis and dermis are separated by a basement membrane, a highly specialized matrix structure, components of which are produced by both the epidermis and the dermis (Iozzo, 2005).

Approximately 95% of cells in the epidermis are keratinocytes. Epidermal keratinocytes exist in a stratified epithelium, with proliferative cells residing in the basal layer. Basal cells periodically detach from the basement membrane, and undertake a differentiation journey. It takes approximately four weeks for a cell that has exited the basal layer to be shed from the surface of the skin.

Intermingled amongst the basal keratinocytes are the epidermal melanocytes, which are dispersed at a 1:10 ratio along the basal layer. Within the epidermis as a whole, the ratio of melanocytes to keratinocytes is approximately 1:36 (Hoath and Leahy, 2003). How this ratio is maintained is an open area in the field. Epidermal melanocytes are not the only melanocytes in the body; they are also found in the iris, inner ear, nervous system and heart. These cells are all able to produce melanin pigment and originate from the neural crest during development.

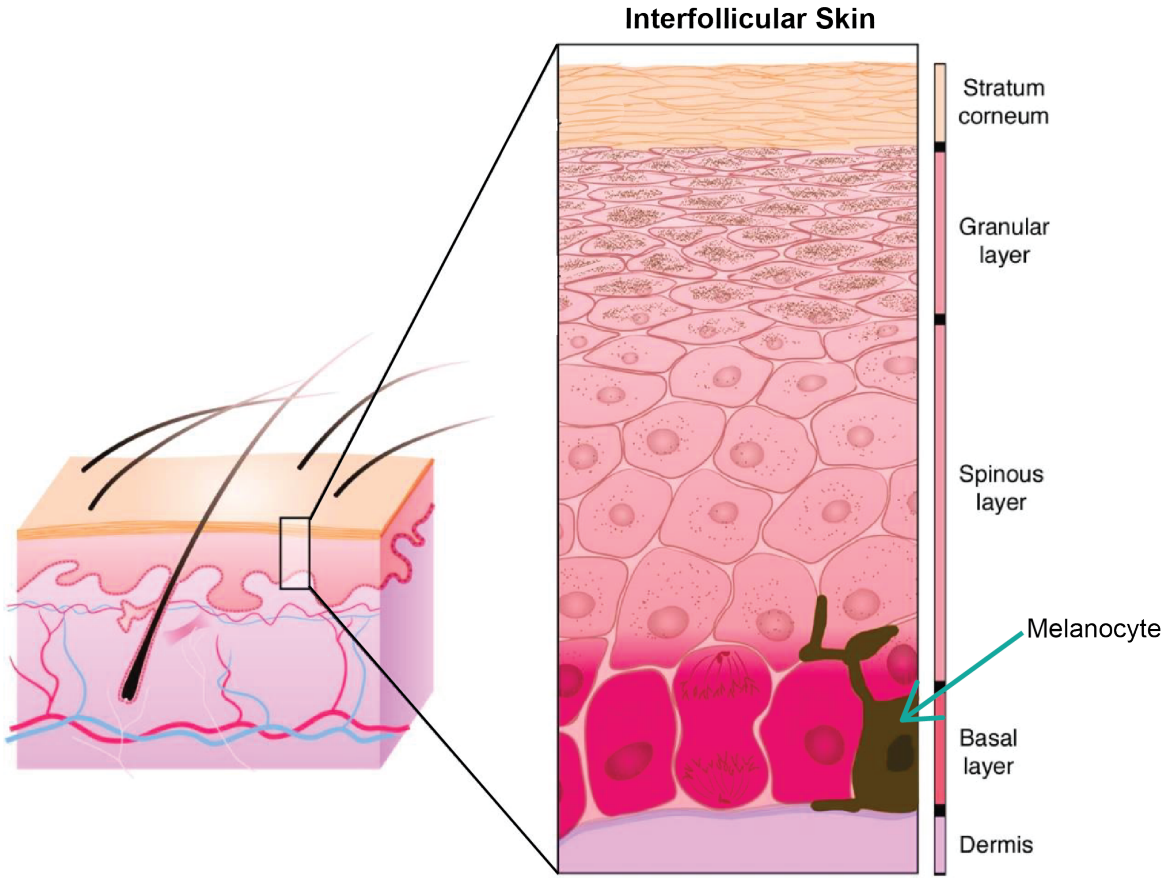

Figure 1 Structure of the Epidermis

Diagram illustrating the dermis and epidermis. The magnified box illustrates the layers of interfollicular skin. Keratinocytes form a stratified epithelium, with dividing cells residing on the basal layer. Melanocytes are interspersed within the keratinocytes of the basal layer. Adapted from (Segre, 2006).

During development, cranial and dorsal neural crest cells give rise to skin melanocytes. These neural crest cells differentiate into melanoblasts, which migrate into the epidermis during innervation of the embryonic skin at around six to eight weeks of human embryonic development, proliferating as they migrate (Adameyko et al., 2009; Cramer and Fesyuk, 2012). Once in the epidermis, the cells continue to proliferate, and eventually differentiate into mature melanocytes, capable of synthesizing melanin. These mature melanocytes have a branching dendritic extensions, which facilitate melanosome transfer to multiple keratinocytes (Cichorek et al., 2013).

1.2 Melanosomes

Melanosomes are characterized by the presence of melanin and melanin producing enzymes. Epidermal melanocytes are able to produce two types of melanin pigment: pheomelanin, a yellow-red pigment, and eumelanin, a brown-black pigment. The ratio of these pigments to each other is responsible for the natural variation of human skin and hair tones. The level of cysteine present in the melanocyte is ultimately responsible for the ratio of these two pigments, as cysteine is necessary for the production of pheomelanin but not eumelanin (Hearing and Tsukamoto, 1991).

Melanosome biogenesis has four distinct stages. Stage I melanosomes (also known as premelanosomes) are early endosomal structures that contain intraluminal vesicles and thin proteinaceous fibrils synthesized by the melanocyte. During Stage II of melanogenesis, the intraluminal vesicles disappear and the quantity of proteinaceous fibrils increases. Stage III of melanogenesis is characterized by the

beginning of melanin synthesis and the deposition of this pigment onto fibrils. The appearance of the fibrils becomes concealed by the heavy deposition in pigment, ultimately resulting in fully mature Stage IV melanosomes (Raposo and Marks, 2007). Fully mature fibrils are characterized by their densely pigmented appearance when visualized through electron microscopy. These densely pigmented fibrils contained within the melanosome membrane are referred to as melanocores.

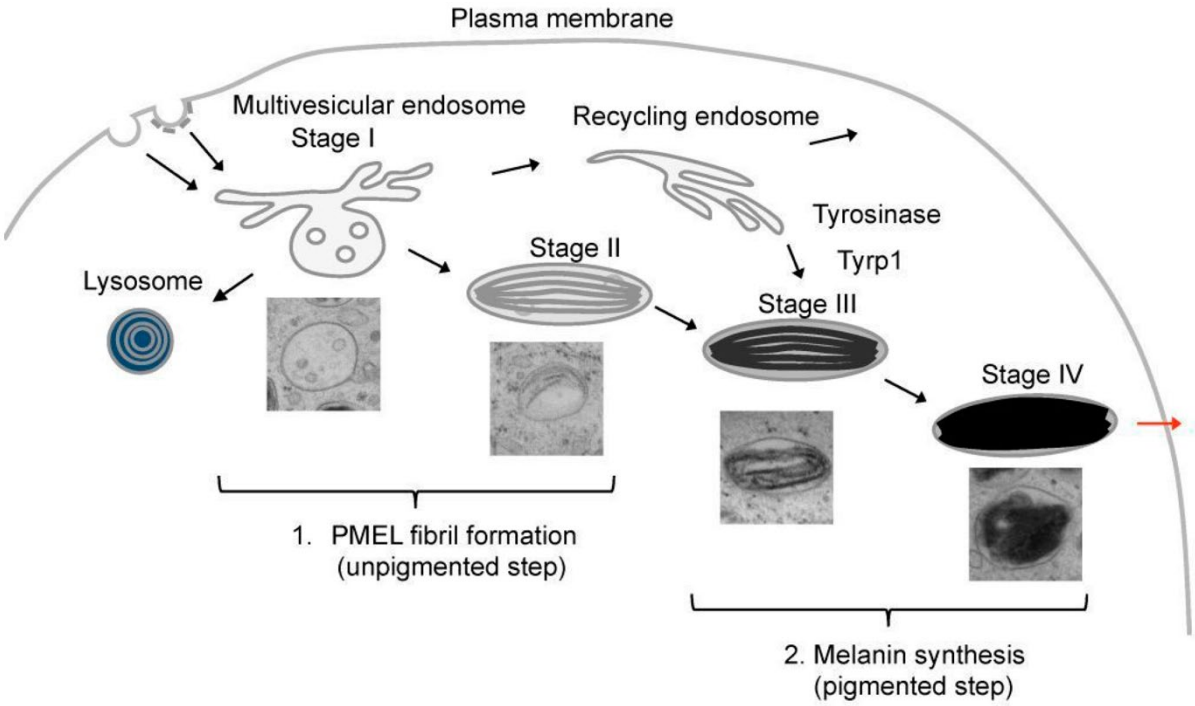

Figure 2 Steps of Melanosome Biogenesis

The different stages of melanosomes are illustrated by parallel illustrations and electron microscopy pictures. PMEL fibrils start to assemble in stage I melanosomes. In stage II melanosomes, PMEL fibrils further assemble, giving the melanosomes their ovular shape and striated appearance. Melanin starts to be produced in stage III melanosomes, which possess melanin synthesizing enzymes. Melanin is deposited on PMEL fibrils, which become entirely covered by melanin in stage IV melanosomes. Mature stage IV melanosomes are then transferred to keratinocytes. Adapted from (Bissig et al., 2016)

Melanogenesis is carried out by a series of enzymes and structural proteins that form the melanosome fibrils, deposit pigment onto the fibrils, and control the size of the melanosome. The luminal fibrils of the melanosome are primarily composed of the protein PMEL17 (also known as gp100 and SILV). PMEL17 is a type 1 integral membrane protein that spans the melanosome membrane. The luminal terminus of this protein undergoes several proteolytic cleavage events, allowing the cleaved domains to assemble into fibrils (Berson et al., 2001). This process is regulated by Melan-A (MART1) (Hoashi et al., 2005). The melanin synthetic enzymes—tyrosinase (TYR), tyrosinase related protein-1 (TRP1) and DOPAchrome tautomerase (DCT)—are also type 1 integral membrane proteins that reside on the melanosome limiting membrane (Newton et al., 2007). The size and distribution of melanosomes within the melanocyte cytoplasm is partly regulated by ocular albinism type 1 (OA1), which is a GPCR that also resides on the melanosome membrane (Giordano et al., 2011).

Melanosomes are carried to the distal tips of melanocyte dendrites on the microtubule network., with Rab27a being an important mediator of this trafficking process. Type 2 Griscelli Syndrome, is a rare autosomal recessive disorder that causes distinctive silvery hair in children with the disease. On a cellular level, it is characterized by improperly trafficked melanosomes that are not able to be transferred to keratinocytes at normal rates. This is the result of a mutation in Rab27a.

Melanosomes are transferred to keratinocytes (discussed in more depth in the next section), where they protect the nuclear DNA of epidermal keratinocytes. Melanosomes absorb and scatter light, thereby reducing reactive oxygen species (Marks and Seabra, 2001). UV radiation penetrates the skin in a wavelength-dependent manner. Longer wavelength UVA (320-400 nm) is able to penetrate into the dermis, while UVB (280-320) is primarily absorbed by the epidermis. UVA radiation generates reactive oxygen species that can damage DNA, while UVB is directly absorbed by DNA. The absorption of UVB by DNA causes photoproducts, that, if not successfully repaired, can be carcinogenic (D'Orazio et al., 2013). Only about 5% of the UV radiation that reaches the surface of the earth is in the UVB range, however, the penetration of UVB grows with the depletion of the ozone layer, and leads to increased carcinogenesis (De Fabo, 2005). Calculations indicate that a 1% decrease in atmospheric ozone leads to a 1-2% increase in melanoma mortality (Kripke, 1988).

Darkly pigmented skin has an average estimated sun protection factor (SPF) of 13.4, while lightly pigment skin has an intrinsic SPF of 3.3 (Kaidbey et al., 1979; Tadokoro et al., 2003). Epidemiologically, light skinned individuals with less melanin pigment develop skin cancers at higher rates (Markovic et al., 2007). On a cellular level, skin from light skinned patients show markedly more cyclopyrimideine dimers after UV exposure than darker skinned patients (Brenner and Hearing, 2008).

1.3 Melanosome Transfer

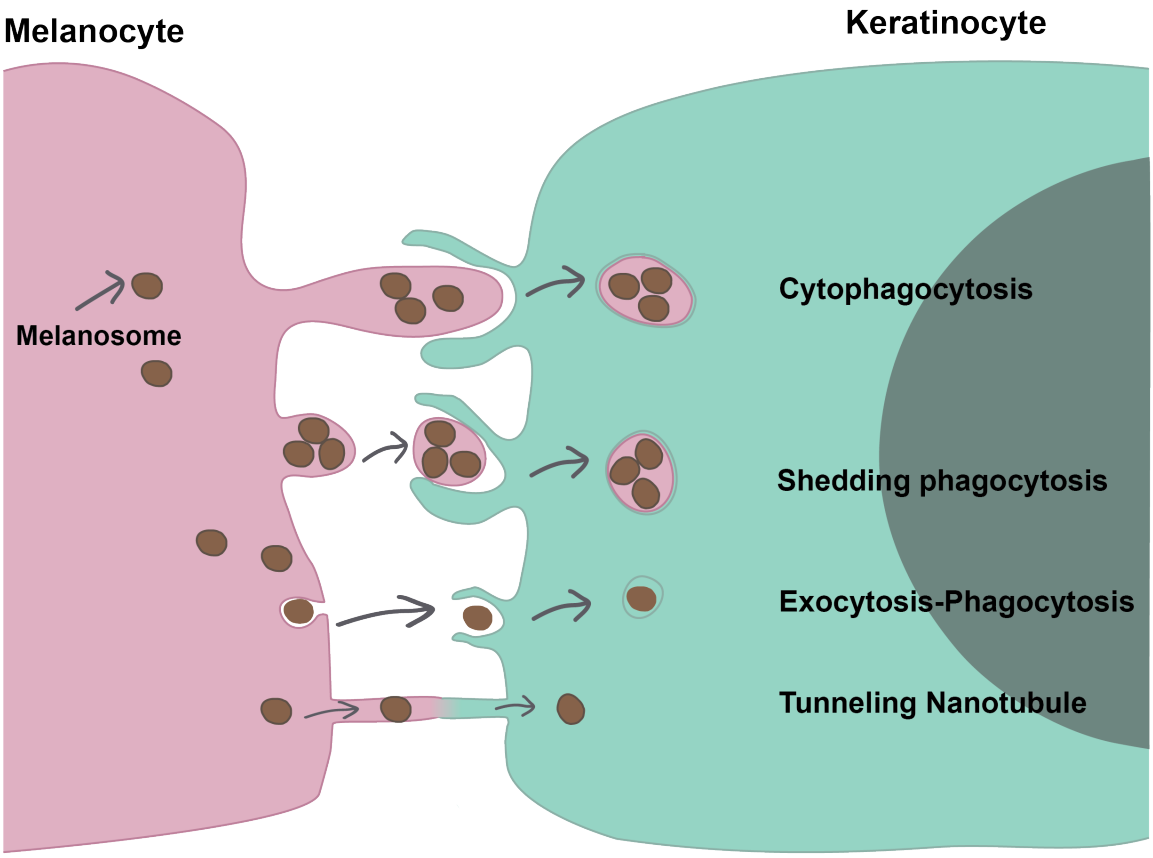

Figure 3 Models of Melanosome Transfer

Four models of melanosome transfer have been hypothesized. In the cytophagocytosis model, a keratinocyte phagocytosis a piece of melanocyte containing melanosomes, while this piece of cell is still attached to the melanocyte. In the shedding phagocytosis model, a keratinocyte phagocytosis a package of melanosomes that has been released from the melanocyte. In the exocytosis-phagocytosis model, the keratinocyte phagocytoses single or multiple melanosomes that have been secreted from the melanocyte. In the tunneling nanotubule model, the melanocyte and keratinocyte membranes fuse, forming a tube through which melanosomes can travel.

In order for keratinocytes to receive the photoprotection benefits of melanocytes, the act of melanosome transfer must occur. However, the molecular mechanism has remained difficult to establish. Numerous models exist for the exact mechanism of melanosome transfer, several of which are not mutually exclusive. What follows is a brief summary of the fundamental features of each:

1.3.1 Cytophagocytosis:

In the cytophagocytosis model, the keratinocyte internalizes a tip of the dendrite of a neighboring melanocyte. This dendrite section could contain single or multiple melanosomes. A distinctive feature of this proposed mechanism is that the keratinocyte phagocytoses of a section of melanocyte plasma membrane that is still attached to the melanocyte. In this model, the nascent phagosome in the keratinocyte will contain plasma membrane from the melanocyte, as well as the melanosome delimiting membranes, and the dense melanin fibrils of the melanocore.

1.3.2 Shedding phagocytosis:

In the shedding phagocytosis model, the melanosome first sheds a vesicle containing single or multiple melanosomes. These are subsequently phagocytosed by the keratinocyte. This model is distinguished from the cytophagocytosis model by the fact that phagocytosis is not initiated until the melanosome-containing package is separated from melanocyte. Most evidence for this model comes from two papers. In Ando et al., the authors used scanning and transmission electron microscopy to observe the release of globules containing multiple melanosomes in a co-culture of primary

human melanocytes and keratinocytes. These globules were seen resting on keratinocyte microvilii, and similar looking packages were observed within keratinocytes. Based on these snapshots, the authors proposed a model wherein melanocytes release melanosome-containing packages which are then internalized by keratinocytes (Ando et al., 2012). This work was performed in cultured, primary human cells.

Using a different model system, Wu et al. also obtained results consistent with the shedding phagocytosis model. They used the “Holly” skin mouse as an experimental system, a transgenic animal which expresses plasma-membrane targeted fluorophores of different colors in melanocytes and keratinocytes (Wu et al., 2012). The experiments were performed in co-cultures of primary melanocytes and keratinocytes derived from these transgenic mice. They observed melanin-containing structures within keratinocytes in these co-cultures that contained both melanocyte and keratinocyte plasma membrane. They also observed instances of melanocyte package shedding. As visualized through fluorescence microscopy, the region behind the tip of the dendrite appeared narrowed and an abscission event occurred. Although the authors interpret this to be evidence in favor of the shedding phagocytosis hypothesis, these results could also be interpreted to support a cytophagocytosis hypothesis. It is not possible from the images shown to conclude that internalization of the package by the keratinocyte does not begin until abscission is complete, because the abscission event is not marked temporally by any clear indicator.

In a study of the inter-feather skin of chicken embryos, Takodoro et al. observed melanocyte dendrites undergo dramatic blebbing followed by the release of melanocyte containing plasma-membrane packages containing melanocytes, which were the taken up by keratinocytes (Tadokoro et al., 2016). This is paper is unique, in that the experiments are performed in live cells *in situ*.

1.3.3 Exocytosis-Phagocytosis:

In the exocytosis-phagocytosis model, a melanosome within the melanocyte fuses its delimiting membrane with the plasma membrane of the melanocyte, thus releasing the melanocore into the extracellular space. The keratinocyte can then phagocytose single or multiple melanocores. In this model, the nascent phagosomes contain neither melanocyte plasma membrane nor melanosome membrane. Evidence for this model is derived from transmission electron microscope ultrathin sections of human tissue. Tarafdar and colleagues observe electron-dense melanocores in the extra-cellular space, with no discernable limiting membrane (Tarafder et al., 2014). They also observe melanosomes enveloped in a single membrane within keratinocytes. This configuration of membranes is only consistent with the exocytosis-phagocytosis model. However, it can be difficult to distinguish fine membranes next to electron-dense structures like the melanosome; the absence of a visible melanosome membrane does not mean that this membrane is not present. Additionally, phagosomes containing multiple membranes around a melanocores (as would be expected from the shedding

phagocytosis or cytophagocytosis model) would be transient structures that could be missed through static imaging. This work was performed in sections of human epidermis, not cultured cells. However, all of the results were obtained through static tomographic images. (Tarafder et al., 2014)

1.3.4 Tunneling nanotubule:

In the tunneling nanotubule model, the melanocyte and keratinocyte plasma membranes join at a juncture to provide direct passage of melanosomes between melanocyte and keratinocyte cytoplasm. Scott et al. observe the presence of melanosome-rich filopodia extending from melanocytes, and particularly from melanocyte dendrites. The abundance of these filopodia are increased by the expression of constitutively active CDC42, a known initiator of filopodia (Scott et al., 2002). Filopodia are not structures that are specific to melanosome transfer. There is no persuasive evidence that these filopodia fuse with keratinocytes to form a tube with openings on both ends, through which melanosomes could transit. Also, the presence of melanosomes in these melanocyte filopodia is not evidence that the filopodia are used as a conduit for melanosomes. The evidence that these filopodia fuse to keratinocytes and allow for transit of melanosomes through a nanotubule is not all that persuasive.

As discussed above, affirmative evidence of various qualities exists for the above models. In particular, the shedding phagocytosis and cytophagocytosis models have many features in common. Given the presence of strong evidence in

favor of both models, it is not unreasonable to speculate that both modes of transfer may occur concomitantly *in situ*. The exocytosis-phagocytosis model also has reasonably strong evidence in its favor. It is not impossible that these three modes of transfer may all occur, perhaps to varying degrees under specific physiological conditions not yet characterized. However, the tunneling nanotubule model does not have sufficient evidence to be considered a credible model at this time. The three models that are in consideration (shedding phagocytosis, cytophagocytosis and exocytosis-phagocytosis) have one important shared feature; they all rely on the keratinocyte phagocytosis. The phagocytic process will be described in more detail in section 1.4, and then explored experimentally in Chapter 5.

1.4 The Fate of the Melanosome within Keratinocytes

Melanosomes reside in lysosomal compartments in keratinocytes. In some humans, melanosomes are grouped in multiples which are contained by a membrane, whereas in other individuals, melanosomes are dispersed individually. This may depend on the skin tone of the individual (Szabo et al., 1969). The first detailed characterization of the melanosome-containing compartment in the keratinocyte came in 1971 from Wolff et al. They observed that *in situ*, guinea pig keratinocytes take up both latex beads and melanosomes of various sizes, but the size of the particle affects both its up-take and storage. The latex beads were delivered in a blister formed in the specimen's skin. Approximately 1 um beads were taken up and stored single, while .5 um beads were taken up in groups and stored together. Using the lysosomal label Thorotrast to label keratinocyte lysosomes, they

found that melanosomes are stored in lysosomal compartments in keratinocytes (Wolff and Honigsmann, 1971).

Melanin is retained through several stages of keratinocyte differentiation, only disappearing from terminally differentiated keratinocytes (Boissy, 2003; Hori et al., 1968). Recently, autophagy has been reported to regulate melanosome degradation in keratinocytes, as melanin levels in human skin cultures are reduced by activators of autophagy and enhanced by its inhibitors (Murase et al., 2013).

In a study of XB-2 cells (a teratoma-derived mouse keratinocyte cell line), Correia et al. found that the uptake of isolated melanocores (but not entire melanosomes) is impaired by the knock-down of Rab5b, an early endocytic regulator, but not Rab7a or Rab9a, two late endocytic regulators (Correia et al., 2018). The fact that these cells can internalize isolated melanocores is evidence in favor of the exocytosis-phagocytosis model discussed in section 1.3. They also found that although keratinocytes possess highly degradative organelles, melanocores do not reside in these compartments. They propose that when keratinocytes take up melanocores, they are stored in hybrid endocytic compartments that are neither highly acidic nor degradative, thus explaining the persistence of melanocores within keratinocytes.

There are important considerations when interpreting these results. These experiments were performed in XB2 keratinocytes, which do not necessarily exhibit the same behaviors as human primary keratinocytes, given that they are both non-human and derived from a teratoma. Equally importantly, the analyses of the acidity and degradative capacity of the melanocore-containing compartments were only

performed following a 4-hour chase following incubation with isolated melanocores. Given that phagolysosomal maturation is expected to occur within the time-course of hours, 4 hours is not long enough to conclude that melanosomes ultimately reside in a non-degradative compartment. The kinetics of phago-lysosome maturation in this system would be interesting to study further, as it is possible that *all* phagosomal or endosomal maturation is delayed in this system. It is equally possible that melanocore-containing compartments are specifically diverted to undergo a delayed processing journey. Also possible is the interpretation put forth by the authors, that melanin ultimately resides in a nondegradative compartment that it is specifically sorted into. If melanin within keratinocytes is preferentially diverted to a slow-maturing or less-degradative compartment compared to other cargos, it will be very interesting to learn more about the mechanism of this trafficking.

Melanin pigment in keratinocytes resides in compartments that represent some part of the endosomal system. However, the studies that address this question come from very different systems; Wolff et al. performed experiments *in situ* in the guinea pig, while Correia et al. used a cultured mouse teratoma cell line. It is hard to speculate from these slightly disparate results the nature of the compartment that melanin resides in *in situ* in humans, and further experimentation in other experimental systems will be necessary.

1.5 Phagocytosis

As mentioned in section 1.3, the three strongest models for melanosome transfer rely on phagocytosis by the keratinocyte. Phagocytosis is carried out by diverse cell types, which consume varied targets. Due to the variety of cell-types and

targets involved, phagocytosis is most broadly defined as the ingestion of particles of at least 0.5 μm in size (Flannagan et al., 2012). In order for this ingestion to occur, the target is recognized and bound by receptors on the phagocytic cell's surface. Following recognition of the target and binding of receptors, a cascade of coordinated signaling, cytoskeletal rearrangement and membrane modeling occurs in concert (Flannagan et al., 2012). Canonically, phagocytosis is a process that is carried out by macrophages and dendritic cells. With the discovery that many other types of cells are capable of phagocytosis, phagocytic cells have been generally divided into the classes of professional phagocytes (macrophages and dendritic cells), and non-professional phagocytes (retinal pigment epithelial cells, fibroblasts and keratinocytes, among others) (Rabinovitch, 1995). The majority of phagocytosis research has been performed on macrophages, so many of the well-characterized phagocytic receptors and pathways are specific to macrophages and may not be fully generalizable to non-professional phagocytes. However, the fundamental steps of recognition, uptake and maturation remain, as far as we know, consistent across cell and tissue.

1.6 Steps of Phagocytosis

1.6.1 Recognition and Internalization

The first step of phagocytosis occurs when the cell recognizes its target. This occurs when receptors on the plasma membrane of the phagocyte engage ligands on the target. There are several common classes of particles that are phagocytosed and corresponding receptors. One class of phagocytic receptors are those that recognize molecules that are found in bacteria, fungi and parasites, but not in

animals or plants. These are termed pattern-recognition receptors. Another type of receptor involved in detection of foreign bodies are opsonic receptors, which bind opsonins. Opsonins are proteins that are deposited onto the surface of pathogens that then mediate phagocytosis by serving as ligands for receptors on the membrane of phagocytes (Anderson et al., 1990).

Pathogens are not the only type of cell that stimulates phagocytosis. Phagocytosis of the corpses of apoptotic cells is another critical process. This process too involves a complex array of ligand-receptor interactions. First, the phagocyte is attracted to the apoptotic cell by soluble “find me” factors, which act as chemoattractants to nearby phagocytes (Chekeni and Ravichandran, 2011). Subsequently, direct binding of the phagocyte to the apoptotic cell is accomplished via the binding of phagocytic receptors to “eat me” signals present on the dying cell (Hanayama et al., 2002; Kobayashi et al., 2007)

One of the most widely characterized receptors is the Fcγ receptor (FcyR), which binds IgG. The FcyR is expressed by multiple immune cells, and particularly macrophages and dendritic cells. Much of our knowledge of the steps of phagocytosis derive from research performed IgG-coated latex beads. For FcγR-mediated phagocytosis, the two major steps of the internalization process, following receptor binding, are clustering of receptors and engulfment of the particle through an actin dependent mechanism. Lateral clustering of the receptors brings the cytosolic sides of multiple receptors into close proximity. This induces a tyrosine kinase signaling cascade, which ultimately induces actin regulating proteins. Actin remodeling occurs, resulting in internalization of the phagosomal target. *In vivo*,

multiple receptors with discrete signaling pathways are generally activated concomitantly, so this is a simplified picture (Flannagan et al., 2012). Although molecular players involved in the uptake process in the case of FcγR-mediated phagocytosis have been characterized, this is not the case for many other phagocytic receptor pathways.

1.6.2 Maturation

The current model for maturation of phagosomes describes internalized phagosomes undergoing several steps that involve fusion with various members of the endosomal system (Yates et al., 2005). Most often, the contents of the phagosome are components that will be digested, be it for the removal of a pathogen, clearance of an apoptotic cell, or for nutrition in the case of some single-celled eukaryotes. In order for the contents of the phagosome to be degraded, the membrane and lumen of the phagosome must be remodeled to take on new properties through a coordinated process of fusion with endosomal compartments. It is unknown whether these fusion events represent complete fusion of the membranes and contents of two organelles, or whether transient, reversible interactions occur, resulting in a limited exchange of components between the compartments (Duclos et al., 2000).

Newly formed phagosomes fuse first with early endosomes, and acquire the GTPase Rab5, which recruits and activates multiple effector proteins. Additional early endosomes are recruited to the early phagosome. Internalized phagocytic receptors are sorted to recycling endosomes, and trafficked back to the plasma membrane for reuse. Formation of the late phagosome occurs when Rab5 is lost

and Rab7 and Lamp1 accumulate on the membrane. Late phagosomes acquire hydrolases and proteases through interactions with late endosomes, and also become increasingly acidified through enrichment of the vacuolar-type H+- ATPase. Late phagosomes fuse with lysosomes, and have an arsenal of degradative enzymes capable of digesting proteins, lipids and sugars. The exact enzymes present in the phagolysosome vary by cell type. The pH of phagosomes also varies by cell type; macrophages contain significantly more acidic phagosomes than do dendritic cells (Flannagan et al., 2012). In macrophages, phagosomal maturation generally occurs within a two hour time-frame, with bone marrow derived macrophage phagosomes acidifying maximally within an hour (Guo et al., 2015).

Most of the work done to characterize these steps has been performed in macrophages phagocytosing opsonized beads, leaving gaps in our knowledge of how this process occurs with the endogenous targets of phagocytosis as well as in cell types that are not macrophages.

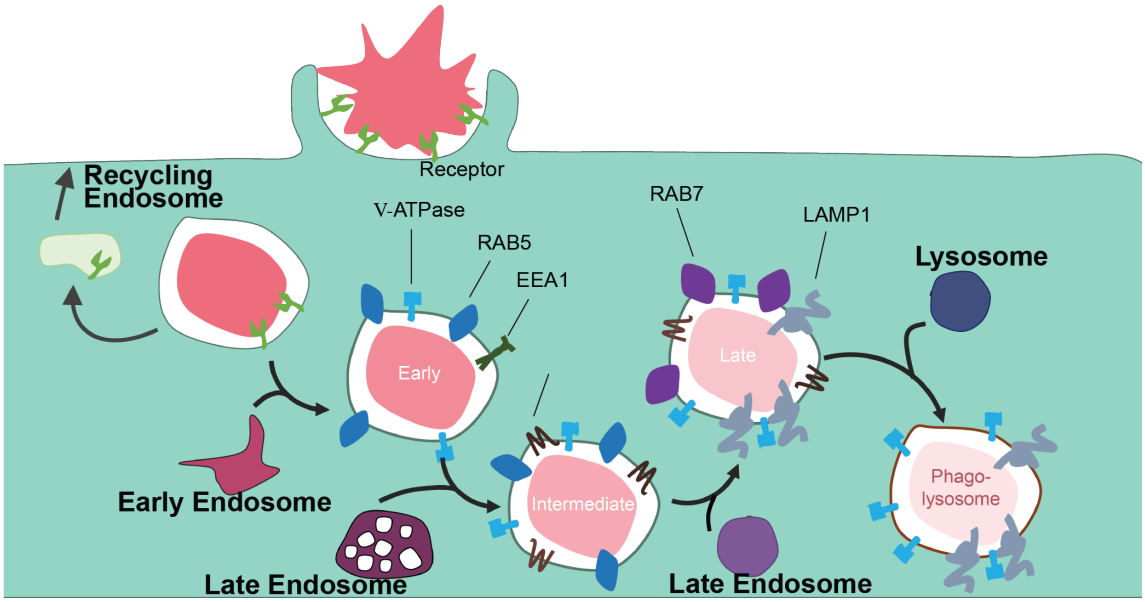

Figure 4 Schematic of Phagosome Maturation

Phagocytes recognize targets through receptors on their cell surface. Targets are internalized, forming phagosomes. Phagosomes mature through a series of interactions with different components of the endosomal system, and each stage of phagosomal maturation is characterized by the presence of particular proteins.

1.7 Epithelial Cells as Phagocytes

Keratinocytes are phagocytic cells and take up both melanocyte-derived materials as well as latex or polystyrene beads if given the opportunity. They are not alone in this capacity; a number of other epithelial cells perform important phagocytic functions. In female mammals, after weaning, there is rapid death of epithelial cells

in mammary glands. These apoptotic cells are phagocytosed by their epithelial neighbors (Monks et al., 2005). Epithelial phagocytes also have an important role to play during spermatogenesis. During spermatogenesis, more than half of the differentiating spermatogenic cells die by apoptosis. These apoptotic cells are phagocytosed by Sertoli cells, which are epithelial cells that reside in the seminiferous tubule (Chemes, 1986; Nakanishi and Shiratsuchi, 2004). A well-known example of a phagocytic epithelial cell comes from the eye. Distal portions of the photoreceptor outer segments (POS) in the retina are turned over daily. These cellular fragments are phagocytosed by retinal pigment epithelial cells, which are the sole phagocytes responsible for this cellular maintenance. 7-10% of POS cell mass is turned over daily, and continuously replaced (Kevany and Palczewski, 2010).

1.8 Keratinocytes as Phagocytic Cells

Evidence exists to support the phagocytic properties of keratinocytes, both in the context of melanosome transfer, and also more generally. As discussed above, time-lapse live-cell microscopy has shown packages being shed from melanocytes and phagocytosed by a neighboring keratinocyte (Wu et al., 2012). Human keratinocytes have been shown to phagocytose plastic beads of various sizes (Wolff and Konrad, 1972). Intriguingly, epidermal cells of the zebrafish have been shown to phagocytose sensory axon debris *in vivo* (Rasmussen et al., 2015). Further evidence that keratinocyte phagocytosis is an important biological process comes from a paper showing that basal keratinocytes in mice clear apoptotic debris of neighboring epithelial cells during catagen, the retraction phase of the hair cycle (Mesa et al., 2015). Understanding keratinocyte phagocytosis, from the binding of receptors

through processing of internalized material, will shed light on the molecular mechanism(s) of melanosome transfer while providing a new level of detail on phagocytosis by a non-professional phagocyte.

1.9 Unresolved Questions in Melanosome Transfer

I have focused so far on what *is* known about melanosome transfer, and the role of keratinocytes in this process. However, the outstanding questions remain numerous. Having discussed and evaluated four different models for the melanosome transfer, it is clear that there is no conclusive answer about which model or models occurs *in situ* in human skin. The evidence for these four models comes from different organisms (human, chicken, mouse and guinea pig), different model systems (cell culture, *in situ* animal tissue) both fixed and live. Given the presence of compelling evidence for three of the proposed models (shedding phagocytosis, cytophagoctysosis and exocytosis-phagocytosis), there are several ways of reconciling these seemingly contradictory findings.

One possibility is that the three phagocytosis-based modes of melanosome transfer all exist in human skin. For example, it may be the case that one mode is predominant in a homeostatic state, and another is more prominent during tanning or another perturbation. To my knowledge, this has not been studied and remains an open possibility. Another possible source of ambiguity is the variety of animal models used to assay this question. The epidermal structure of both chickens and mice differ from interfollicular human skin. It is possible that in both of these species, melanosome transfer does not proceed identically to human skin. In particular, a co-culture of mouse melanocytes and keratinocytes may be a poor model for

melanosome transfer. In the mouse, melanocytes reside in the hair bulb, not dispersed in the basal layer of the epidermis as they are in interfollicular human skin. Finally, the cytophagocytosis model and shedding phagocytosis model have more in common than they do differences. It is entirely plausible that in the dense environment of the epidermis, the difference between a keratinocyte phagocytosing a piece of melanocyte that is still attached to the cell vs a piece that has entirely pinched off is negligible.

To my mind, one of the most compelling questions in melanosome transfer is whether it is a receptor-mediated process. While receptors have been characterized to be involved in regulating the melanosome transfer process, no particular receptor has been identified as specific to the uptake of melanosomes. Relevant to this question is whether the keratinocyte is internalizing pieces of melanocyte that are enclosed in plasma membrane or membrane-less melanocores. If melanosome transfer is a phagocytic process mediated by a specific receptor-ligand pairing, identifying both the receptor and ligand would clarify which model is accurate. It is also possible that this uptake is not a specific process. Given that keratinocytes will readily internalize latex and polystyrene beads, it may be the case that they are constitutively phagocytosing their surroundings and take up melanosomes as a byproduct of constant phagocytic internalization.

1.10 Signaling Between Keratinocytes and Melanocytes

In the basal layer of the epidermis, melanocytes and keratinocytes reside together. In this shared environment, information is conveyed from one cell type to another. In particular, keratinocytes generate a number of factors that regulate

melanocyte proliferation and differentiation. More factors by which keratinocytes signal to melanocytes have been characterized than in the reciprocal direction. I will elaborate on the factors that are either specific to keratinocyte phagocytosis, or play a role in subsequent chapters. Not discussed below, but implicated in keratinocyte-melanocyte signaling, are the following factors: a-MSH, ACTH, bFGF, granulocyte-macrophage colony-stimulating factor, steel factor, leukemia inhibitory factor and hepatocyte growth factor (Costin and Hearing, 2007).

1.10.1 NGF

Nerve Growth Factor (NGF) is an important molecule that keratinocytes secrete that regulates melanocytes. NGF is a signaling protein that was initially discovered based on its ability to modulates the growth and viability of certain sensory neurons in the chick embryo (Cohen and Levi-Montalcini, 1956). Keratinocytes produce and release NGF, which in turn regulates both dendritogenesis and melanogenesis of melanocytes (Yaar et al., 1991). Keratinocyte expression of NGF is upregulated by UV radiation. Melanocytes express the NGF receptor as well as other receptors that have a high affinity for NGF (Peacocke et al., 1988).

1.10.2 PAR-2

Protease-Activated Receptor 2 (PAR-2) is a seven-transmembrane domain G-protein coupled receptor that resides on the plasma membrane of keratinocytes, and has been identified as promoting melanosome transfer (Nystedt et al., 1994; Santulli et al., 1995; Seiberg et al., 2000). It is related to the thrombin family of receptors (TRs) that also include the TRs PAR-1, PAR-3 and PAR-4 (Ishihara et al.,

1997; Vu et al., 1991; Xu et al., 1998). These receptors are activated by proteolytic cleavage of the N-termini of their extracellular domains, which reveals a new N-terminus that functions as a tethered ligand (Nystedt et al., 1994). PAR-2 is activated by trypsin and mast-cell tryptase (Molino et al., 1997; Nystedt et al., 1994; Nystedt et al., 1995). PAR-2 is also able to be activated by exogenous addition of peptides that correspond to its cleaved N-terminus without the necessity of proteolytic activity (Bohm et al., 1996; Nystedt et al., 1995).

PAR-2 is expressed in keratinocytes and not melanocytes, and its expression is upregulated in human skin in response to ultraviolet radiation (Santulli et al., 1995; Scott et al., 2001; Seiberg et al., 2000). Human skin grafted onto mice shows increased pigmentation when treated with PAR-2 activating peptides. PAR-2 appears to regulate melanosome transfer by modulating the phagocytic capacity of keratinocytes (Seiberg et al., 2000). Its activation in cultured HaCaT keratinocytes increases their phagocytic activity in a non-specific manner; their uptake of both beads and E. coli bioparticles is increased (Sharlow et al., 2000). The HaCaT cell line is a spontaneously transformed, aneuploid human keratinocyte cell line. The mechanism by which PAR-2 activation induces increased phagocytic activity is not well understood. However, it has been observed that activation of PAR-2 induces actin reorganization, and also increases the length and decreases the diameter of podia that extend from keratinocytes, which hints at a possible mechanism of action (Sharlow et al., 2000). Interestingly, PAR-2 activation upregulates keratinocyte secretion of proteases that are in turn capable of cleaving and activating PAR-2. This suggests that PAR-2 activation enhances further activation of PAR-2 (Scott et al., 2001).

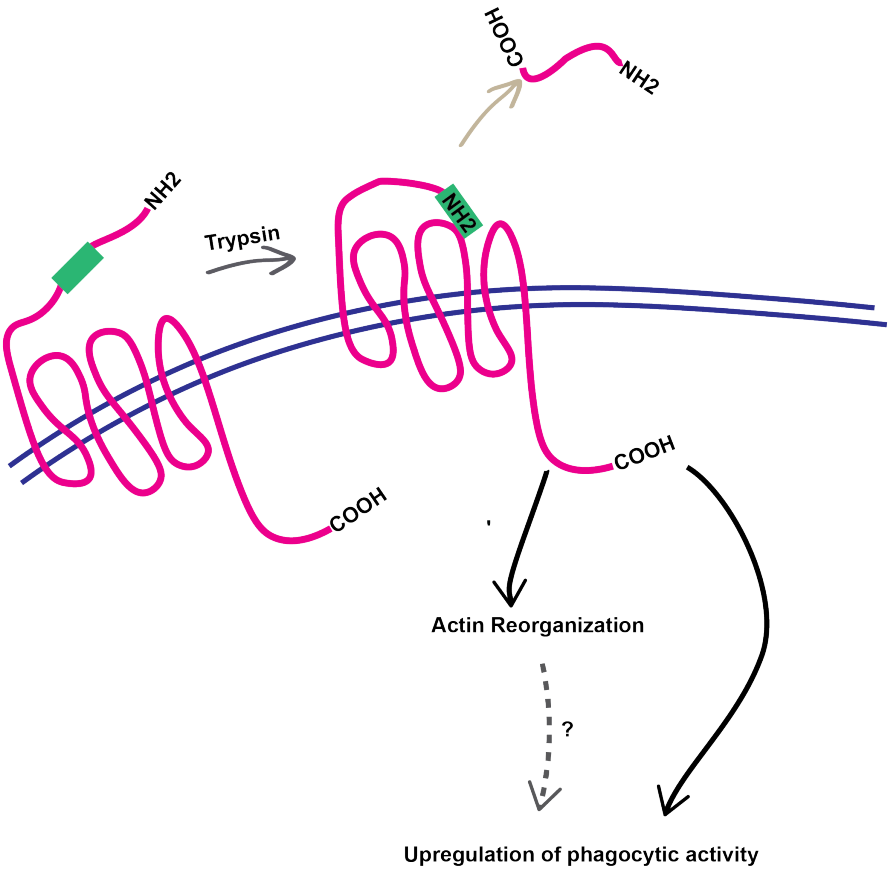

Figure 5 Schematic of Par-2 Activation

PAR-2 is activated when its amino terminus is cleaved, revealing a new amino terminus that serves as a tethered ligand, activating the receptor. Activation of PAR-2 leads to an upregulation of phagocytic activity and actin reorganization.

1.10.3 Keratinocyte Growth Factor

Keratinocyte Growth Factor is produced by mesenchymal cells, in this case, fibroblasts, which reside in the dermis. It specifically affects epithelial cells, which it binds to through the KGF receptor (KGFR), a splice variant of Fibroblast Growth Factor Receptor 2 (Tsuboi et al., 1993). KGF acts as a mitogen on cultured keratinocytes; it promotes early differentiation but prohibits terminal differentiation and apoptosis (Hines and Allen-Hoffmann, 1996; Marchese et al., 1990). In addition to its role in growth promotion, KGF promotes melanosome transfer in culture, as quantified by measuring the number of melanosomes in keratinocytes. KGF treatment also stimulates increased phagocytosis of beads by keratinocytes, suggesting that KGF non-specifically promotes the phagocytic activity of keratinocytes (Cardinali et al., 2005).

1.10.4 Endothelin

Endothelins (ETs) are secreted peptides that function as growth factors for a variety of cell types in the body. Endothelin-1 (ET-1) was originally discovered as an endothelium-derived vasoconstrictor. However, the role of ET-1 extends beyond the vascular system. ET-1 can bind to two G-protein coupled receptors, termed endothelin receptors A and B. In many cell types, binding of ET-1 to endothelin receptors on the cell surface induces changes in calcium (Ca^{2+}) concentration, with calcium serving as a second messenger in the cell. Depending on the cell-type in question, the Ca^{2+} involved in ET-1-induced signaling can derive from intracellular or extracellular stores (Tykocki and Watts, 2010).

Human melanocyte proliferation and melanosome production are both stimulated by ET derivatives (Yada et al., 1991). Keratinocytes produce and secrete ET-1, and this production of ET-1 is stimulated by UVB exposure, increasing in a dose-dependent manner (Imokawa et al., 1992). Endothelin treatment has been shown to increase the free cytoplasmic calcium level of cultured melanocytes (Yada et al., 1991). Conditioned media from UV-exposed keratinocytes also causes an increase in the cytoplasmic calcium level of melanocytes (Imokawa et al., 1992). Work from our lab has shown that endothelin and acetylcholine trigger local compartmentalized Ca^{2+} transients within melanocyte dendrites. These calcium transients are generated on discrete dendritic spine-like structures on the melanocytes. The calcium in these transients is derived from both intracellular and extracellular stores. Preincubation of melanocytes with a selective inhibitor of endothelin receptor B, but not an endothelin receptor A, blocks the increase in Ca2+ transients induced by ET-1 (Belote and Simon, 2020). It has also been observed that melanocyte dendritogenesis is stimulated by ET-1 (Hara et al., 1995).

1.11 Summary

Despite the body of research discussed above, there are quite a few outstanding questions relating to how melanocytes and keratinocytes interact, the cellular consequences of these interactions, and the process of melanosome transfer itself. It is not clear what is the predominant mode of melanosome transfer, or even if one mode predominates *in vivo*. Related to this question is the issue of whether the uptake of melanosomes by keratinocytes is a phagocytic process

mediated by a specific receptor-ligand interaction. If it is, what are the receptors on the keratinocyte, and what are they detecting on the melanosome or melanocyte plasma membrane?

There are also open questions in the field of melanocyte-keratinocyte signaling. Although a number of molecules have been characterized as having a role in signaling between melanocytes and keratinocytes as described above, it is unlikely that we have characterized every molecule involved in the process. The possibility remains that there are other molecules involved in signaling between melanocytes and keratinocytes. Additionally, the downstream effectors of both the identified and as of yet unidentified signaling molecules are not fully elucidated.

In my doctoral work, I have sought to address two goals. My first broad goal was to identify novel genes involved in communication between melanocytes and keratinocytes. This work is described in Chapters 2, 3 and 4. My second goal was to identify proteins involved in keratinocyte phagocytosis with the aim of better understanding melanosome transfer from the perspective of the keratinocyte. This work is described in Chapter 5.

CHAPTER 2: Transcriptomic Analysis of Melanocytes and Keratinocytes from Intact Skin

In order to better understand the homeostatic state of a healthy epidermis, we sought to assemble a transcriptome of cells derived directly from an intact epidermis. The transcriptome here refers to the full suite of messenger RNA (mRNA) and long-noncoding RNA (lncRNA) found in a given cell type at a moment in time. Understanding the transcriptome of a particular cell population provides insight about the biological state of the cells at the moment that the RNA is isolated by revealing what genes are expressed. Transcriptomes are dynamic, as cells modulate their gene expression patterns in response to different environmental conditions, including signaling molecules, environmental stressors and physical growth conditions. It has been reported that cells can change their transcriptomes as they adapt from growth *in situ* to *in vitro* (Kim et al., 2018). We wanted to capture the transcriptome of melanocytes and keratinocytes (both basal and suprabasal) in a state as close to *in situ* as possible, before the cells had ever been grown in a tissue culture environment.

This transcriptome then serves as a comparative data set for us and others; experiments performed *in vitro* can be cross-referenced to this data set to see whether genes of interest found through cell culture experiments are expressed in the living tissue. This is the first data set of its kind for these cell populations in from human neonatal foreskin, and is a useful resource.

To generate this data, we took a fresh piece of human skin tissue, isolated the epidermal cells, and used fluorescence activated cell sorting (FACS) with antibodies to separate out melanocytes, basal keratinocytes and suprabasal keratinocytes. The RNA from the FACS sorted cells was promptly isolated, prepared for next generation sequencing, and the sequences analyzed.

2.1 Preparation of Epidermal Cells for FACS Sorting

To establish a transcriptome that is as close as possible to that of the cells *in situ*, we focused on reducing the time from sample excision to RNA extraction. We waited to perform the experiment until we obtained a sample that could be collected immediately prior to the cell isolation. The details of the sample preparation process are described in more detail in Chapter 6. Once the sample was obtained, we dissected the tissue and separated the epidermis from the dermis with dispase followed by manual dissection. The epidermis was minced and separated into single cells with trypsin, and the cells resuspended in FACS buffer and strained. Cells were prepared for FACS by staining with three antibodies: anti-Alpha-6 Integrin, anti-C-Kit and anti-CD11c. Alpha-6 Integrin is a cell adhesion molecule that serves as a marker for basal keratinocytes (Metral et al., 2017). C-Kit (also known as CD117) is receptor that is expressed by melanocytes, and plays an important role in melanocyte cell homeostasis. It serves as a cell surface marker for melanocytes in the epidermis (Willemsen et al., 2020). CD11c is a classical marker of dendritic cells, and was used to remove dendritic cells from our collection (Haniffa et al., 2013). A diagram of the cell labeling scheme is shown in Figure 6A. There was clear separation of each of the three cell populations being sorted, as seen in Figure 6B.

The cells were sorted directly into a cell lysis buffer, and the RNA was isolated immediately after sorting. The RNA obtained from this procedure was all of appropriately high quality, with RNA integrity number (RIN) scores uniformly greater than or equal to 9, as indicated in Figure 7. The RIN calculation is generated by an propriety algorithm that analyzes electropherograms generated on an Agilent Bioanalyzer, and high quality RNA is essential for the production of interpretable RNA-sequencing results.

A

Cell Type	Cell Number	CD-11c	C-Kit	α6-Integrin
Basal Keratinocyte	3,572	-	-	+
Suprabasal Keratinocyte	10,779	-	-	-
Melanocyte	10,343	-	+	-

B

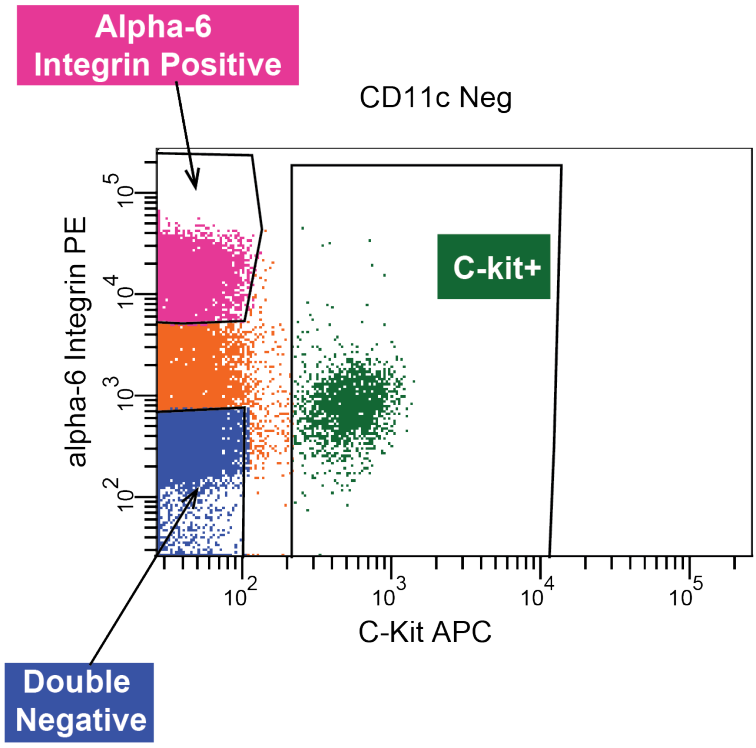

Figure 6 Flow Cytometry of Keratinocytes and Melanocytes Derived from Human Tissue

A) Table showing the number of cells sorted from each cell population, and the gating scheme for each cell type. Basal keratinocytes were positive for a6-Integrin, and negative for CD-11c and C-Kit. Suprabasal keratinocytes were triple negative. Melanocytes were positive for C-Kit and negative for CD-11c and a6-Integrin. B) Plots generated during FACS sorting melanocytes and keratinocytes showing the gating strategies employed. This plot shows all CD11c negative cells. The double negative cells are suprabasal melanocytes, the alpha-6 Integrin positive cells are basal keratinocytes, and the C-Kit positive cells are melanocytes.

A

Cell Type	Cell Type
Basal Keratinocyte	9
Suprabasal Keratinocyte	9.8
Melanocyte	9.5

B

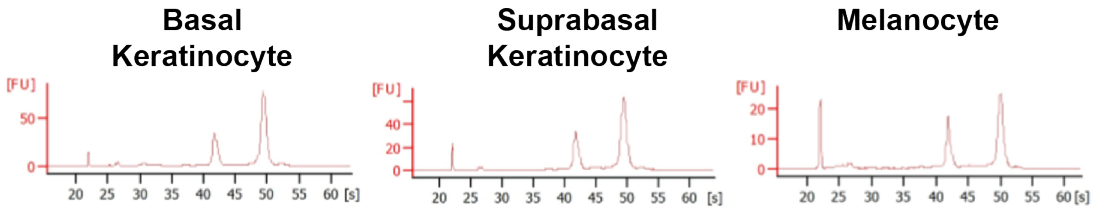

Figure 7 Quality of RNA from FACS Sorted Cells

A) RNA Integrity Number (RIN) scores of samples derived from basal keratinocytes, suprabasal keratinocyte and melanocytes. All are above 9. B) Electropherograms of each sample measured on an Agilent Bioanalyzer Picochip. The x-axis is in seconds, and the y-axis is Fluorescent Units.

2.2 Building a Primary Cell Transcriptome

RNA libraries were prepared using the SMARTer Universal Low Input RNA kit (Takara Bio), and were sequenced on the Illumina NextSeq 500 system, using paired-end reads of 75 base pairs. Details of the bioinformatic analysis are included in Chapter 6, but in brief: reads were subjected to quality control using FastQC (Babraham Institute), trimmed using BBduk (Joint Genome Institute), and were aligned and counted using Salmon (Patro et al., 2017). The counts were normalized by FPKM.

The quality control results from all three samples were excellent. The nucleotide position relative to the read-length was consistent, and the quality score was excellent throughout the position in the sequence (Figure 3.2B)

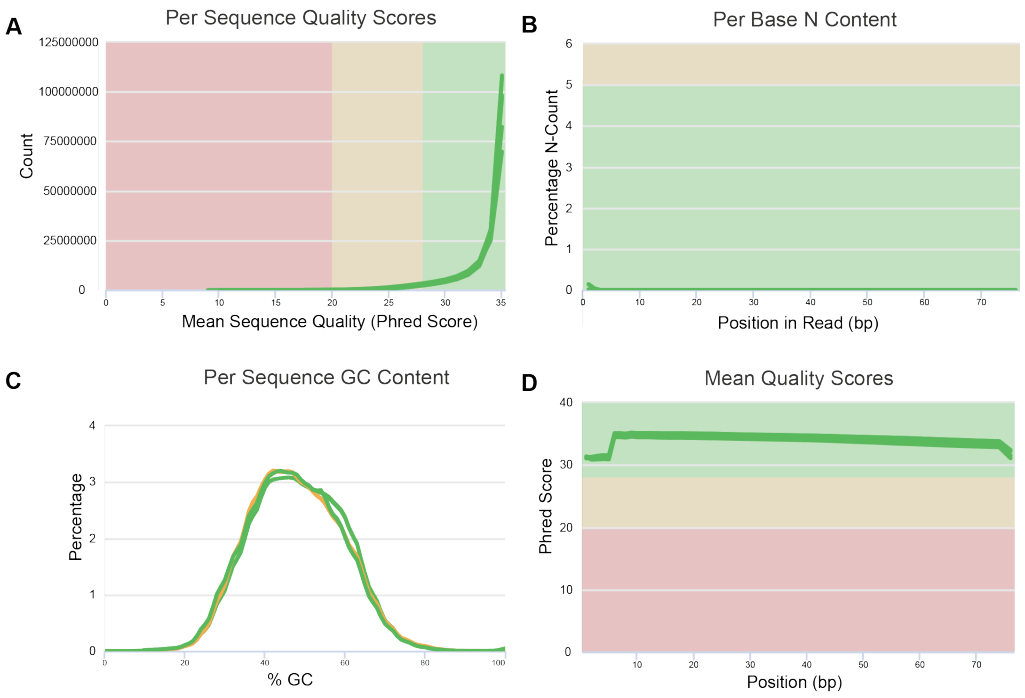

Figure 8 Quality Control Analyses of RNA Sequencing Data for FACS Sorted Samples

Samples were analyzed using Fast QC and visualized using MultiQC. All of the samples used had appropriate per sequence quality scores (A), a negligible per base N content (B), per sequence GC content distributed around 50% (C), and mean quality scores over 30 throughout the length of the read (D).

2.3 Expression Profile of Basal Keratinocytes

I sorted the genes present in each sample by normalized count. The samples were not normalized to each other, and only internal comparisons were made. The top 15 genes present in the basal keratinocyte sample are shown in Table 1. The top two genes expressed are keratin 14 (K14) and keratin 5 (K5). This is consistent with what is known about keratin expression in keratinocytes. Basal keratinocytes predominantly express K14 and K5. As keratinocytes differentiate, they downregulate their expression of K14 and K5 and increase their expression of K10 and K1 (Fuchs, 1995; Fuchs and Green, 1980). This pattern is reflected in this sequencing data, as K10 and K1 are the top expressed genes in the suprabasal keratinocyte population. Although K10 and K1 are both expressed in this basal keratinocyte population, K14 is expressed 4-fold over K10, and K5 is expressed 5-fold over K1. This canonical pattern of differentiation-specific keratin expression confirms the identity of the populations that were sorted through FACS.

Table 1 Top 15 Most Expressed Genes in Basal Keratinocytes

	Ensembl Number	Normalized Count	Symbol	Description
1	**ENSG00000186847**	**4567343**	**KRT14**	**keratin 14**
2	**ENSG00000186081**	**2539384**	**KRT5**	**keratin 5**
3	**ENSG00000186395**	**1147661**	**KRT10**	**keratin 10**
4	**ENSG00000198804**	**993249**	**MT-CO1**	**mitochondrially encoded cytochrome c oxidase I**
5	**ENSG00000075624**	**860067**	**ACTB**	**actin beta**
6	**ENSG00000156508**	**845738**	**EEF1A1**	**eukaryotic translation elongation factor 1 alpha 1**
7	**ENSG00000171346**	**802056**	**KRT15**	**keratin 15**
8	**ENSG00000065618**	**663415**	**COL17A1**	**collagen type XVII alpha 1 chain**
9	**ENSG00000198938**	**591027**	**MT-CO3**	**mitochondrially encoded cytochrome c oxidase III**
10	**ENSG00000198727**	**532369**	**MT-CYB**	**mitochondrially encoded cytochrome b**
11	**ENSG00000112378**	**528935**	**PERP**	**p53 apoptosis effector related to PMP22**
12	**ENSG00000096696**	**510387**	**DSP**	**desmoplakin**
13	**ENSG00000167768**	**488824**	**KRT1**	**keratin 1**
14	**ENSG00000184009**	**487303**	**ACTG1**	**actin gamma 1**
15	**ENSG00000151914**	**482056**	**DST**	**dystonin**

2.4 Expression Profile of Suprabasal Keratinocytes

As alluded to in the previous section, K10 and K1 are the top expressed genes in the suprabasal keratinocyte population, seen in Table 2. In the suprabasal keratinocyte population, K10 is expressed 59-fold higher than K14 and K1 is

expressed 21-fold higher than K5. This again is confirmation of the correct identity of this cell population.

Table 2 Top 15 Most Expressed Genes in Suprabasal Keratinocytes

	Ensembl Number	Normalized Count	Symbol	Description
1	**ENSG00000186395**	**5954189**	**KRT10**	**keratin 10**
2	**ENSG00000167768**	**2977007**	**KRT1**	**keratin 1**
3	**ENSG00000112378**	**888507**	**PERP**	**p53 apoptosis effector related to PMP22**
4	**ENSG00000096696**	**883353**	**DSP**	**desmoplakin**
5	**ENSG00000198804**	**830155**	**MT-CO1**	**mitochondrially encoded cytochrome c oxidase I**
6	**ENSG00000156508**	**694614**	**EEF1A1**	**eukaryotic translation elongation factor 1 alpha 1**
7	**ENSG00000075624**	**673461**	**ACTB**	**actin beta**
8	**ENSG00000188508**	**610327**	**KRTDAP**	**keratinocyte differentiation associated protein**
9	**ENSG00000251562**	**501212**	**MALAT1**	**metastasis associated lung adenocarcinoma transcript 1**
10	**ENSG00000184009**	**496467**	**ACTG1**	**actin gamma 1**
11	**ENSG00000198938**	**413036**	**MT-CO3**	**mitochondrially encoded cytochrome c oxidase III**
12	**ENSG00000134760**	**408418**	**DSG1**	**desmoglein 1**
13	**ENSG00000150991**	**388510**	**UBC**	**ubiquitin C**
14	**ENSG00000165272**	**388014**	**AQP3**	**aquaporin 3**
15	**ENSG00000173801**	**366636**	**JUP**	**junction plakoglobin**

2.5 Expression Profile of Melanocytes

The top 15 genes expressed in the melanocyte sample are shown in Table 3. Of just this top 15, 8 genes code for proteins that are localized to melanosomes. The rows containing these genes are highlighted in blue. This is confirmation that we did indeed isolate melanocytes from the epidermis, as expression of the genes for these melanosome proteins are characteristic of melanocytes.

Table 3 Top 15 Most Expressed Genes in Melanocytes

	Ensembl Number	Normalized Count	Symbol	Description
1	**ENSG00000107165**	**5031704**	**TYRP1**	**tyrosinase related protein 1**
2	**ENSG00000185664**	**3879456**	**PMEL**	**premelanosome protein**
3	**ENSG00000080166**	**3672680**	**DCT**	**dopachrome tautomerase**
4	**ENSG00000075624**	**1350902**	**ACTB**	**actin beta**
5	**ENSG00000198804**	**851108**	**MT-CO1**	**mitochondrially encoded cytochrome c oxidase I**
6	**ENSG00000136235**	**789522**	**GPNMB**	**glycoprotein nmb**
7	**ENSG00000120215**	**763217**	**MLANA**	**melan-A**
8	**ENSG00000077498**	**702626**	**TYR**	**tyrosinase**
9	**ENSG00000163453**	**697667**	**IGFBP7**	**insulin like growth factor binding protein 7**
10	**ENSG00000184009**	**613709**	**ACTG1**	**actin gamma 1**

11	**ENSG00000157404**	**593545**	**KIT**	**KIT proto-oncogene, receptor tyrosine kinase**
12	**ENSG00000115828**	**557318**	**QPCT**	**glutaminyl-peptide cyclotransferase**
13	**ENSG00000137575**	**532220**	**SDCBP**	**syndecan binding protein**
14	**ENSG00000164733**	**485722**	**CTSB**	**cathepsin B**
15	**ENSG00000198727**	**472400**	**MT-CYB**	**mitochondrially encoded cytochrome b**

2.6 Conclusions

This data set showed differential keratin expression in each of the keratinocyte populations, and the dramatic enrichment of genes involved in melanogenesis in melanocytes indicating that this transcriptome is reflective of the biology of each of these cell types. Although all possible care was taken to reduce the time from sample excision from the patient to transcriptomic analysis, the sample processing and FACS sorting both take time. This transcriptome only reflects a snapshot of the RNA present in each of these cell populations at a particular point in time and may not be identical to that of the cells *in situ*, but the quality scores and expression patterns suggest that it is biologically relevant.

The main function of the data set described here is to serve as a reference for ourselves and others. In subsequent chapters, I will identify genes of interest through experiments performed on cultured primary cells. The transcriptomes

described here allowed me to validate that my genes of interest are expressed *in situ* in the cell populations I am interested in. I also hope that this transcriptome will serve as a similar reference for other researchers interested in studying these cell types.

CHAPTER 3: THE EFFECTS OF MELANOCYTES ON KERATINOCYTE GENE EXPRESSION

In this chapter, I will detail work I have done to characterize the effect of the presence of melanocytes on keratinocytes in culture. As discussed in the introduction, signaling from keratinocytes to melanocytes has been studied for decades. However, what effects the melanocytes have on keratinocytes when these cells are grown together remains less understood. In order to address this question, I decided to study how the transcriptome of keratinocytes changes when keratinocytes are grown in co-culture with melanocytes or in monoculture. I took two approaches to isolate keratinocyte mRNA from cells grown in co-culture: (1) using flow cytometry to separate keratinocytes from melanocytes and (2) using a cell-specific ribosomal purification to isolate keratinocyte mRNA transcripts. Each of these approaches has pros and cons, which I will explore within this chapter. I executed both, with the intention that the benefits and caveats of each method would balancing out the other and serve as validation of the results.

3.1 Characterizing Changes in Keratinocytes Due to the Presence of Melanocytes Using Flow Cytometry

To address alterations in the keratinocyte transcriptome in the presence of melanocytes, I first developed a flow cytometry and sequencing workflow (Figure 9). I grew keratinocytes in cell culture both with and without melanocytes. All of the cells used were primary epidermal cells (melanocytes and keratinocytes) from neonatal foreskins, isolated from tissue as described in Chapter 6. All cells used were below passage 5. The keratinocytes grown in co-culture with melanocytes were seeded at

a ten-fold higher density than the melanocytes, to recapitulate the 10:1 ratio of keratinocytes to melanocytes in the basal layer of the epidermis. The co-cultures were not composed of melanocytes and keratinocytes from the same donor. Once the cultures reached confluency, I increased the calcium level of the media to 1.06 μM, which allows for more physiologically accurate cell-cell junctions but reduces keratinocyte proliferation (Belote and Simon, 2020). The cells were grown in co-culture or monoculture in these conditions for 42 hours.

In both conditions, after 72 hours, I dissociated the cells into a single-cell suspension, and prepared them for flow cytometry, as described in Chapter 6. The antibodies used to discriminate melanocytes from the keratinocytes were Alpha-6 Integrin and C-Kit. Keratinocytes that were selected for sequencing were alpha6-integrin positive and C-Kit negative. Both conditions were treated identically and subjected to flow cytometry. The results of the FACS sort were as expected, with the melanocyte-keratinocyte co-culture samples having a C-Kit positive population (which was not analyzed for this experiment), and the keratinocyte monoculture samples not having this C-Kit positive population (Figure 10). The Alpha-6 Integrin positive, C-Kit negative samples were selected and sorted directly into a cell lysis buffer. The RNA from these samples was isolated and was of appropriately high quality, with RNA integrity number (RIN) scores uniformly greater than or equal to 9. The samples were sequenced, and the quality of the sequencing results was analyzed and deemed suitable (Figure 11).

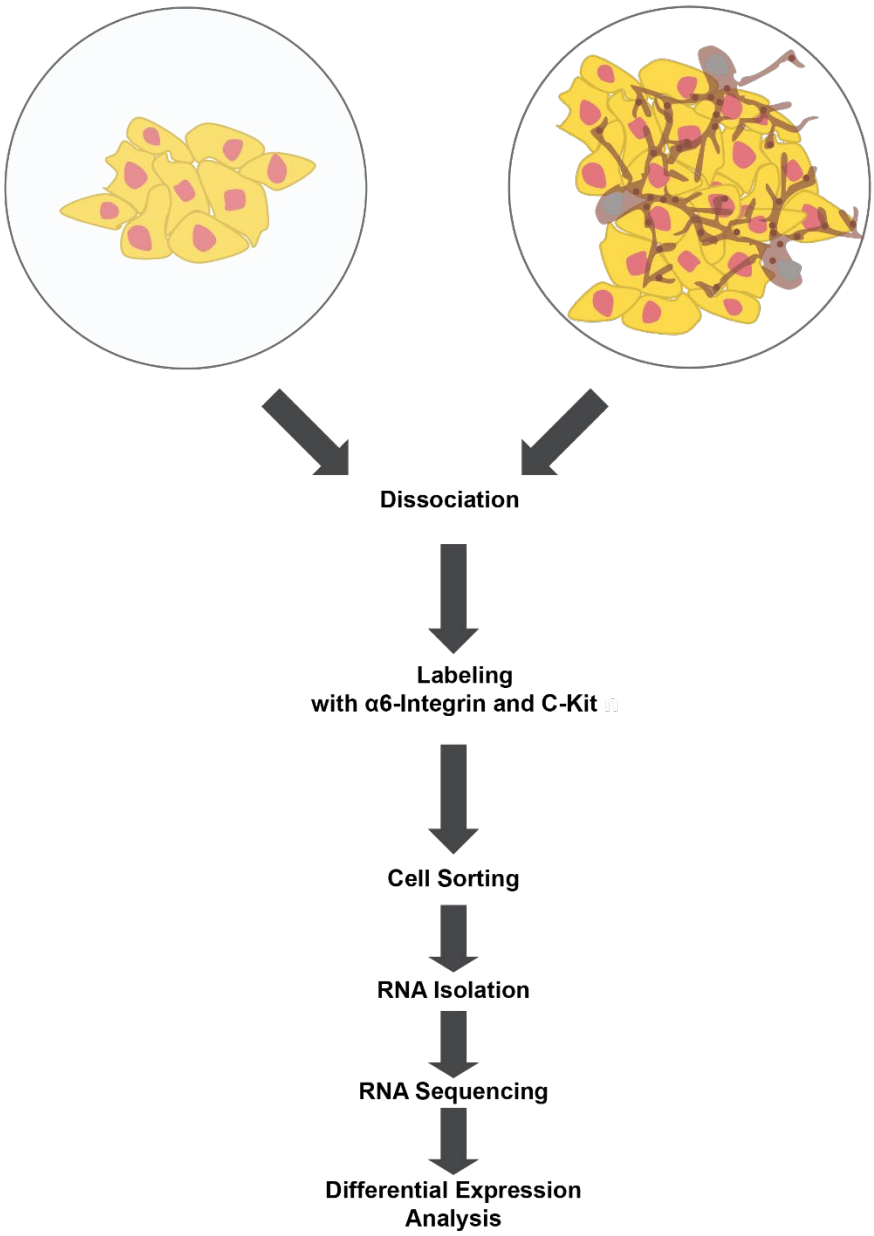

Figure 9 Schematic of Experimental Workflow Used to Study Keratinocyte RNA from Keratinocytes Grown in Monoculture and Co-Culture

Primary keratinocytes derived from neonatal human foreskins were cultured either independently or in co-culture with primary human melanocytes in **technical** triplicate. Cells were dissociated, stained for flow cytometry, and sorted based on the presence/absence of alpha6-Integrin and C-Kit. The RNA was isolated, libraries prepared, and RNA sequencing performed. The transcriptomes of the keratinocytes grown in co-culture and monoculture were compared to each other.

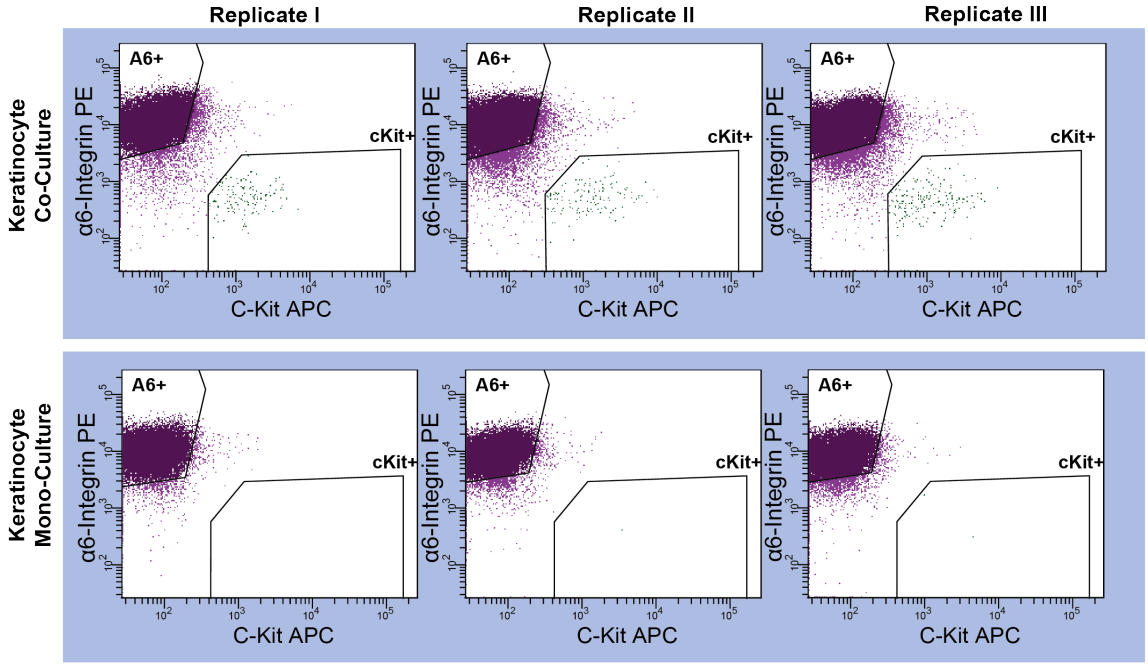

Figure 10 FACS Plots for Keratinocyte Co-Culture and Monoculture

Keratinocyte monocultures and keratinocyte-melanocyte co-cultures were labeled with alpha-6 integrin and C-Kit in triplicatevand sorted on a BD FACS Aria instrument. The established gates are shown as black geometric shapes. The alpha-6 Integrin positive cells (in the top left corner of each plot) were sorted directly into cell lysis buffer, and other cells were discarded. The C-Kit positive population is only present in the co-culture condition, seen in the top row.

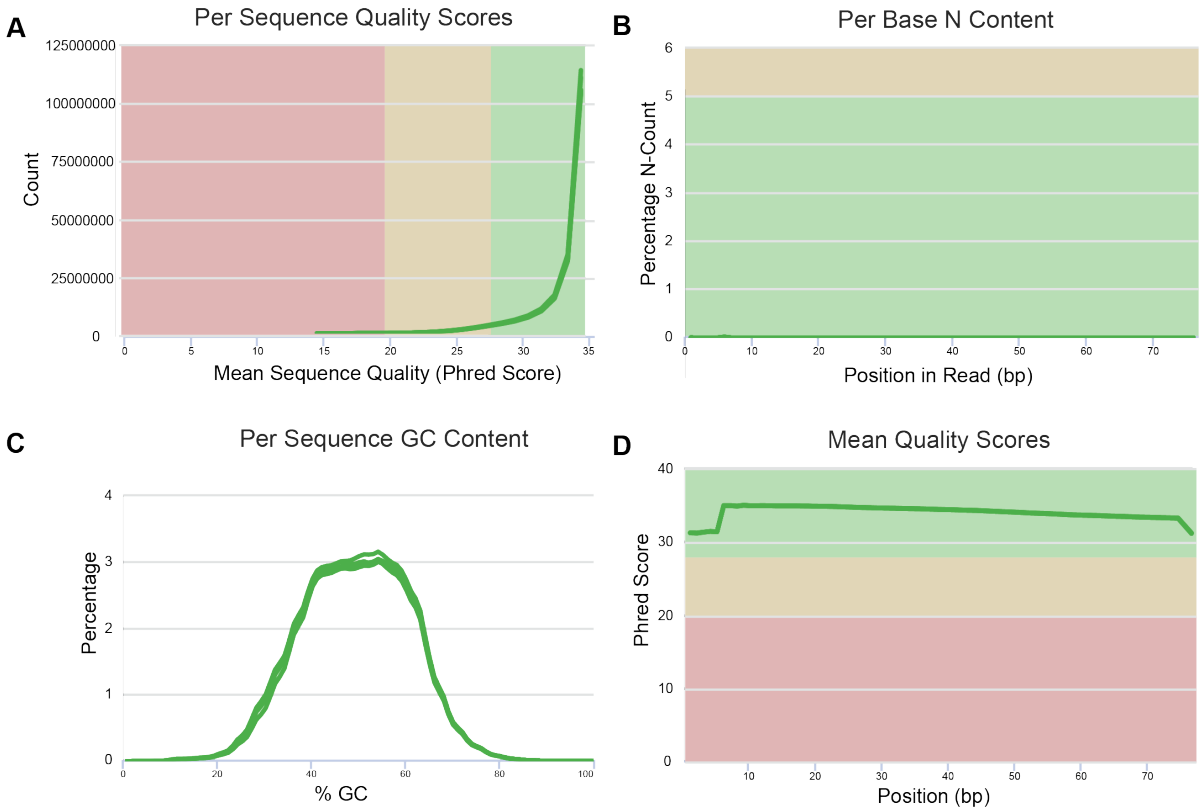

Figure 11 Quality Control Analyses of RNA Sequencing Data for FACS Sorted Keratinocytes

Samples were analyzed using Fast QC and visualized using MultiQC. All of the samples used had appropriate per sequence quality scores (A), a negligible per base N content (B), per sequence GC content distributed around 50% (C), and mean quality scores over 30 throughout the length of the read (D).

3.2 Analyzing Changes in the Keratinocyte Transcriptome

We performed principal component analysis and hierarchical clustering to visualize, in bulk, differences between the transcriptomes of keratinocytes grown under these two conditions (Figure 12). The co-culture transcriptome did not separate from the monoculture transcriptome when analyzed through both principal component analysis and hierarchical clustering. However, when we looked at the

results of differential expression analysis performed via DeSeq2 (Love et al., 2014), we found that a small but significant group of transcripts were upregulated in keratinocytes when they were cultured with melanocytes. The lack of separation by PCA and hierarchical clustering is probably due to how few genes were differentially expressed between the samples. A full list of these RNAs (P-value <= 0.05, and log_2FoldChange >= 0.9) is included in Table 4. 12 RNAs met these criteria. Two of the transcripts were for novel proteins of unknown function, and two transcripts represented a previously uncharacterized long noncoding RNA (lncRNA). : In recent decades, evidence has accumulated suggesting that lncRNAs play an important role in cell differentiation and gene regulation (Statello et al., 2021). Seven transcripts were found to be downregulated, meeting the criteria of P-value <= 0.05, and log_2FoldChange <= -0.9 (Table 5).

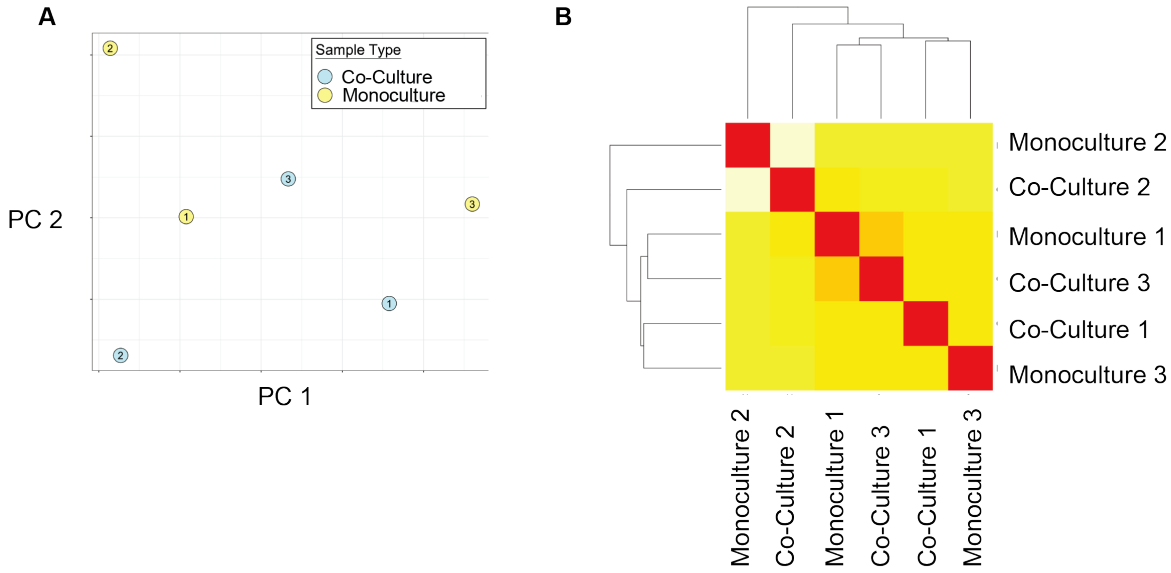

Figure 12 Principal Component Analysis and Hierarchical Clustering of Keratinocytes Grown Alone and with Melanocytes

Keratinocytes grown with and without melanocytes do not separate from each other by principal component analysis (A) or hierarchical clustering (B).

Table 4 Differentially Expressed Genes (Upregulated) in Keratinocytes Cultured with Melanocytes

Gene Name	Base Mean	log_2FoldChange Change	Stat	P-value	P-adjusted
Novel lncRNA	41.0365	8.7864	7.0836	1.404E-12	3.2212E-08
MFSD4A	99.6846	1.8200	6.3908	1.650E-10	9.4633E-07
BORCS7-ASMT	24.1850	8.0237	6.0232	1.710E-09	7.8453E-06
NPM1P7	16.9542	7.5120	5.7206	1.062E-08	3.4791E-05
AEBP1	109.5618	1.6403	5.4251	5.792E-08	1.6609E-04
Novel Protein	13.7881	7.2218	5.1259	2.961E-07	7.5457E-04
NRCAM	199.6205	1.4196	4.8878	1.020E-06	1.9494E-03
SLC8A1	34.5629	2.6520	4.2690	1.963E-05	2.5019E-02
SOCS3	119.0286	1.3031	4.1997	2.673E-05	3.1359E-02
Novel lncRNA	418.0040	0.9677	4.1429	3.429E-05	3.5317E-02
MSI2	388.9358	0.9174	4.1355	3.541E-05	3.5317E-02
TRANK1	119.7991	1.2436	3.9771	6.977E-05	5.3352E-02

Full list of transcripts that meet the criteria of P-value ≤ 0.05, and log_2FoldChange ≥ 0.9. List is sorted by stat.

Table 5 Differentially Expressed Genes (Downregulated)

Gene Name	Base Mean	log_2FoldChange Change	Stat	P-value	P-adjusted
Novel lncRNA	26.2222	-8.1701	-6.4385	1.206E-10	9.2251E-07
Novel lncRNA	20.5268	-7.8177	-5.8925	3.805E-09	1.4545E-05
KLRD1	31.0691	-2.6131	-5.0162	5.271E-07	1.2091E-03
MYCBP2	3158.5844	-1.1412	-4.9193	8.684E-07	1.8109E-03
IFITM10	26.8128	-2.5834	-4.6288	3.677E-06	6.0251E-03
RNF39	372.3944	-1.2896	-4.4627	8.093E-06	1.1603E-02
LRRC7	64.8481	-1.3390	-4.1934	2.748E-05	3.1359E-02

Full list of transcripts that meet the criteria of P-value <= 0.05, and log_2FoldChange ≤ - 0.9. List is sorted by stat.

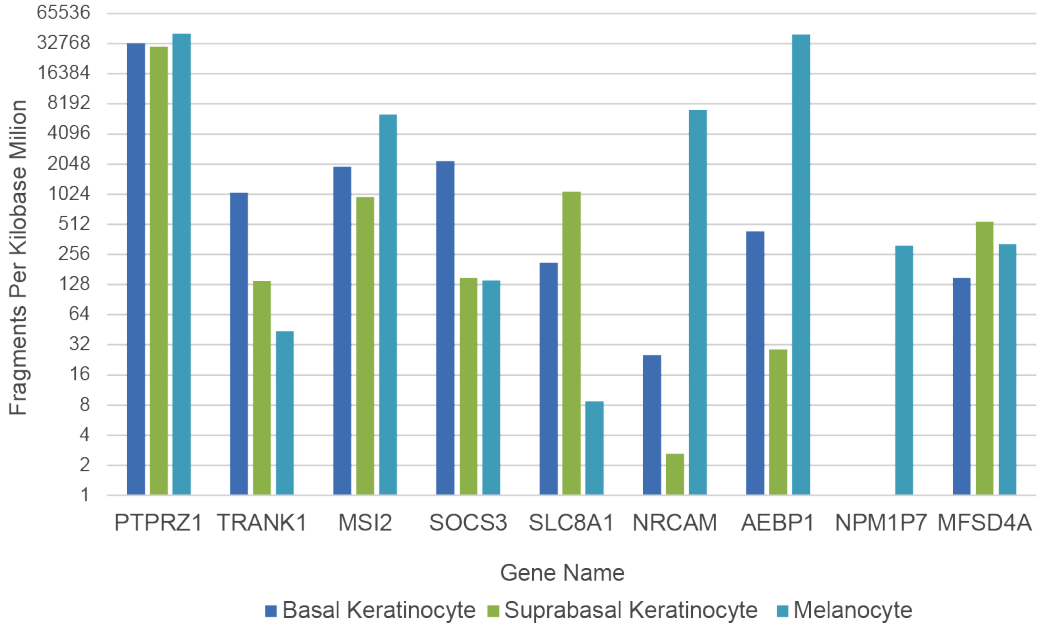

Figure 13 Expression Levels of Upregulated Genes in Basal Keratinocyte, Suprabasal Keratinocyte and Melanocyte Transcriptomes from *In Situ* Cells

For each of the upregulated genes of interest from Table 4, I plotted the fragments per kilobase million (FPKM). With the exception of NPM1P7, each gene examined is expressed in both basal and suprabasal keratinocytes. With the exception of SLCA8 and MFSD4A, the transcripts are expressed more highly in basal keratinocytes than suprabasal keratinocytes.

We wanted to confirm that these genes of interest are indeed expressed in keratinocytes in tissue, and that they are not an artifact of the cells being grown in culture. To this end, we cross-referenced these genes to the data set described in Chapter 3, the transcriptomic analysis of basal keratinocytes, suprabasal keratinocytes and melanocytes from intact human tissue. We found that with the exception of NPM1P7 (a pseudogene of nucleophosmin 1), all of the genes were

expressed *in situ* in keratinocytes. We excluded from this analysis the lncRNAs and the previously uncharacterized proteins. Of the 8 genes that were expressed in keratinocytes (both basal and suprabasal), 6 were expressed at higher levels in the basal keratinocytes than the suprabasal keratinocytes (Figure 13).

Of the genes that were upregulated in the keratinocyte population, we were particularly interested in one, neuronal cell adhesion molecule (NRCAM), also called neuron-glial related cell adhesion molecule (Nr-CAM). NRCAM is one of a class of integral plasma membrane proteins (the L1 group of the immunoglobulin superfamily) containing 6 immunoglobulin domains and 5 fibronectin III repeats that face the extracellular matrix. NRCAM and related proteins have been found to be important for axon guidance (Brummendorf and Rathjen, 1996) and for interactions between Schwann cells and neurons (Haney et al., 1999). Through an ankyrin binding domain on the cytoplasmic domain of the protein, NRCAM can induce actin remodeling, resulting in changes to cell morphology and migration (Maness and Schachner, 2007). NRCAM facilitates these cell-adhesion based processes through both homophilic and heterophilic interactions, and although its role is best characterized in the immune system, it also plays a role in leukocytes, intestinal crypt cells and kidney tubule epithelia (Kadmon and Altevogt, 1997).

NRCAM was particularly interesting because we were seeking novel mechanisms of cell-cell interactions between melanocytes and keratinocytes. Our RNA-seq data from cells derived from intact tissue confirms that NRCAM is expressed in both melanocytes and keratinocytes, and the differential expression analysis from FACS sorted co-cultured keratinocytes shows that NRCAM is

upregulated in keratinocytes in the presence of melanocytes. We sought to confirm the presence of the protein *in situ* through immunofluorescence, and validated that NRCAM is expressed in both melanocytes and keratinocytes (Figure 14).

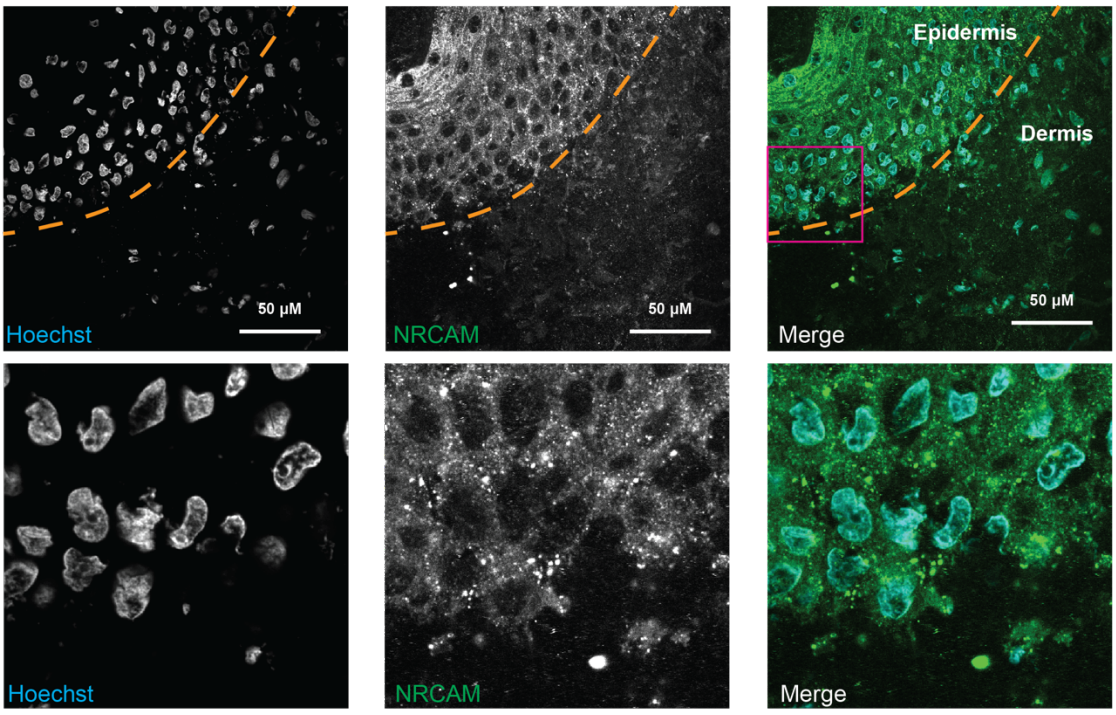

Figure 14 Human Keratinocytes Express NRCAM *In Situ*

Human epidermal tissue was fixed, cryopreserved, and embedded in OCT. 10 micron slices were prepared on a cryostat, and the tissue mounted on a glass slide and subjected to immunofluorescent staining with an anti-NRCAM antibody and Hoechst stain. Images were taken on an Olympus confocal microscope.

3.3 TRAP-Seq of Keratinocytes Grown With and Without Melanocytes

As a complementary, we used an entirely different method of preferentially sequencing keratinocyte RNA from a co-culture. Rather than separating whole cells using flow cytometry, we used a ribosomal affinity purification approach, called Translating Ribosome Affinity Purification Sequencing, subsequently referred to as TRAP-seq (Heiman et al., 2014). In brief, we expressed a fluorescently tagged ribosomal protein subunit (referred to as GFP-L10) in keratinocytes through viral transduction. Keratinocytes were infected with virus for inducing the expression of GFP-L10 while in monoculture prior to plating in a co-culture condition. Keratinocytes were grown alone or with melanocytes interspersed at a 1:10 ratio. After 72 hours of co-culturing, the cells were treated with cycloheximide to pause RNA transcripts currently interacting with ribosomes. Cycloheximide was maintained in the subsequent buffers during the isolation of ribosomes and their associated mRNAs. The entire plate of cells was lysed, and ribosomes containing the GFP-L10 tag were pulled down using an anti-GFP nanobody conjugated to beads. The beads were washed thoroughly, and the beads ultimately suspended in an RNA lysis buffer containing no cycloheximide. The RNA was isolated from this supernatant, subjected to quality analysis, and sequenced.

Unfortunately, we found significant contamination of the sample with melanocyte RNA. In the group of genes most differentially expressed in the keratinocyte co-culture compared to the keratinocyte monoculture, a number of genes that are likely to be of melanocyte origin are present (Table 6). Of the top 15 differentially expressed genes, seven were genes that were specifically involved in

melanogenesis, including tyrosinase (TYR), tyrosinase related protein one (TYRP1) and pre-melanosome protein (PMEL). Although these genes stood out as being derived from melanocytes due to their distinct function in melanogenesis, it is not possible to sort out which other genes in this data set are melanocyte derived. Due to the presence of melanocyte derived transcripts, this data set cannot be used to draw conclusions about changes in the keratinocyte transcriptome.

3.4 Conclusions

Keratinocytes experience specific, reproducible changes in the expression levels of a small sub-set of genes. One of these genes codes for NRCAM, a protein that has previously been reported to be involved in cell adhesion and axon guidance. I validated that NRCAM is expressed *in situ* in human epithelial keratinocytes. Although these results suggest a possible role for NRCAM in melanocyte-keratinocyte adhesion or signaling, more experiments will be necessary to identify what consequences NRCAM has on the physiology of both of these cell types. In particular, I propose knocking down NRCAM in keratinocytes grown in co-culture with melanocytes and observing the effects on both melanocyte and keratinocyte morphology and on melanosome transfer.

1

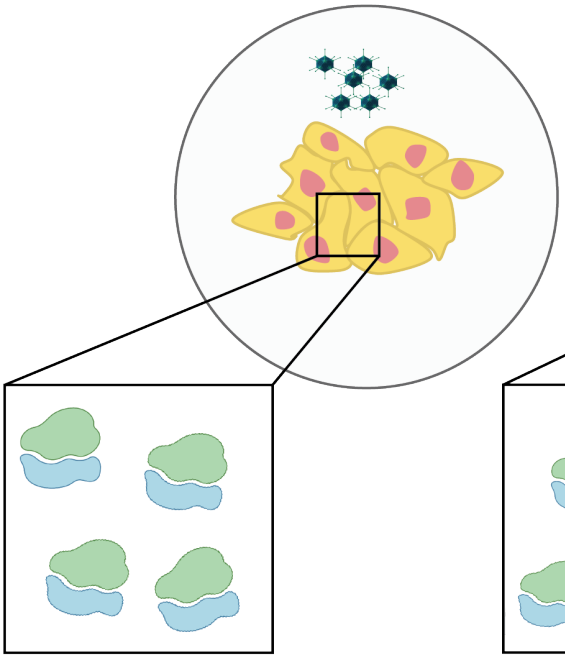

Add GFP-L10 expression virus to primary keratinocytes

2

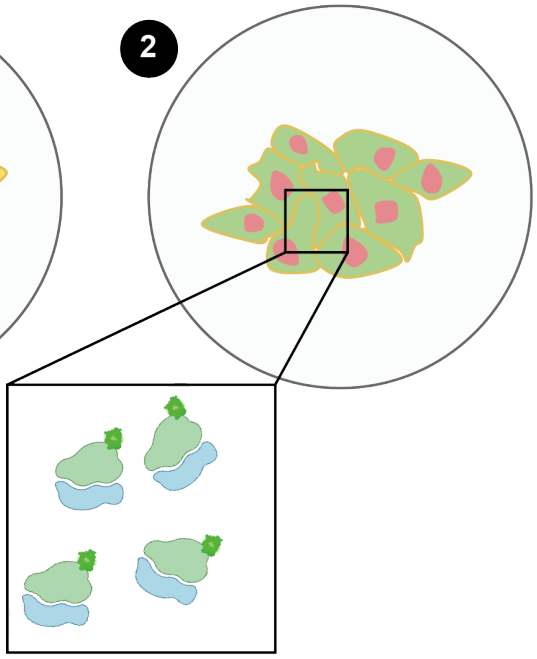

Induce and confirm expression of GFP-L10

3

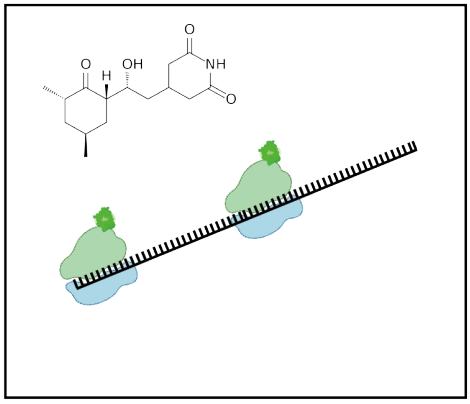

Treat with cycloheximide. Ribosomes stall on mRNA

4

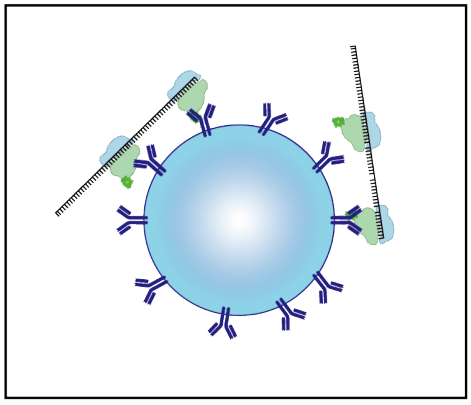

Pull-down GFPL10 labeled ribosomes with beads covered in anti-GFP nano-bodies

5

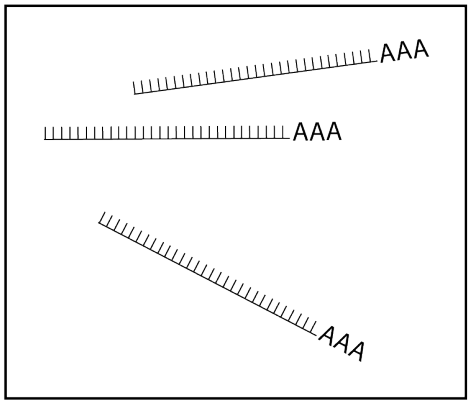

Release RNA from ribosomes and purify RNA

Figure 15 Schematic of TRAP-Seq Experiment

1-2) Keratinocytes were transduced with lentivirus to induce GFP-L10 expression, and confirmation of GFP-L10 expression was detected by microscopy. 3) Cells were treated with cycloheximide to stall ribosomes on mRNA. 4) Beads covered in anti-GFP nanobodies were used to pull down GFP-L10 labeled ribosomes. 5) RNA was released from ribosomes and isolated.

Table 6 Top Differentially Expressed Genes in Pull-Down of Keratinocyte Ribosomes from Keratinocyte-Melanocyte Co-Culture Compared to Keratinocyte Monoculture

Gene Name	Base Mean	log_2Fold Change	Stat	P-value	P-adjusted
TYR	236.8164	11.2756	7.5518	4.294E-14	5.1119E-11
MLANA	4716.6431	10.2944	28.8733	2.586E-183	4.6178E-179
PHACTR1	476.0212	9.9448	12.8230	1.220E-37	5.4441E-34
DCT	314.2168	9.4484	8.7703	1.782E-18	2.8926E-15
SLC24A5	229.6199	8.2947	8.9560	3.367E-19	6.0126E-16
TYRP1	1311.3424	7.3895	21.7445	7.793E-105	6.9575E-101
COL1A2	309.6015	5.3956	10.1483	3.372E-24	1.0034E-20
TRPM1	206.5496	5.1303	11.1805	5.080E-29	1.8140E-25
RRAGD	193.6946	4.9850	9.8406	7.527E-23	1.9201E-19
PMEL	1185.9752	4.4751	14.4808	1.602E-47	9.5377E-44
GNG11	291.6964	4.1211	8.3992	4.495E-17	6.1739E-14
NNMT	167.9347	4.0918	8.3889	4.907E-17	6.2589E-14
CAPN3	540.4231	2.4756	9.3334	1.025E-20	2.0339E-17
QPCT	617.4010	2.3898	8.5146	1.672E-17	2.4872E-14
TYR	236.8164	11.2756	7.5518	4.294E-14	5.1119E-11

Top 15 transcripts that meet the criteria of P-value ≤ 0.05, and log2 Fold Change ≥ 0.9. List is sorted by log2 Fold Change. Genes involved in melanogenesis are highlighted in orange.

CHAPTER 4: THE EFFECTS OF ENDOTHELIN ON MELANOCYTE GENE EXPRESSION

The presence of keratinocytes has a number of effects on melanocytes. We had previously observed that primary human melanocytes grow extensive dendrites in the presence of keratinocytes, but not when cultured independently. Additionally, we found that fine dendritic spines were only observed on the melanocyte dendrites in the presence of keratinocytes. Further, these dendrites and their spines only demonstrate repetitive calcium “spikes” in the presence of keratinocytes (Belote and Simon, 2020). We had also shown that these “spikes” can be specifically elicited by endothelin-1 secreted by keratinocytes. It has been previously shown that keratinocytes secrete endothelin-1. We demonstrated that pharmacological blockers of the endothelin-1 beta receptor (and not the endothelin-1 alpha receptor) block the spikes in melanocytes when keratinocytes are present. Further, introduction of shRNA against the endothelin-1 beta receptor into the melanocytes also blocks the calcium spikes and addition of 10 nM endothelin-1 was sufficient to elicit these spikes.

To explore the effects of keratinocytes on melanocyte signaling, we utilized three approaches. 1) We tried a TRAP-seq based approach, as described in Chapter 3 in which we monitored the translatome of melanocytes grown alone or in the presence of keratinocytes. 2) We also attempted to FACS sort melanocytes grown both with and without keratinocytes in the same manner that we did for keratinocytes in Chapter 3. 3) We observed gene expression changes induced by ET-1 signaling.

Ultimately, the third approach, observing transcription changes in the melanocytes in the presence of endothelin-1 provided the signal that was easiest to interpret. The only cell present was the melanocytes – there was no cross-contamination from the keratinocytes. In contrast, both the TRAP approach did not yield sufficient purity of signal, and the FACS approach did not yield sufficient RNA. I will discuss the two unsuccessful methods used to address changes in melanocyte gene expression. With better enrichment, they may yet yield a clean signal as an orthogonal validation.

I will then focus on the results of the experiment examining ET-1 induced changes. We identified a population of genes that are upregulated in response to ET-1 treatment and found that a significant portion of these genes are involved in cytoskeletal regulation and dendritogenesis. We further validated two of these genes, and investigated the consequences of ET-1 signaling on the actin structure of melanocytes.

4.1 TRAP-seq of Melanocytes Grown With and Without Keratinocytes

As with the experiment performed in keratinocytes described in Chapter 3, I expressed a fluorescently labeled ribosomal protein in melanocytes, but not in keratinocytes. I cultured the GFP-L10-expressing melanocytes alone, or with keratinocytes at ten-fold excess, or with HeLa cells at ten-fold excess. The purpose of including this HeLa cell condition was to control for gene expression changes in melanocytes resulted from making contact with neighboring cells of other types, which could differ from changes specifically caused by making contact with

keratinocytes. We pulled down the GFP-L10 ribosomes and sequenced the associated RNA transcripts.

Unfortunately, as with the experiment performed in keratinocytes, the preparation of ribosome-associated RNA from melanocytes contained substantial content of RNA derived from keratinocytes, evident from the significant presence of several keratin genes which are the characteristic gene expression signature of keratinocytes (as seen in Chapter 2). This contamination of keratinocyte RNA rendered these data sets unusable for analysis. Although it is difficult to assign with confidence whether a given transcript is derived from melanocytes or keratinocytes, the four keratin genes (KRT16, KRT6A, KRT6B, KRT6C) in the top 15 differentially expressed genes (ranked by stat) are most likely originated from keratinocytes. There has been controversy about whether melanocytes express Keratin 16 (Bhawan et al., 2005, 2010; Ramot et al., 2009); my own transcriptomic results suggest that melanocytes do express a relatively low level of the KRT16 gene (FPKM of 156). However, there is little evidence that melanocytes can express other three keratin genes at such high level. These remarkably high log2Fold changes of multiple keratin genes are therefore most likely the result of contamination, especially in light of the results from Chapter 3. For this reason, we did not use this data set for further analysis.

Table 7 Top 15 Differentially expressed genes in melanocytes cultured with keratinocytes compared to melanocytes cultured with HeLa cells

Gene Name	Base Mean	log2Fold Change	Stat	P-value	P-adjusted
KRT16	245889.6	14.8822	23.6187	2.5E-123	4.9E-119
KRT6A	255521.3	13.4902	20.4757	3.55E-93	3.49E-89
KRT6B	54233.53	16.0952	19.8747	6.73E-88	4.42E-84
LY6D	8592.489	10.7631	19.2799	7.92E-83	3.9E-79
FXYD3	44142.18	11.2264	19.0065	1.51E-80	5.94E-77
IFI6	22592.47	9.9998	17.8532	2.73E-71	7.23E-68
FGFBP1	5947.845	8.0480	17.8491	2.94E-71	7.23E-68
LAD1	6114.151	12.9481	17.4454	3.73E-68	8.17E-65
TMEM40	9976.819	11.4164	17.4144	6.42E-68	1.26E-64
IFI27	13629.67	9.7345	17.1653	4.83E-66	8.65E-63
KRT6C	22961.44	14.8667	16.9985	8.42E-65	1.38E-61
LYPD3	10105.53	10.1463	16.7715	3.94E-63	5.97E-60
HOPX	14525.73	11.7597	16.2688	1.64E-59	2.16E-56
SUGCT	6173.642	10.4654	15.9257	4.2E-57	5.17E-54
SPRR2D	32307.82	10.9739	15.9014	6.2E-57	7.18E-54

Top 15 transcripts that meet the criteria of P-value ≤ 0.05, and log2 Fold Change ≥ 0.9. List is sorted by stat. Keratin genes are highlighted in orange.

4.2 Characterizing Changes in Melanocytes Due to the Presence of Melanocytes Using Flow Cytometry

As with keratinocytes, we attempted to use flow cytometry to sort melanocytes from co-cultures of melanocytes and keratinocytes. The design for this experiment was almost identical to the one shown in Figure 9 in the previous chapter, but instead of sorting out keratinocytes from monocultures and co-cultures, we sorted melanocytes from monocultures and co-cultures. We were able to sort out a population of C-Kit positive and Alpha-6 Integrin negative cells, and isolated RNA from the samples. However, the number of sorted cells obtained with this strategy

did not yield sufficient RNA, which prevented us from proceeding with the experiment. This experiment is more difficult with melanocytes than with keratinocytes, because melanocytes are the minority cell population present. I also observed large amounts of melanocyte cell-death during the preparation for the FACS sort. Further optimization of the sample preparation may preserve the health of the melanocytes and facilitate the success of this experiment.

4.3 Characterizing Changes in Melanocytes due to Endothelin Signaling

Despite the difficulty in characterizing changes in melanocytes co-cultured with keratinocytes, we were able to specifically examine the changes in melanocytes induced by ET-1 signaling. We focused on ET-1 signaling because it is implicated in melanocyte morphology and melanosome transfer. Previous work from our lab showed that melanocytes exhibit localized calcium transients in spine-like structures on their dendrites, and that these calcium transients are induced by ET-1 signaling. The Ca2+ transients were reduced by antagonists to the endothelin receptor B (EDNRB), shRNA in the melanocytes to reduce expression of the EDNRB, and shRNA in keratinocytes to reduce production of ET-1 (Belote and Simon, 2020). However, the downstream effects of ET-1 signaling on melanocytes has not been studied at the level of gene-expression. For this reason, we sought to characterize the transcriptome of melanocytes after exposure to ET-1 for varying time periods.

I grew melanocytes in their normal growth media and supplement (described in the Materials and Methods), which contains ET-1 in addition to other growth supplements. Once the melanocytes were 70% confluent, I replaced the media with one lacking any added growth factors (and thus no ET-1). The cells were deprived of

ET-1 for 24 hrs, at which point the control condition was treated with vehicle, while the two experimental conditions were treated with 10 nM ET-1 for either 5 or 24 hrs. At these time-points, the cells were lysed in RNA extraction buffer, their RNA isolated and sequenced (Figure 16). The reason for the selection of these two time points was that existing studies on the effects of ET-1 on melanocytes have spanned various time points, but there have not been any studies on the time-dependence of the effects of ET-1. Belote et al. saw the induction of calcium transients in melanocytes within minutes after the addition of ET-1 to the media (Belote and Simon, 2020), while morphological changes to melanocytes reported by Hara et al. were observed after a 48-hour incubation with ET-1 (Hara et al., 1995). Therefore, we selected 5 and 24 hours as two intermediate time-points within the timescale at which ET-1 induced changes had been previously observed.

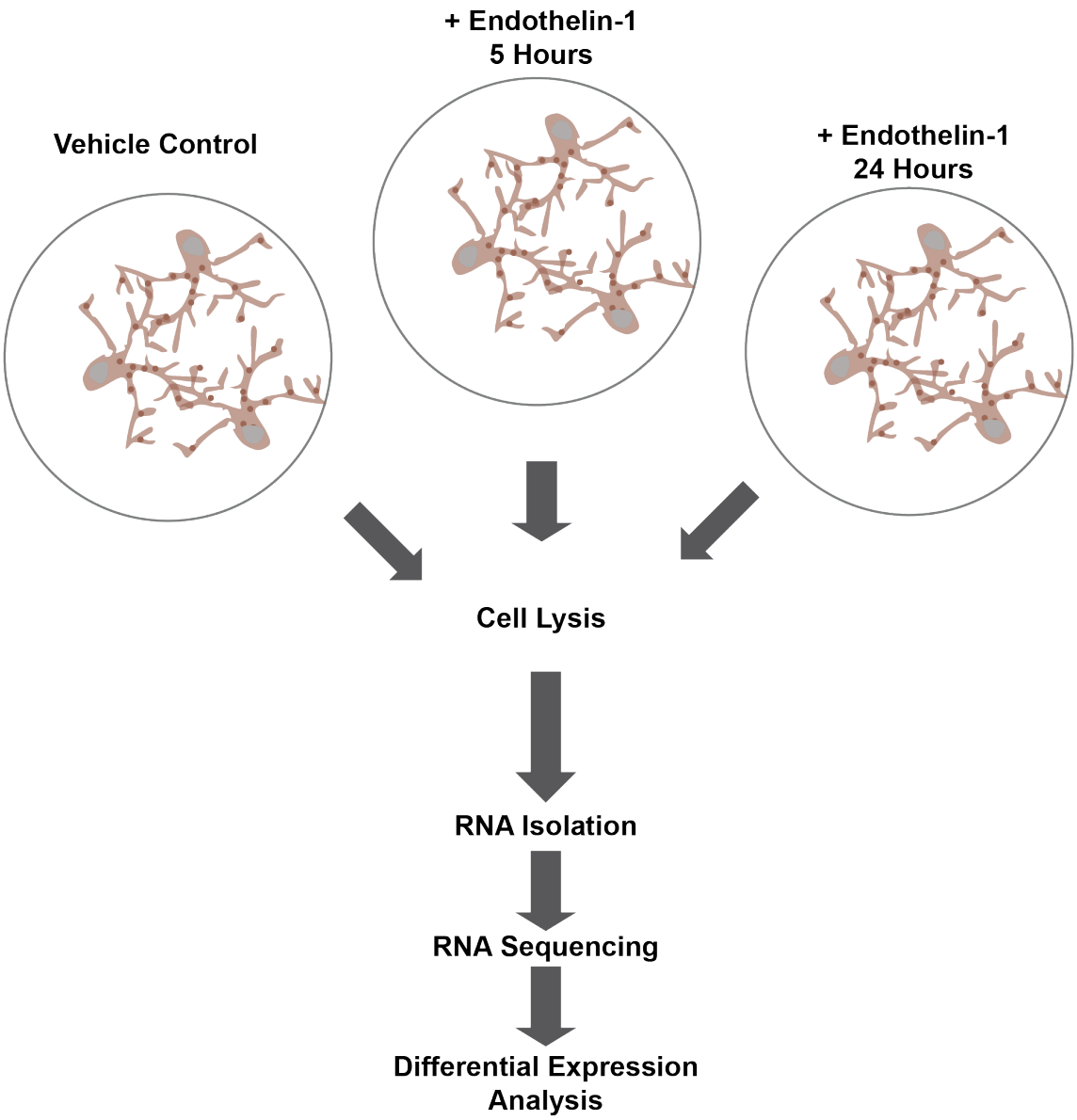

Figure 16 Schematic of Melanocyte Endothelin-1 Treatment

Melanocytes were cultured treated with ET-1 for 5 or 24 hours, at which point the cells were lysed and the RNA isolated. The RNA was sequenced, and the transcriptomes of each condition compared to each other through differential expression analysis.

The quality of the sequencing results was excellent as measured by several metrics (Figure 17), which allowed us to confidently proceed with differential expression analysis. We used DeSeq2 to compare differentially expressed genes in the three conditions: vehicle control, 5-hour ET-1 treatment and 24-hour ET-1 treatment. We performed principal components analysis on the data and found that each of the conditions separated from each other, with the three replicates of each experiment clustering together (Figure 18A). This result suggests that gene expression changes induced by ET-1 in melanocytes occur in a time-dependent manner. When we performed hierarchical clustering on these data, we again found that each replicate of the conditions clustered together, and that the three conditions clustered separately from each other. Interestingly, the 24-hour ET-1 treatment and control clustered more closely than the 5-hour ET-1 treatment. This suggests that certain changes induced by ET-1 signaling are more pronounced at the shorter time scale. In total, 242 transcripts met the threshold of P-value ≤ 0.05, and log2FoldChange ≥ 0.9 in the 24-hour condition and 271 in the 5-hour treatment condition.

I focused my subsequent analysis on the genes that were upregulated in both the 5- and 24-hour conditions. The list of the genes upregulated in both these conditions is shown in Table 7. Here, while 65 total transcripts were upregulated in this population, only 63 are listed, as we removed two novel lncRNAs and one novel coding sequence from the table.

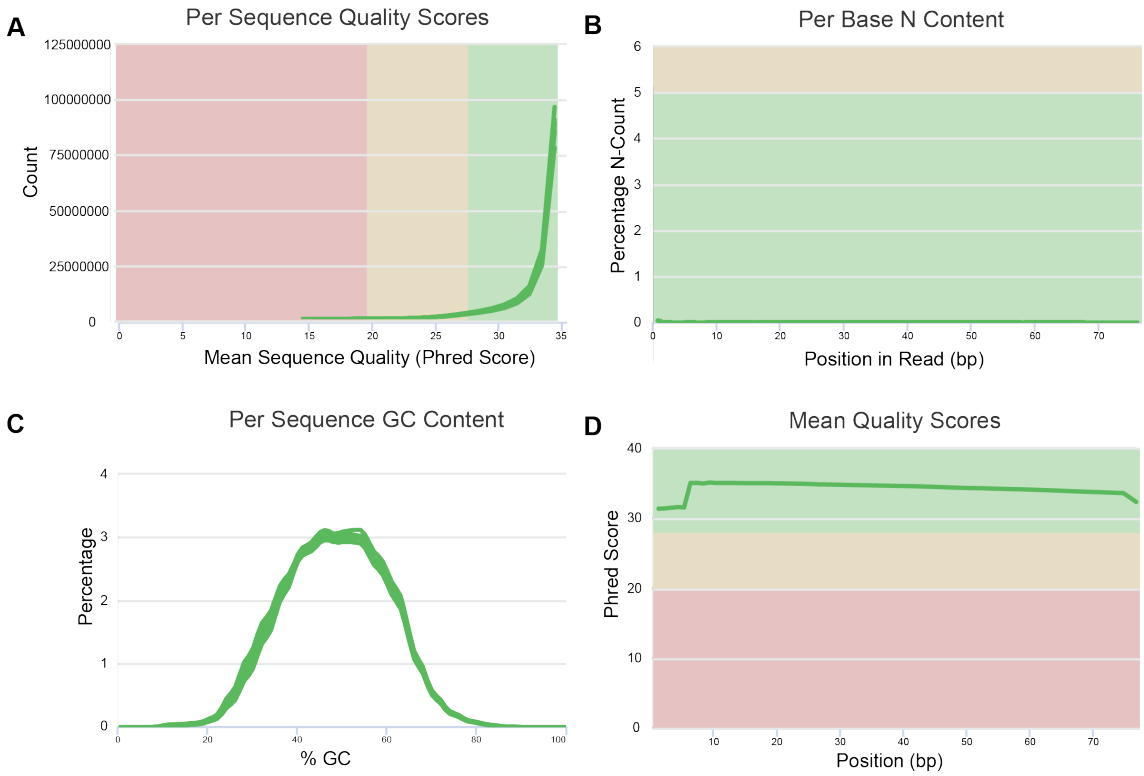

Figure 17 Quality Control Data of ET-1 Treated Melanocytes

Samples were analyzed using Fast QC and visualized using MultiQC. All of the samples used had appropriate per sequence quality scores(A), a negligible per base N content (B), per sequence GC content distributed around 50% (C), and mean quality scores over 30 throughout the length of the read (D).

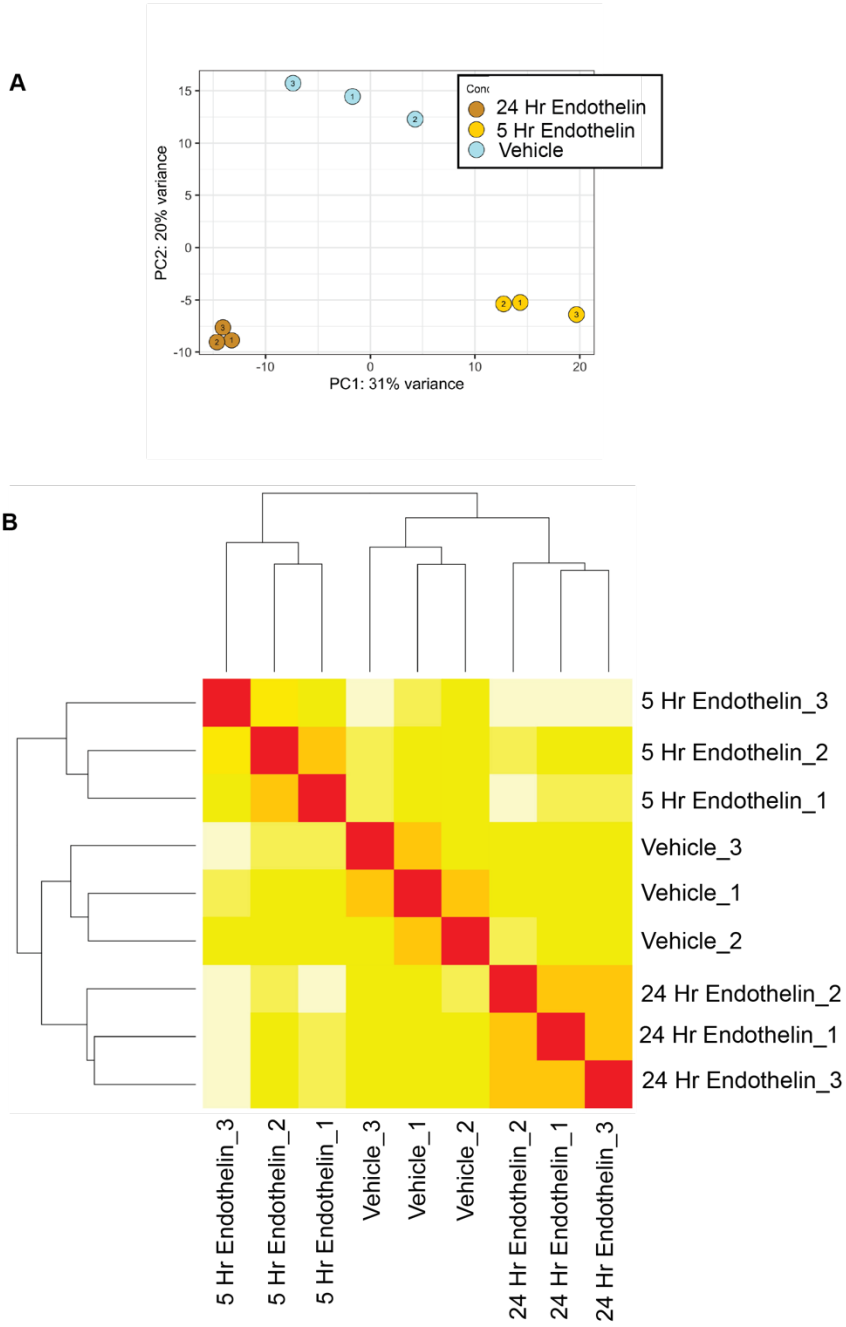

Figure 18 Principal Component Analysis and Hierarchical Clustering of ET-1 Treated Melanocytes

Melanocytes treated with ET-1 for 5- and 24-hours separate from each other, and from a vehicle control by principal component analysis, while replicates of each condition cluster with each other (A). The same pattern is observed by hierarchical clustering (B).

Table 8 Genes Upregulated After 5 and 24 Hour Treatments with Endothelin-1

Gene Name	Base Mean	log2Fold Change	Stat	P-value	P-adjusted
HDAC9	727.1965	2.9026	18.3506	3.267E-75	2.848E-71
CEMIP	14574.5220	1.8231	17.4214	5.681E-68	3.301E-64
MTSS1	581.7226	2.3280	13.4627	2.593E-41	5.023E-38
TAGLN	3507.6772	1.6450	12.4478	1.438E-35	2.089E-32
MAP3K7CL	1730.2971	1.4642	11.1374	8.246E-29	7.986E-26
TRIB1	418.8246	1.9419	11.0673	1.807E-28	1.658E-25
DEPP1	8104.9205	1.5313	10.7270	7.600E-27	6.023E-24
ZBTB16	1376.2282	1.3153	10.3549	3.976E-25	2.391E-22
GMNC	868.3532	1.5912	10.2193	1.625E-24	9.140E-22
BACH1	5317.4353	1.3219	9.6654	4.228E-22	1.755E-19
ABHD17C	1117.6767	1.4474	8.9306	4.238E-19	1.192E-16
SHROOM3	1404.4101	1.0080	8.1633	3.259E-16	7.103E-14
ABL2	1311.9026	1.4756	7.8613	3.800E-15	6.761E-13
SAMD4A	790.8011	1.0489	7.3594	1.847E-13	2.496E-11
SLAIN1	153.9084	1.7657	7.2665	3.689E-13	4.694E-11
RNF128	298.5476	1.2652	7.2088	5.643E-13	6.928E-11
FABP3	387.0162	1.5239	7.0667	1.587E-12	1.740E-10
LINC00518	164.8486	1.6276	6.7330	1.662E-11	1.566E-09
COBLL1	293.6195	1.8836	6.6316	3.322E-11	3.016E-09
CITED1	112.9404	1.8180	6.5855	4.534E-11	4.033E-09
KCNK15	194.2470	1.2439	6.5489	5.796E-11	5.129E-09
FOXQ1	50.0734	2.4373	6.4791	9.226E-11	7.963E-09
NGFR	236.1684	1.1710	6.2717	3.571E-10	2.743E-08
NNMT	5261.3965	1.2563	6.2452	4.233E-10	3.187E-08
CDH19	322.0140	1.0797	5.8182	5.949E-09	3.384E-07
TRPC6	87.0377	1.8538	5.5305	3.193E-08	1.595E-06
PKD1P1	30.8400	21.1049	5.4002	6.658E-08	3.095E-06
PDLIM3	254.1119	1.3206	5.3789	7.492E-08	3.456E-06
C1orf167	18.7598	7.4946	5.2476	1.541E-07	6.490E-06
ATF3	107.9502	1.2396	5.2216	1.774E-07	7.311E-06
MAP2	305.8413	1.3879	5.1349	2.822E-07	1.119E-05
RUBCNL	48.5926	2.0226	4.9366	7.950E-07	2.800E-05
HRH2	89.5245	1.2708	4.8092	1.515E-06	4.931E-05
HSPB3	17.1985	3.6266	4.7775	1.775E-06	5.699E-05
HES4	135.6341	1.2391	4.5454	5.482E-06	1.534E-04
LYPD1	71.7840	1.8794	4.5071	6.572E-06	1.788E-04
SEMA3E	69.6824	1.9525	4.3961	1.102E-05	2.753E-04
CYP24A1	15.5786	5.6183	4.3104	1.630E-05	3.875E-04
BIRC3	67.6522	1.5039	4.3091	1.639E-05	3.889E-04

TRIM6-TRIM34	52.7234	9.2152	4.2556	2.085E-05	4.697E-04
LINC00702	57.5434	2.4479	4.2453	2.183E-05	4.904E-04
MMP12	15.3329	3.0437	4.1273	3.670E-05	7.701E-04
HRK	118.5584	1.6328	4.0814	4.477E-05	9.035E-04
PTGS2	159.7302	1.2181	3.9332	8.381E-05	1.538E-03
CNN1	36.5935	1.9666	3.6440	2.684E-04	4.126E-03
INHBB	24.2976	1.7852	3.5098	4.485E-04	6.273E-03
WFDC1	24.8078	2.1559	3.3778	7.307E-04	9.388E-03
IL6	199.4227	1.0668	3.3457	8.208E-04	1.026E-02
ERG	60.3782	1.2471	3.2574	1.124E-03	1.332E-02
DOK5	23.5972	1.7042	3.2474	1.165E-03	1.375E-02
PTPN2	1773.4732	1.7274	3.1566	1.596E-03	1.774E-02
BIK	17.8990	1.7280	3.1045	1.906E-03	2.046E-02
CHDH	30.4188	2.0711	3.0641	2.183E-03	2.263E-02
SHTN1	390.6882	1.3583	3.0374	2.386E-03	2.414E-02
SRPK3	61.1076	1.7208	2.9715	2.964E-03	2.856E-02
SHROOM3-AS1	18.8808	1.8179	2.9175	3.529E-03	3.262E-02
RBM20	20.9707	2.2399	2.8958	3.781E-03	3.428E-02
FAM221A	24.9295	1.5767	2.8545	4.310E-03	3.759E-02
NR4A3	17.1851	2.3238	2.8399	4.512E-03	3.893E-02
NR4A1	53.8026	1.6660	2.7800	5.436E-03	4.515E-02
IL1RAPL1	55.0285	1.3163	2.7609	5.764E-03	4.715E-02
ZNF321P	50.5480	1.3967	2.7476	6.003E-03	4.867E-02

Genes meet the cut off of P-value ≤ 0.05, and log2FoldChange ≥ 0.9, and are ordered by stat.

We further analyzed this list of genes by gene ontology (GO) to identify the molecular functions and biological processes represented in the list of upregulated genes (Table 8). There were four molecular functions that met the significance value threshold of ≤ 0.05, all of which were related to cytoskeletal proteins, and three were specific to actin binding.

Table 9 Molecular Functions of Genes Upregulated in Melanocytes after ET-1 Treatment

Name and ID	Hit Count in Query List	Hit Count in Genome	Hit in Query List
actin binding GO:0003779	10	456	SHROOM3,ABL2,PDLIM3,MAP2,COBLL1,TRPC6,MTSS1,TAGLN,SHTN1,CNN1
actin monomer binding GO:0003785	3	28	ABL2,COBLL1,MTSS1
cytoskeletal protein binding GO:0008092	11	1053	SHROOM3,ABL2,PDLIM3,MAP2,COBLL1,TRPC6,MTSS1,TAGLN,SHTN1,CNN1,FABP3
actin filament binding GO:0051015	5	222	SHROOM3,ABL2,MTSS1,TAGLN,SHTN1

We also investigated the biological processes that were upregulated through GO analysis. A total of 206 biological process pathways met the criteria of statistical significance. Many of these pathways overlap with each other, describing similar if

not identical cellular processes by slightly different names. A selection of these pathways is shown in Table 9. In the analysis, pathways involved in cell morphogenesis, cell projections, adhesions and tissue morphogenesis were all identified as upregulated, as predicted. This result shows that we were able to detect transcriptomic changes that reflected the observed morphological changes.

Interestingly, a number of the pathways that were upregulated have been previously identified as involved in neuron differentiation, neuron development, dendrite morphogenesis and axon morphogenesis. Melanocytes are neural crest derived cells are known to share some signaling pathways with neurons (such as NGF). Additionally, melanocytes share certain morphological features with neurons, as they possess dendrites that are studded with spines, and also engage in localized calcium transients in response to ET-1 signaling from keratinocytes (Belote and Simon, 2020). Part of our interest in understanding the consequences of ET-1 signaling on the melanocyte transcriptome was to understand the molecular origins of the observable changes in melanocyte morphology induced by ET-1 signaling, and this data set gives us a basis for understanding the genes that underly these changes. I have found that melanocytes express sets of genes implicated both in general cell projection organization and in neuronal projection development (both axon and dendrite). This is a novel finding.

Table 10 Subset of Biological Pathways of Genes Upregulated in Melanocytes after ET-1 Treatment

Name	Hit Count in Query List	Hit Count in Genome	Hit in Query List
cell morphogenesis 0000902	13	1197	IL1RAPL1,DOK5,SHROOM3,ABL2,MAP2,TRPC6,NGFR,HRH2,NR4A3,CDH19,SHTN1,IL6,SEMA3E
cell migration 0016477	12	1812	HDAC9,ABL2,ERG,NR4A3,NR4A1,MMP12,SHTN1,TRIB1,PTGS2,IL6,SEMA3E,CEMIP
plasma membrane bounded cell projection organization 0120036	12	1863	GMNC,IL1RAPL1,DOK5,ABL2,MAP2,TRPC6,MTSS1,NGFR,NR4A3,SHTN1,IL6,SEMA3E
cell projection organization 0030030	12	1904	GMNC,IL1RAPL1,DOK5,ABL2,MAP2,TRPC6,MTSS1,NGFR,NR4A3,SHTN1,IL6,SEMA3E
biological adhesion 0022610	11	1578	IL1RAPL1,PTPN2,ZBTB16,ABL2,INHBB,MTSS1,NR4A3,CDH19,MMP12,IL6,SEMA3E

neuron differentiation 0030182	11	1639	IL1RAPL1,HDAC9,DOK5,ABL2,MAP2,TRPC6,NGFR,NR4A3,SHTN1,IL6,SEMA3E
tissue morphogenesis 0048729	10	874	SHROOM3,ABL2,FOXQ1,MTSS1,NGFR,NR4A3,CITED1,MMP12,IL6,SEMA3E
neuron projection development 0031175	**10**	**1197**	**IL1RAPL1,DOK5,ABL2,MAP2,TRPC6,NGFR,NR4A3,SHTN1,IL6,SEMA3E**
neuron development 0048666	**10**	**1358**	**IL1RAPL1,DOK5,ABL2,MAP2,TRPC6,NGFR,NR4A3,SHTN1,IL6,SEMA3E**
cell morphogenesis involved in neuron differentiation 0048667	**9**	**715**	**IL1RAPL1,DOK5,ABL2,MAP2,TRPC6,NGFR,NR4A3,SHTN1,SEMA3E**

neuron projection morphogenesis 0048812	9	770	IL1RAPL1,DOK5,ABL2,MAP2,TRPC6,NGFR,NR4A3,SHTN1,SEMA3E
plasma membrane bounded cell projection morphogenesis 0120039	9	785	IL1RAPL1,DOK5,ABL2,MAP2,TRPC6,NGFR,NR4A3,SHTN1,SEMA3E
cell projection morphogenesis 0048858	9	790	IL1RAPL1,DOK5,ABL2,MAP2,TRPC6,NGFR,NR4A3,SHTN1,SEMA3E
regulation of neuron projection development 0010975	**8**	**558**	**IL1RAPL1,ABL2,MAP2,TRPC6,NGFR,SHTN1,IL6,SEMA3E**
regulation of cell projection organization	8	800	IL1RAPL1,ABL2,MAP2,TRPC6,NGFR,SHTN1,IL6,SEMA3E

0031344			
regulation of nervous system development 0051960	7	548	IL1RAPL1,MAP2,TRPC6,NGFR,SHTN1,IL6,SEMA3E
actin cytoskeleton organization 0030036	7	768	SHROOM3,ABL2,PDLIM3,MTSS1,SHTN1,CNN1,SEMA3E
Axonogenesis 0007409	6	552	DOK5,MAP2,NGFR,NR4A3,SHTN1,SEMA3E
dendrite development 0016358	5	310	IL1RAPL1,ABL2,MAP2,TRPC6,NGFR
dendrite morphogenesis 0048813	4	186	IL1RAPL1,ABL2,MAP2,TRPC6
regulation of axonogenesis 0050770	4	193	MAP2,NGFR,SHTN1,SEMA3E

4.4 Validating Genes Identified in ET-1 Differential Expression

I wanted to further validate the genes that we identified through GO analysis. I rereferred back to the data set described in Chapter 2, the transcriptome of cells isolated from an intact epidermis. In Table 10, I have listed each of the genes included in the pathways in Table 9, and cross referenced it to the *in-situ* transcriptome of melanocytes. All but two of the genes were expressed *in situ*, which provides further evidence that the genes play a role in melanocyte biology. After validating that these genes are expressed *in-situ* by transcriptomic analysis, we wanted to use a complementary method to further validate the expression results of two of the genes. We selected NGFR and MAP2 for immunofluorescent investigation, because of the availability of well-documented antibodies against the corresponding proteins of these two genes. We were also particularly interested in each of these genes for reasons that are discussed below. We cross-referenced the genes of interest identified through GO analysis in Table 9 to the *in-situ* transcriptome created in Chapter 3. All but two of the genes of interest were expressed in *in-situ* melanocytes.

Table 11 Validation of *In-Situ* Expression of Subset of Genes Identified in ET-1 Differential Expression

Gene Name	Description	Expressed In-Situ
MAP2	microtubule associated protein 2	Yes
NGFR	nerve growth factor receptor	Yes
SHTN1	shootin-1	Yes
SEMA3E	semaphorin 3E	Yes
ILRAPL1	interleukin 1 receptor accessory protein like 1	No
ABL2	ABL proto-oncogene 2, non-receptor tyrosine kinase	Yes
TRPC6	transient receptor potential cation channel subfamily C member 6	No
DOK5	docking protein 5	Yes
NR4A3	nuclear receptor subfamily 4 group A member 3	Yes
SHROOM3	shroom family member 3	Yes
PDLIM3	PDZ and LIM domain 3	Yes
MTSS1	MTSS I-BAR domain containing 1	Yes
CNN1	calponin 1	Yes

4.4.1 NGFR

As discussed in section 1.10, NGF signaling has been implicated as important for melanocyte dendritogenesis and melanosome transfer, and it has previously been reported that melanocytes express the NGFR, which I confirmed through RNA sequencing of melanocytes from an intact epidermis in Chapter 2.

We performed immunofluorescence on melanocytes grown in monoculture treated with 10 nM ET-1 for 5 hours, treated with a vehicle control, or else grown in co-culture with keratinocytes for 72 hours (Figure 19). For time points selected, At 5 hours was the point when the greatest effect of ET-1 treatment was seen by transcriptomic analysis, while 72 hours was the point at which a melanocyte-keratinocyte co-culture is established well enough to allow for maximal observable calcium transients (Belote and Simon, 2020). NGFR labeling was visible on cells in

all three conditions. However, the morphology of the melanocytes in each condition varied so dramatically that quantitative comparison was difficult. The ET-1 deprived melanocytes did not appear healthy and were somewhat balled-up with no projections (Figure 20 top row). The melanocytes treated with ET-1 for 5 hours were more spread out (Figure 20 middle row). The melanocytes culture with keratinocytes for 72 hours had their characteristic dendritic morphology and had clear NGFR labeling on the cell periphery. Once again, there was no melanocyte marker co-staining in these conditions because of antibody species incompatibility. However, the morphology of melanocytes and keratinocytes is well differentiated from each other, and it is clear based on morphology that the cells whose membranes are labeled with NGFR are melanocytes. Due to the difference in the morphology of the cells in each condition as well as the differential localization of NGFR in the samples, I was not able to quantify these images to confirm an increase in protein level consistent with the increase in RNA level observed by RNA-seq. NGF signaling had previously been implicated in melanocyte biology, and the expression of NGFR by melanocytes was previously observed. This is the first evidence that NGFR expression is upregulated directly in response to ET-1, demonstrating how keratinocytes are able to regulate melanocyte dendritogenesis at a molecular level.

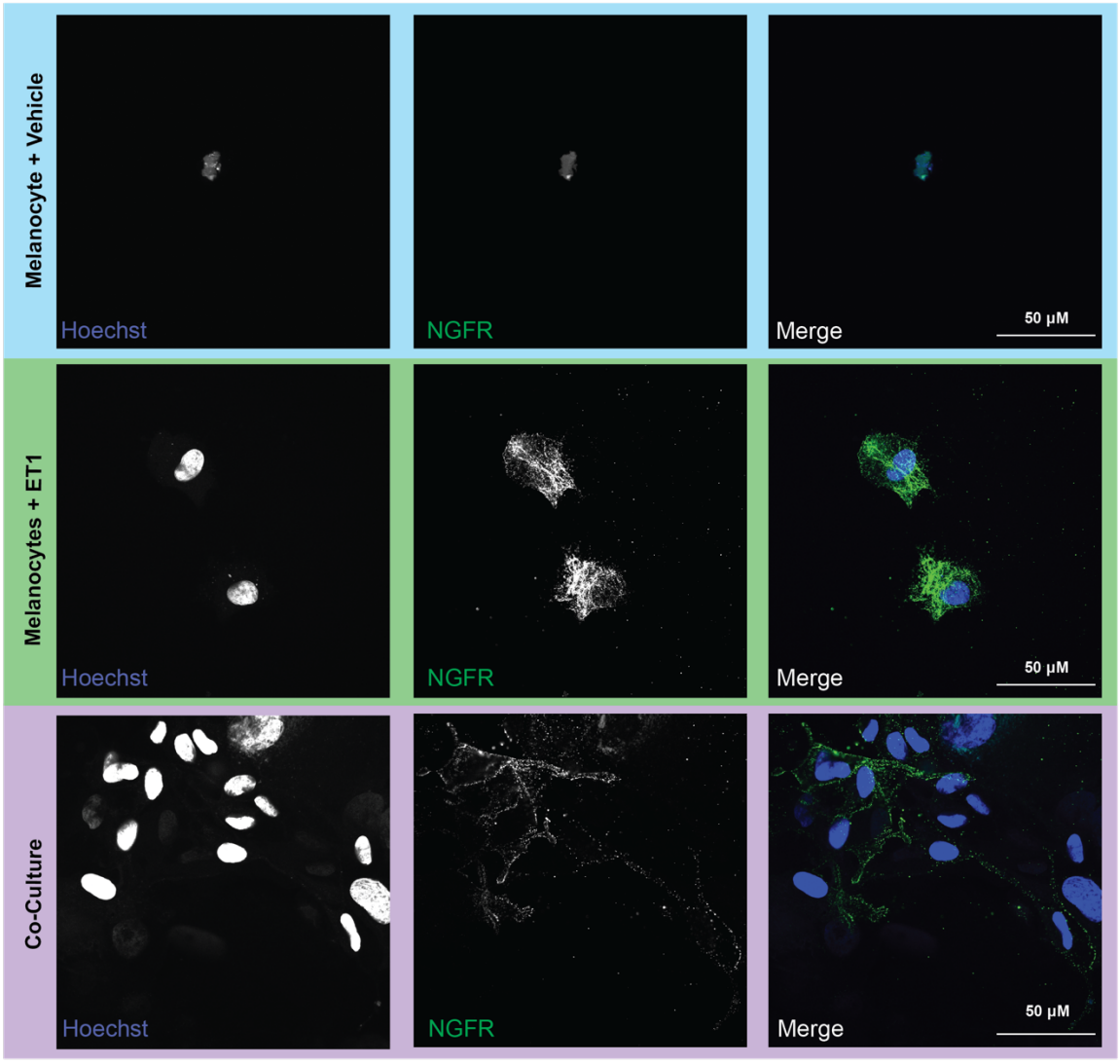

Figure 19 Immunofluorescence of NGFR in Melanocyte Monoculture and Melanocyte-Keratinocyte Co-Culture

Melanocytes were grown in three conditions, and subjected to immunofluorescence with an anti-NGFR antibody, and labeled with Hoechst nuclear stain. The top row shows melanocytes were treated with vehicle, the middle melanocytes treated with 10 nM ET-1 for 5 hours, and the bottom row melanocytes and keratinocytes grown in co-culture for 72 hours.

4.4.2 MAP2

I was also particularly interested in further investigation into microtubule associated protein 2 (MAP2). MAP2 is primarily expressed in neuronal cells, and serves to both stabilize microtubules and crosslink microtubules with actin (Mohan and John, 2015). GO analysis identified cytoskeleton and dendritogenesis as two broad pathways of interest that are upregulated in melanocytes by ET-1, and MAP2 was a gene involved in both processes. We performed immunofluorescence on MAP2 in skin cross sections, and co-stained with a cocktail of two melanocyte labeling antibodies (TRP1 and C-Kit) to provide more thorough labeling of melanocytes (Figure 20). We found that virtually all epidermal cells express MAP2, including melanocytes and keratinocytes. The *in situ* transcriptomes that I assembled in Chapter 2 confirmed that both basal and suprabasal keratinocytes express MAP2.

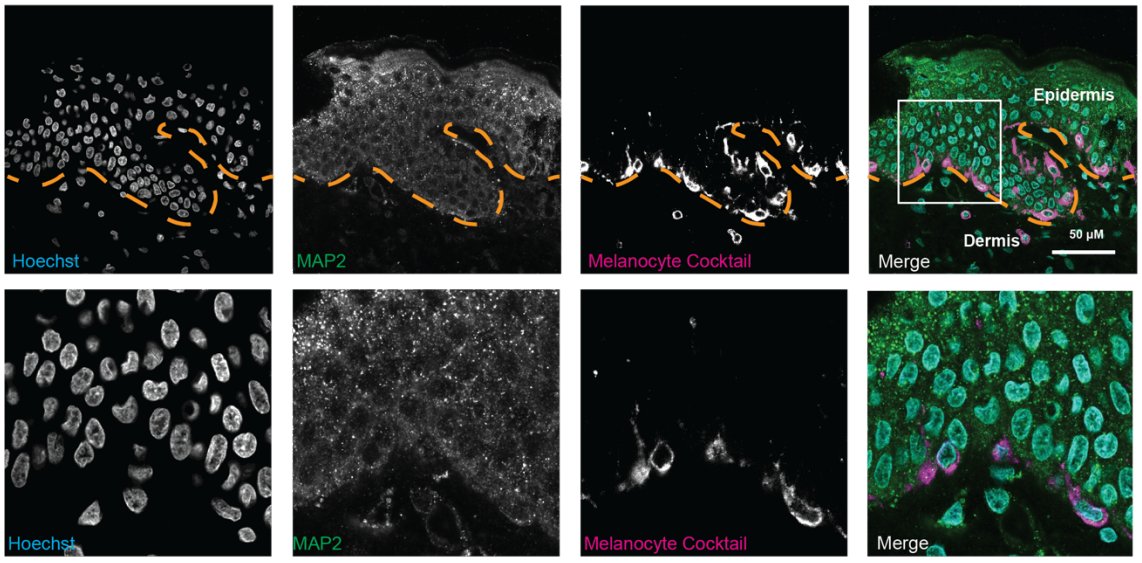

Figure 20 Immunofluorescence of MAP2 *In Situ*

Human epidermal tissue was fixed, cryopreserved, and embedded in OCT. 10 micron slices were prepared on a cryostat, and the tissue mounted on a glass slide and subjected to immunofluorescent staining with an anti-MAP2 antibody, melanocyte cocktail, a combination of two melanocyte labeling antibodies (TRP1 and C-Kit)l, and Hoechst nuclear stain. Images were taken on an Olympus confocal microscope.

In order to validate the upregulation of MAP2 expression in melanocytes in response to ET-1 signaling, we performed immunofluorescence on melanocytes that were treated with ET-1 for 5 hours, or a vehicle control (Figure 20A). We saw an increase in the brightness of the MAP2 staining in melanocytes, although it was not statistically significant upon quantification (Figure 20B). Quantification was performed by drawing a region of interest (ROI) within the cell and measuring the fluorescence mean intensities within that region. Three cells were selected at random from each condition, and the means of the intracellular fluorescence mean intensities were compared by a paired t-test.

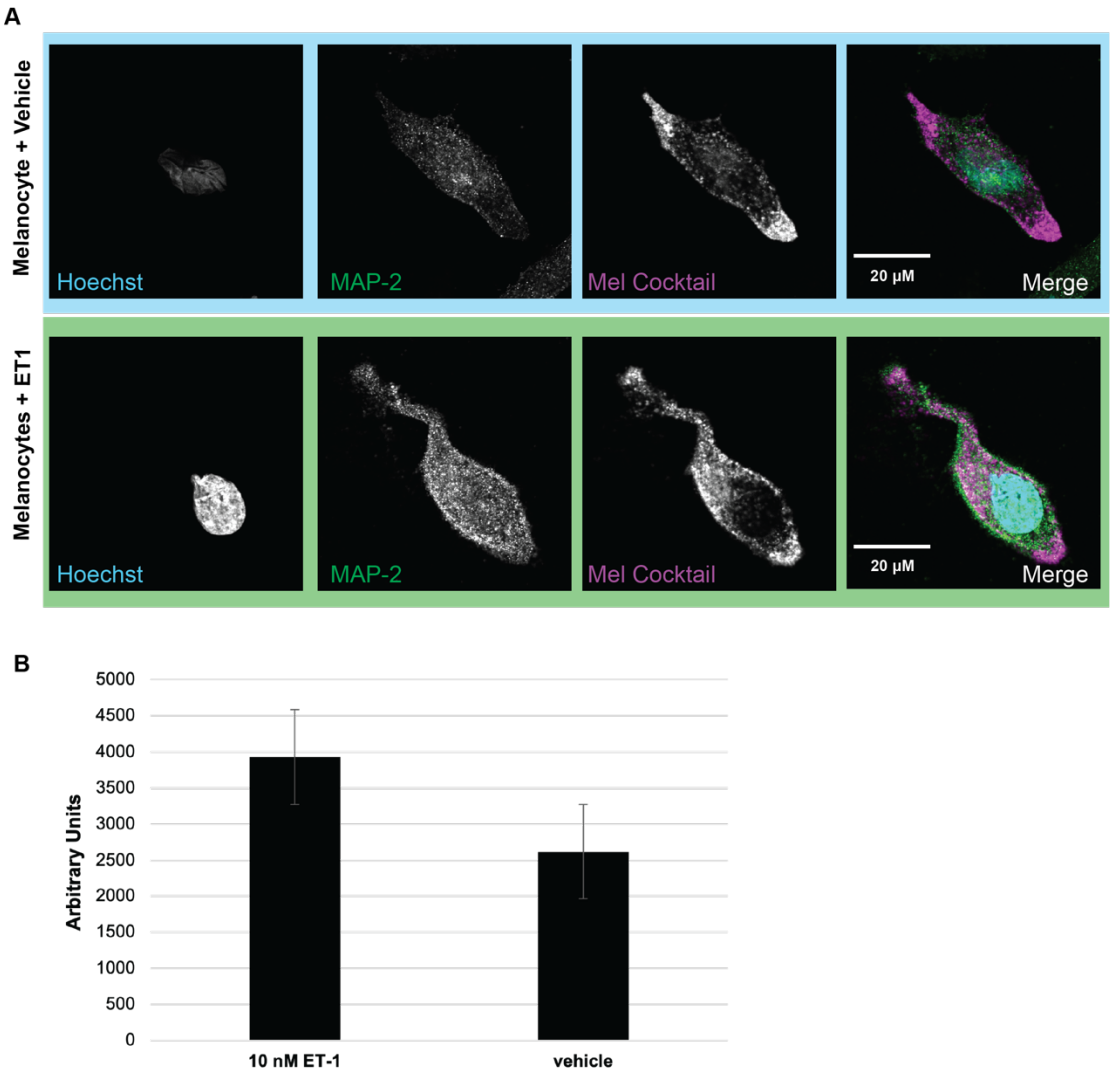

Figure 21 Immunofluorescence of MAP-2 in Melanocytes

A) Melanocytes were treated with either a vehicle control, or 10 nM ET-1 for 5 hours, and subjected to immunofluorescence with a melanocyte cocktail and an anti-MAP2 antibody, and labeled Hoechst nuclear stain. B) Quantification was performed by drawing a round region of interest (ROI) within a cell and measuring the mean fluorescence within that region. Three cells were selected at random from each condition, and the means were compared by a paired t-test (P= .13). Error bars indicate standard error.

4.4.3 Actin Structure

Melanocytes change their cell morphology when treated with ET-1 and also when grown in culture with keratinocytes. These differences have been previously reported, and are also recapitulated as shown in the images presented here (Figure 20 being a clear example). It is important to note that the 5-hour ET-1 treatments used for these experiments, although sufficient to induce changes in gene expression, are much shorter than the 48 hours used in published studies on melanocyte dendritogenesis . Although we observe some changes in melanocyte morphology after 5 hours, the cells do not make long projections in that time period.

The GO analysis drew our attention to proteins involved in cytoskeletal structure, including MAP2. The cytoskeleton, along with the proteins that regulate it and interact with it, give cells their shape (Wickstead and Gull, 2011). For this reason, I wanted to look directly at the actin structure of melanocytes, to determine if there were any observable alterations in actin structure in response to ET-1, or to co-culturing with keratinocytes. I fixed the cells, performed immunofluorescence with the melanocyte cocktail, and labeled with phalloidin-488, which binds preferentially to F-actin. Two characteristic images for each condition are shown in Figure 22. I observed an increase in bright actin puncta in the ET-1 treated cells, chiefly near the cell peripheries (Figure 22B&D). In the vehicle control cells, the phalloidin staining was more diffuse, with fewer bright puncta (Figure 22A&D). The phalloidin staining in the melanocytes in co-culture were also more punctate (Figure 22C&D).

It is difficult to quantitatively compare the staining in the co-cultured cells to monocultured cells. The co-cultures are confluent, and are not entirely restricted to a

monolayer, with some differentiating keratinocytes resting on top of the other cells. For this reason, antibodies and stains do not evenly permeate to the bottom layer of the culture. The melanocyte cocktail staining in the co-culture is dimmer, suggesting that comparing the brightness of phalloidin staining from the co-culture to the monoculture conditions is not appropriate. Although it is difficult to quantitate by how much the actin network is changed, I observed alterations.

These results will require further confirmation by replicates of this experiment. Additionally, extending the time-course of ET-1 treatment up to 48 hours will be informative. The microscopy experiments described above were performed after 5 hours of ET-1 treatment, but the published changes in dendritic architecture are more pronounced by 48 hours. In order to work around the difficulty of comparing phalloidin staining between co-cultures and monocultures due to permeance issues, it will also be advantageous to use a different method of visualizing F-actin. For example, an actin chromobody (a camelid-derived, GFP-fused nanobody) can be expressed in melanocytes (Melak et al., 2017), which will allow for a cleaner comparison of the actin-structure between monocultured and co-cultured melanocytes. Because only the melanocytes will express the chromobody, this improves the specificity of the signal over the phalloidin staining which also stains the F-actin of neighboring keratinocytes. This also circumvents the cell-permeance issue, because the actin label comes from within the cell. Finally, it will allow live-cell imaging of actin, rather than relying on fixed cells, avoiding the possibility of fixation artifacts and also enabling the actin structure of individual cells to be monitored after

the addition of ET-1. Visualizing actin changes in live cells after ET-1 treatment would be compelling evidence that ET-1 does induce actin rearrangements.

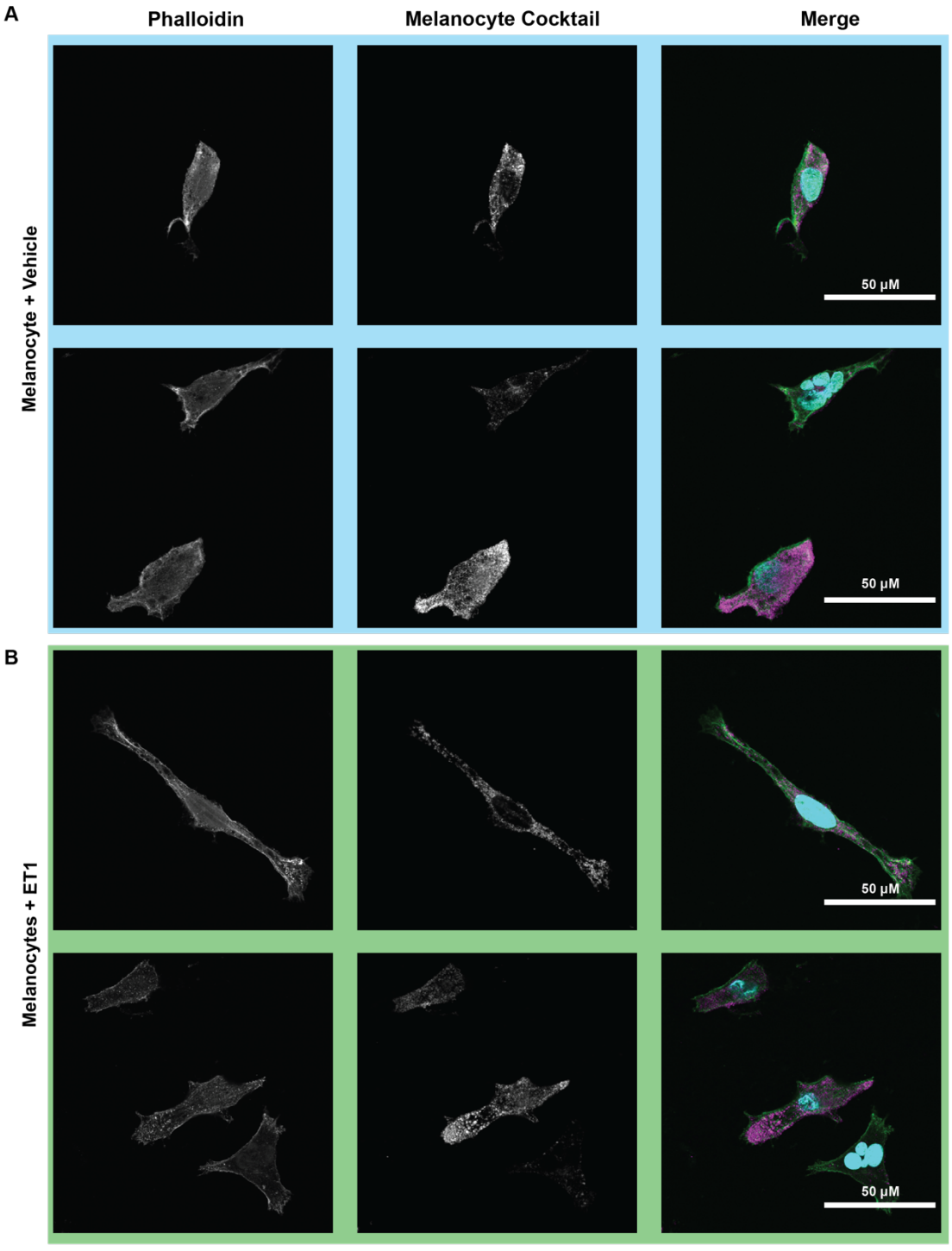
A
Phalloidin
Melanocyte Cocktail
Merge
Melanocyte + Vehicle
50 µM
50 µM
B
Melanocytes + ET1
50 µM
50 µM

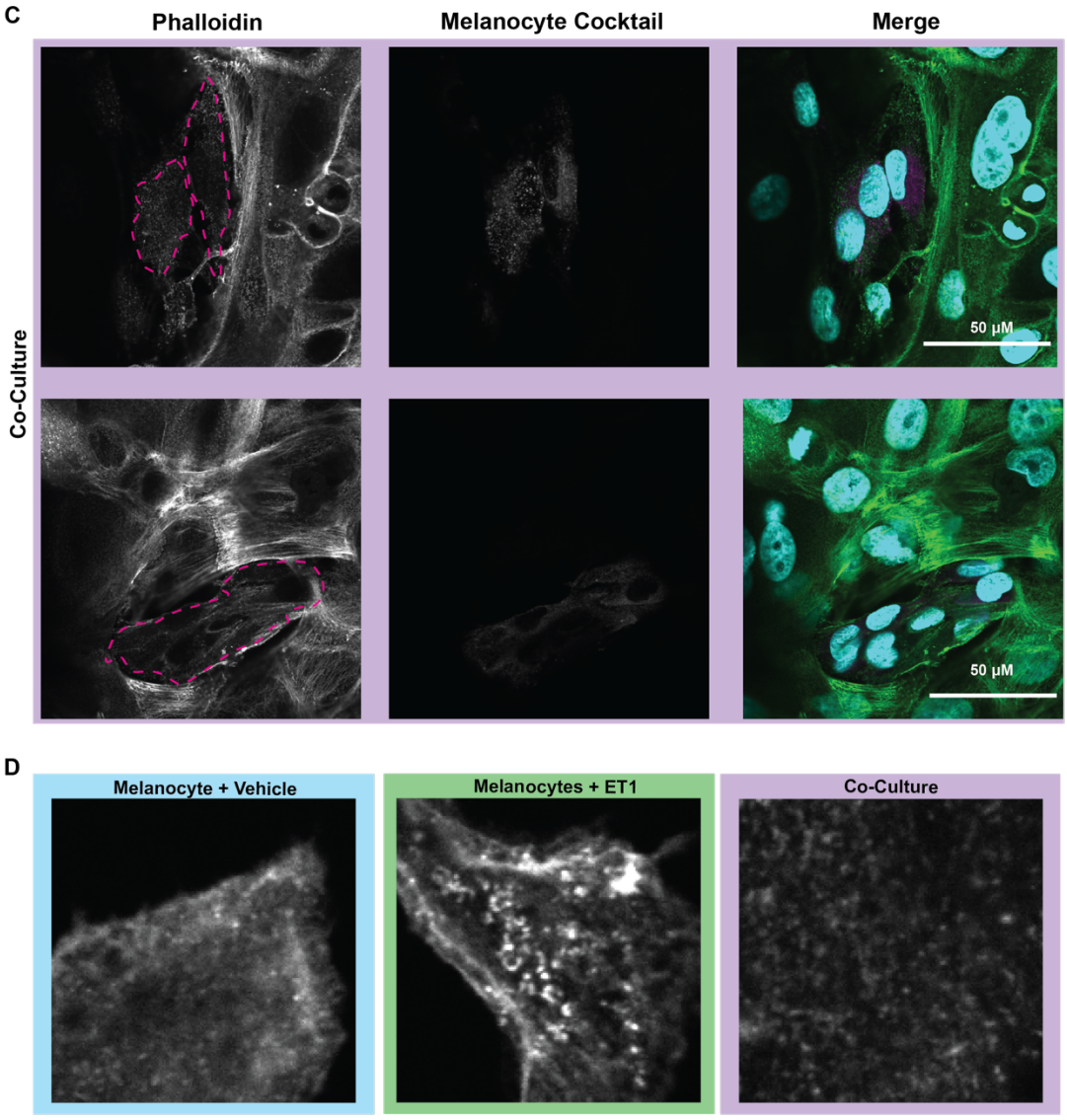

Figure 22 Phalloidin Staining of melanocytes in monoculture and co-culture

Melanocytes were grown in three conditions, and subjected to immunofluorescence with a melanocyte cocktail, and labeled with phalloidin-488 and Hoechst nuclear stain. A) Melanocytes were treated with vehicle. B) Melanocytes were treated with 10 nM ET-1 for 5 hours. C) Melanocytes and keratinocytes grown in co-culture for 72 hours. Cell outlines were traced in the melanocyte cocktail condition and superimposed on the phalloidin condition. D) Close up views (same magnification) of actin structure in melanocytes.

4.5 Conclusions

I have shown that in response to ET-1 treatment, melanocytes upregulate a specific population of genes. Through GO analysis, I have shown that a large number of these genes are involved in cytoskeleton regulating functions, and in dendritogenic pathways. I confirmed that these genes are expressed *in-situ* through transcriptomic analysis—and microscopy, in the case of MAP2 and NGFR—and further validated these genes through immunofluorescence of monocultured and co-cultured melanocytes. Finally, we observed the F-actin structure of melanocytes treated with ET-1, and grown in monoculture and co-culture, and observed a novel change in the arrangement of melanocyte actin, which will require further investigation and validation.

CHAPTER 5: CHARACTERIZATION OF PRIMARY KERATINOCYTE PHAGOSOMES

Keratinocytes are phagocytically active cells, as are several other non-immune cells discussed in the introduction. However, the study of phagocytosis has primarily been relegated to cells of the immune system, in particular macrophages and dendritic cells. In this chapter, I describe work I have done to characterize the protein content of keratinocyte phagosomes, in order to better understand phagocytosis in a primary epithelial cell.

In addition to wanting to contribute to our knowledge of how phagocytosis works in non-immune cells, I also wanted to better understand keratinocyte phagocytosis for the purpose of potentially learning more about the melanosome transfer process. As discussed in Section 1.3, melanosome transfer is a process that likely depends on the keratinocyte phagocytosing melanosomes produced by melanocytes. The three models of melanosome transfer for which there is the most evidence have, as a key step, a keratinocyte internalizing a particle of at least .5 microns. In addition to keratinocytes likely performing phagocytosis during melanosome transfer events, keratinocytes also phagocytose cell debris during the hair cycle in mice (Mesa et al., 2015).

In this chapter, I characterize the proteome of keratinocyte phagosomes following the uptake of a generic package. The data set allows for comparison to phagosomes from other cell types. It was also initially intended to serve as a comparison for proteomic analysis of keratinocyte phagosomes containing different, biologically specific, targets. Although these experiments were not able to be

completed, this generic package control serves as a complete data set in its own right.

5.1 Phagocytosis of Microspheres

I took advantage of a classic method used extensively to characterize the phagosomal proteome of immune cells: phagocytosis of a polystyrene bead, and subsequent fractionation and proteomic analysis of the proteins surrounding the bead (Desjardins et al., 1994). To my knowledge, no published results exist of this experiment performed on an epithelial cell. The scheme of the experiment is as follows: the phagocyte initiates internalization of the bead and envelopes it, forming a phagosomal membrane around the bead. The bead is internalized and undergoes steps of phagosome maturation**.** This experiment has several theoretical advantages. By introducing an exogenous phagosomal target, one can control the timing of the initiation of phagocytosis. If one performs an initial incubation of the cells with beads on ice, it is possible to roughly synchronize phagosomes by releasing them from this pause synchronously. Another benefit of this experimental design is that it is relatively straight-forward to fractionate bead-containing phagosomes. The phagosomes are of a consistent size and density and can be isolated through flotation fractionation on a sucrose gradient.

A potentially important caveat in interpreting results from these experiments is that the proteome of the bead phagosome does not necessarily reflect the proteome of the endogenous target of the phagocyte. One way of addressing this is to coat the bead with a ligand that is native to the substrate of the phagocyte. However, phagocytic cells are sensitive to the size and density of the target, and so even a

ligand-coated bead does not accurately recapitulate all aspects of target-mediated phagocytosis (Baranov et al., 2020). Despite these caveats, this method has proved useful and has been one of the main techniques that has grounded our understanding of phagocytosis.

5.2 Establishing Bead Phagocytosis in Keratinocytes

Although the fact that keratinocytes phagocytose latex and plastic beads has been previous reported (Wolff and Konrad, 1972), I first tested that this held true in my hands. I incubated primary keratinocytes with .96 μm FlashRed beads (Bangs Laboratories) for one hour. Melanosomes are approximately .5 μm, and I would have ideally used bead of the same size for this experiment. However, this was the closest size of fluorescent bead available to me. After one-hour, extraneous beads were removed and the cells were fixed and stained with phalloidin and Hoechst stains, to allow for visualization of the actin structure and nucleus of the cells. Beads appeared within the periphery of the cells when viewed by epifluorescence (Figure 23) I observed that beads appeared to accumulate in the perinuclear area of the cell. However, only viewing the cells in two dimensions did not rule out the possibility that the beads were lying on top of the cells rather than being internalized. For this reason, I epifluorescently imaged the cells using z-stacks that started below and ended above the plasma membrane of the cell. I then deconvolved these images, which allowed for a clear assessment of the location of the beads relative to the cell body. By viewing cross sections of the deconvolved cells, it was clear that the majority of beads were located within the cells (Figure 23).

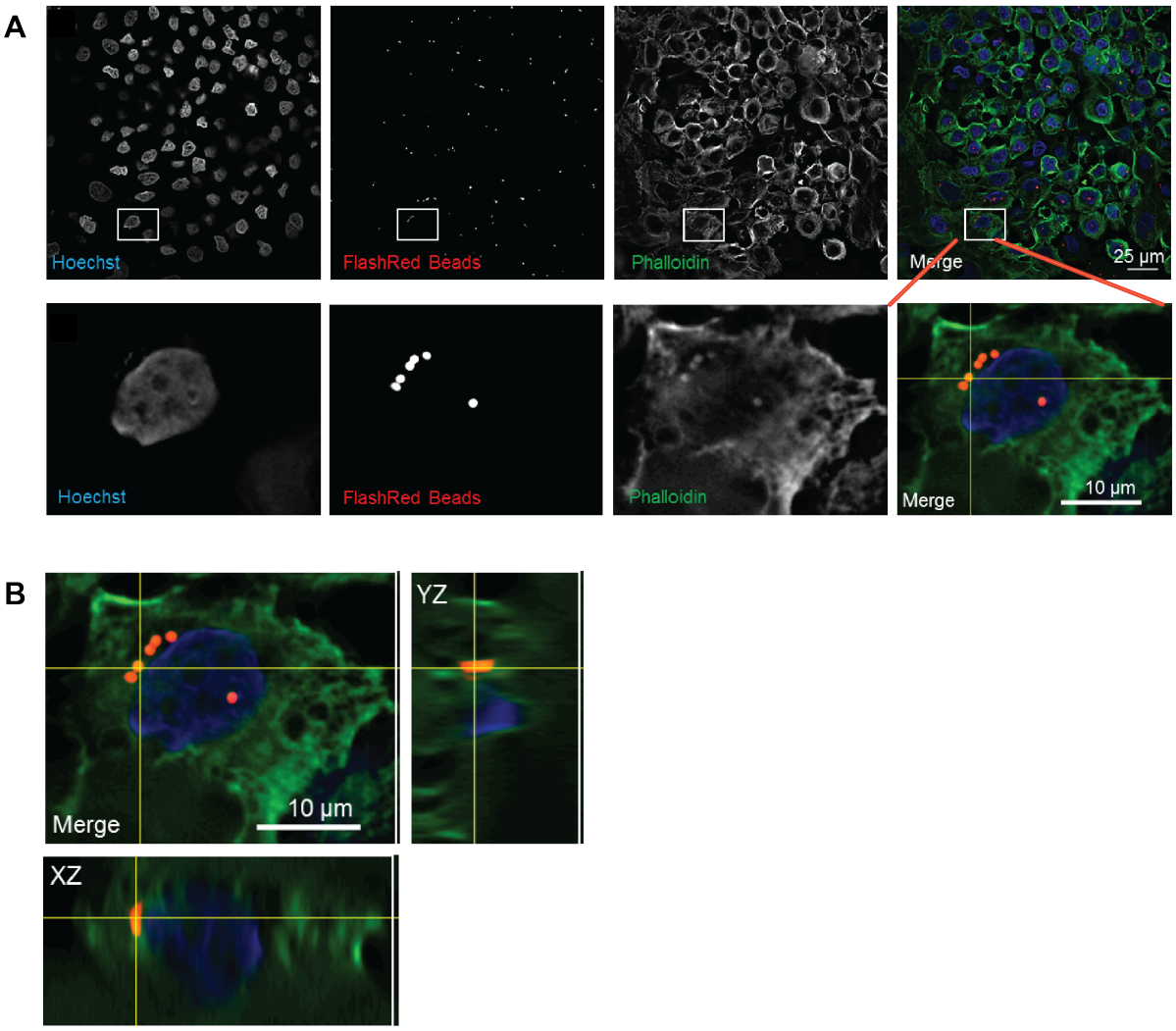

Figure 23 Primary Keratinocytes Internalize Microspheres.

A) Representative image of primary human keratinocytes after an hour long incubation with FlashRed beads. Cells were labeled with Phalloidin-488 and Hoechst stain. B) Visualization of the z- dimension, showing that the microsphere is surrounded by actin on all sides, and thus resides within the cell, not on top of it. Images acquired on Olympus upright microscope with a 63x objective, deconvolved using Autoquant software.

The next issue to address was whether cell density and media composition affected internalization of beads, in order to determine the optimal conditions for subsequent experiments. I cultured cells at two different densities, a sparser condition of approximately 60% confluency, and a denser condition at 100% confluency (Figure 24). For the denser condition, I also cultured the cells in keratinocyte growth media supplemented to a calcium concentration of 1.06 mM, which closer reflects physiological conditions and allows for calcium-dependent intercellular interactions and differentiation of keratinocytes (Belote and Simon, 2020). Each of these conditions was further divided into a 2 and 4 hour-long bead incubation. I observed that the sparser cells internalized more beads, and used this to inform the conditions of the subsequent proteomic experiments. I suspect that this is due to the fact that the dense cells do not have as much exposed plasma membrane available, because they are pressed up against each other. In particular, the “sides” of the cells are not available for phagocytosis because they are contacting other keratinocytes.

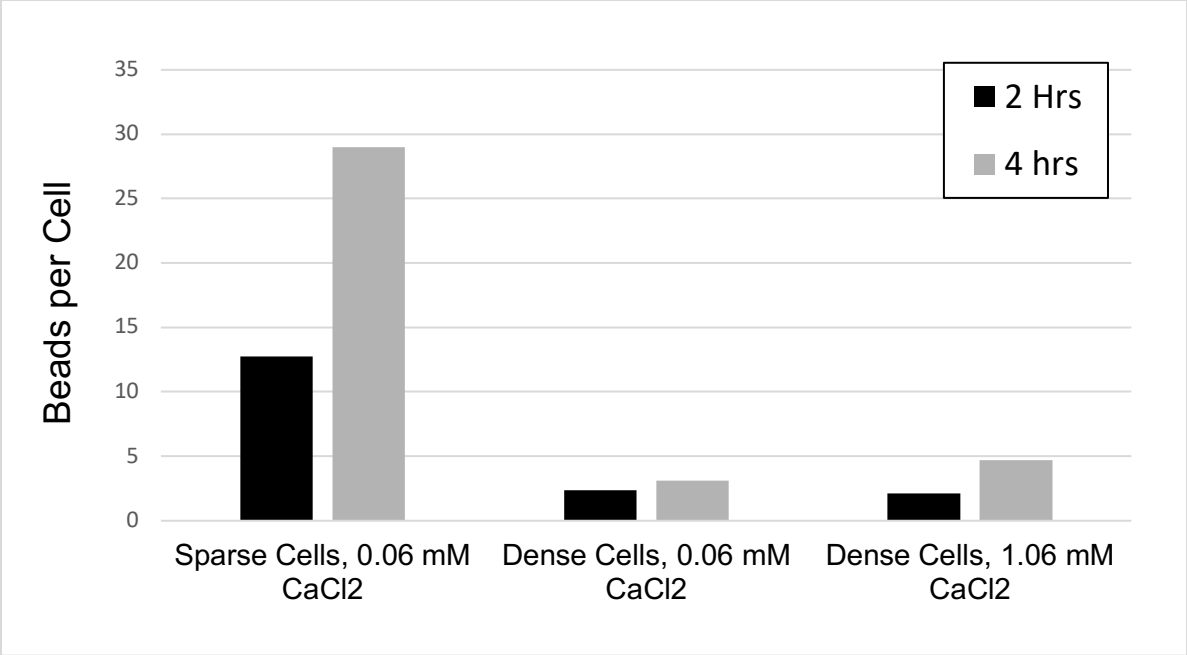

Figure 24. Number of Beads Internalized by Primary Keratinocytes Under Different Conditions.

Primary keratinocytes were treated with beads for two or four hours. Cells were plated at two densities, and the denser cells were grown at both 0.06 mM $CaCl_2$ or 1.06 mM $CaCl_2$.

5.3 Fractionation of Bead Phagosomes in Keratinocytes.

After establishing some experimental parameters via microscopy as described above, we moved our attention to establishing a phagosome preparation that I could use for proteomic analysis (Figure 25). Keratinocytes are highly adherent cells, and do not survive even the most delicate of scraping off of a culture dish. For this reason, I removed the cells from the dish with trypsinization. After trypsinization, the cells were homogenized using nitrogen cavitation. Nitrogen cavitation works by first dissolving nitrogen in the cytoplasm of cells under high pressure. After the cells

are equilibrated, the pressure is rapidly returned to atmospheric levels, causing expansion of nitrogen bubbles in the cytoplasm that cause rupturing of the plasma membrane. This technique has advantages over mechanical homogenization methods; it reduces the risk of accidentally damaging the membranes of subcellular compartments and introduces no heat (Simpson, 2010). I removed the nuclei with centrifugation and separated the phagosomes by ultracentrifugation on a sucrose gradient. The bead phagosomes float above cell debris and other organelles and reside at the interface of the 10% and 25% sucrose layers. I removed them carefully with a Pasteur pipette. The bead-containing phagosomes were solubilized, and the proteins analyzed by mass spectrometry. More details of this sample preparation and mass spectrometric analysis are included in Chapter 7.

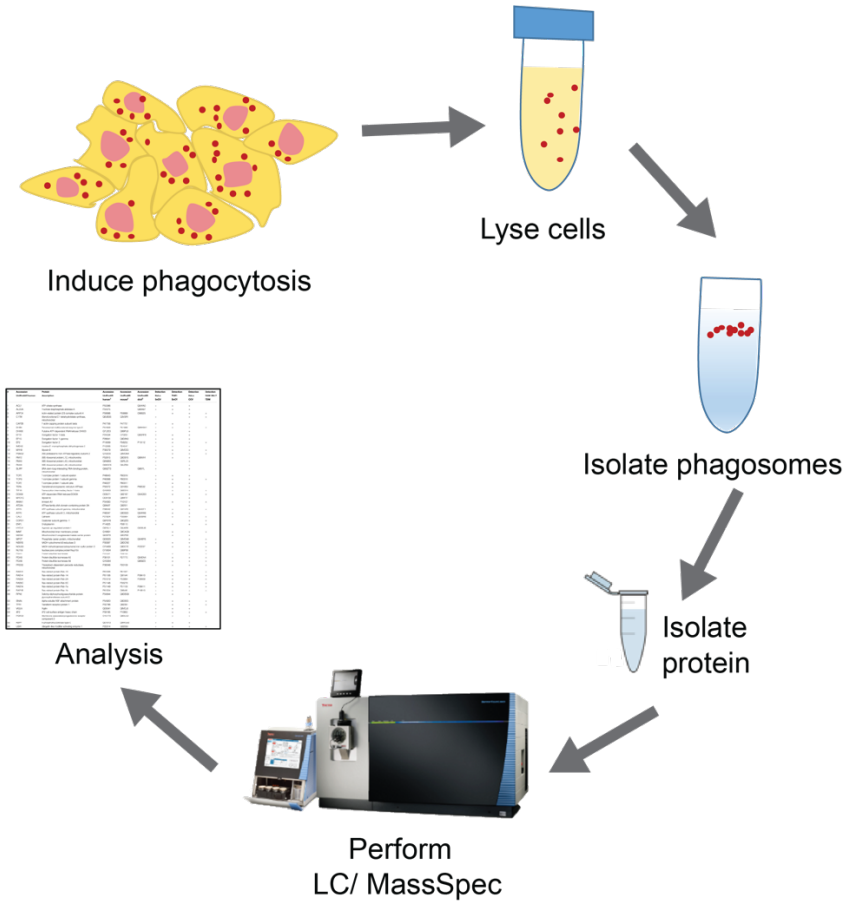

Figure 25 Schematic of Phagosome Fractionation and Mass Spectrometry

Cells were incubated with polystyrene beads. The cells were lysed by nitrogen cavitation, phagosomes were isolated via sucrose fractionation, and their proteome analyzed by LC/MassSpec.

5.4 Validation of Fractionation by Comparison to Sodium Azide Treatment

To confirm that the protein fraction we were analyzing was truly an internalized phagosomal fraction, we compared two conditions, one where substantial internalization of bead phagosomes would not occur. For this non-internalization condition, cells were treated with 0.1% sodium azide to ATP-

dependent halt cellular processes. Sodium azide treatment causes a rapid depletion of intracellular ATP by inhibiting cytochrome oxidase, the final enzyme of the electron transport chain (Tsubaki, 1993). Cells were also placed on ice in a cold room, to further retard internalization. The same cell lysis and fractionation procedures were performed on the non-internalization control as on the experimental condition. In this condition, we expect that the number of beads that are internalized through phagocytosis are greatly reduced, although there is still the possibility of beads sticking to the dish and the surface of cells.

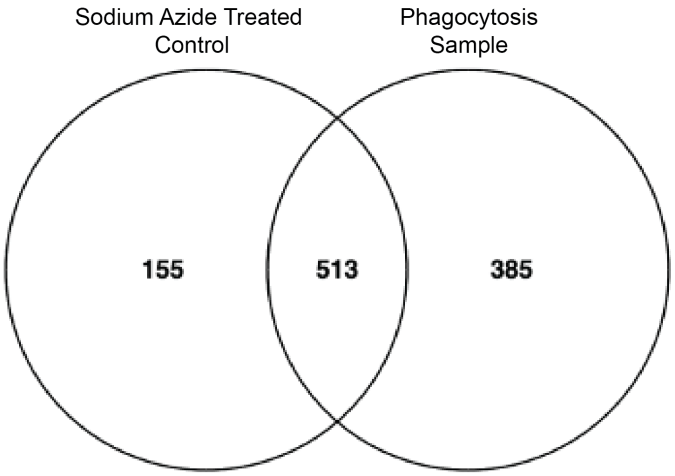

Figure 26 Venn Diagram of Proteins Present in Phagocytosis Sample Compared to Non-Internalization Control

Comparison of proteins present in the sodium azide treated control compared to the phagocytosis sample. There are 385 distinct proteins found in the sample compared to the non-internalization control, 513 overlapping proteins, and 155 distinct proteins found in the sodium azide treated control. Comparison is of proteins for which a peptide spectrum match was found, and does not compare relative levels of proteins.

I found that these protein content of these two conditions were not the same as each other, which indicates that the proteome we are analyzing in the experimental condition is the result of phagocytic internalization (Figure 26). However, there is a substantial overlap in proteins present in the two conditions. I consider this preparation to be an “enrichment” of phagosomes, not an ideal purification. It is possible that in the process of cell lysis, membranes or proteins stuck to the naked beads in the non-internalization control, and that this is the source of proteins present. In the phagocytosis experimental condition compared to the non-internalization control, there was an increase in the amount of Lamp1, CD63, EEA1, Rab5a and Rab7 (Figure 27). We specifically checked the levels of these proteins, as they are proteins that are expected to be present in a phago-lysosomal fraction, as seen in Figure 4 of Chapter 1.

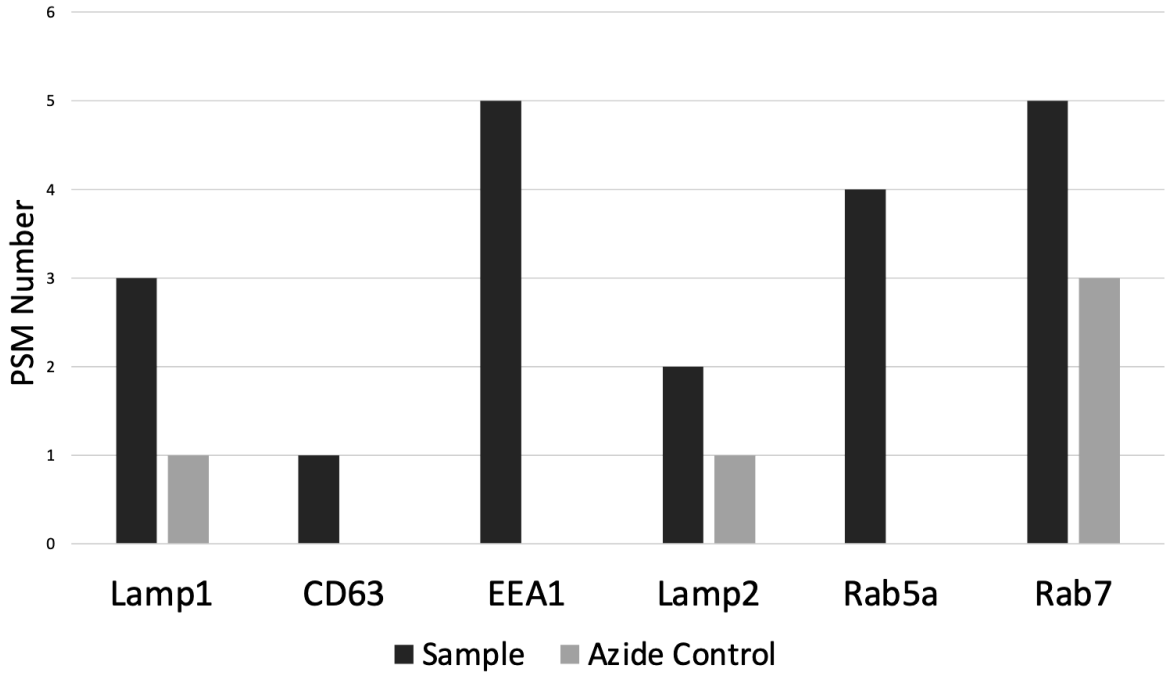

Figure 27 Comparison of Specific Proteins in Phagocytosis Sample and Non-Internalization Control

Comparison of peptide spectrum match (PSM) numbers of specific proteins of interest in the phagocytosis sample compared to the sodium azide treated control sample.

5.5 Analysis of Keratinocyte Phagosome Proteome

Next, we analyzed the proteome of these keratinocyte phagosomes. For this experiment, samples from a single experiment were grown in triplicate. Through mass spectrometry, 2065 proteins were identified to have at least one peptide spectrum match in the phagosomal fraction. I performed network analysis of the proteins present by STRING analysis, and formatted the resulting diagrams using

Cytoscape (Shannon et al., 2003; Szklarczyk et al., 2019). Through unbiased pathway analysis, I identified proteins that have been previously characterized to be present in phagosomes and endosomes. Figure 28 shows the network of proteins identified that are previously characterized to be associated with endosomal compartments. These proteins include Rab7a, Lamp1, Annexins A1, A2, A6 and A8.

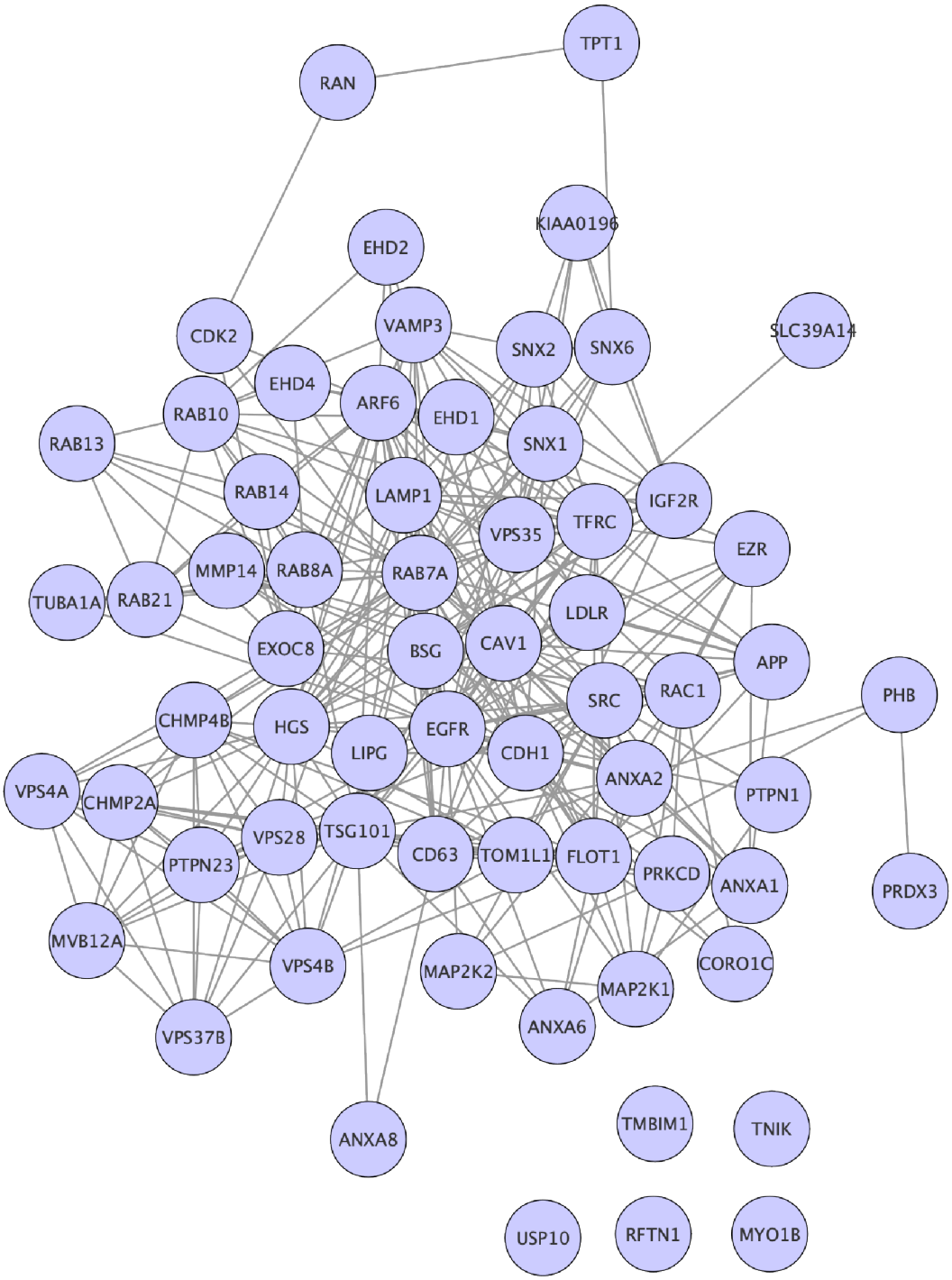

Figure 28 String Plot of Endosomal and Phagosomal Proteins Present in Keratinocyte Phagosomes.

String analysis of endosomal and phagosomal proteins in the keratinocyte bead phagosome, visualized in Cytoscape.

The same pathway analysis also revealed lysosomal proteins that were present in the sample (Figure 29). This included LAMP1 and CD63. This indicates that keratinocyte phagosomes do undergo some sort of canonical lysosomal maturation, at least with this cargo. Keratinocytes are capable of phagocytosing polystyrene beads, and they do so in a manner that is similar to other phagocytes. This interpretation comes with the caveat that the phagosomes studied here contain carboxylated polystyrene beads, not melanosomes.

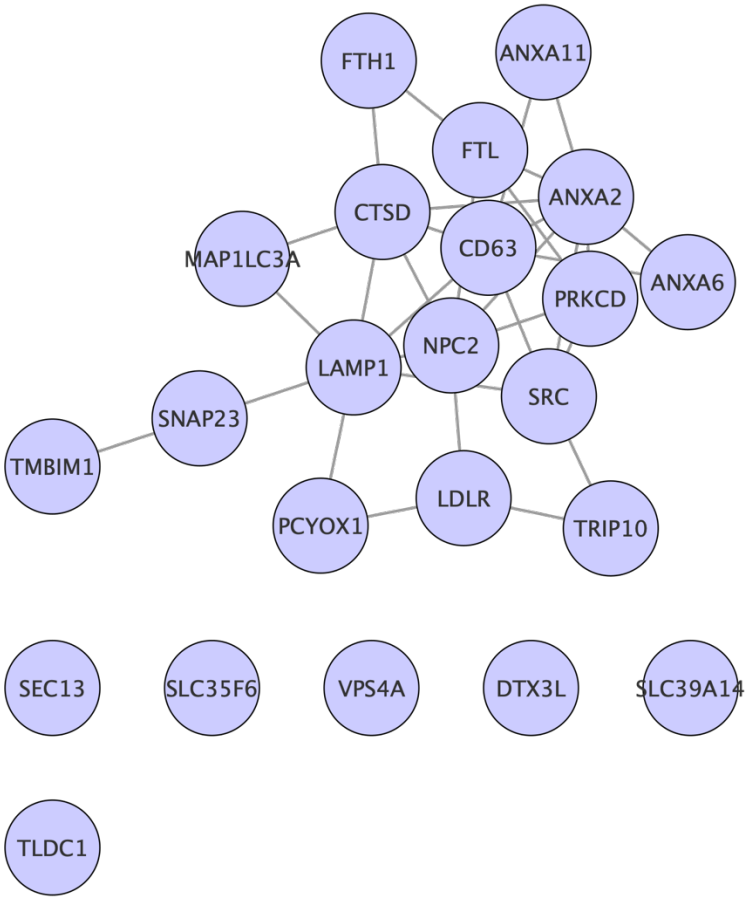

Figure 29 String Plot of Lysosomal Proteins Present in Keratinocyte Phagosomes.

String analysis of lysosomal proteins in the keratinocyte bead phagosome, visualized in Cytoscape.

5.6 Proximity Labeling as a Method of Studying Phagosomes

In order to identify keratinocyte proteins that are involved in the uptake of melanosomes, I designed an alternative approach to studying phagosome proteomes. This method was based not in fractionation but proximity labeling. I specifically used a BioID2-based approach, a method whereby a promiscuous biotin ligase is fused to a protein of interest (Roux et al., 2018). In the presence of biotin, this biotin ligase biotinylates proximal proteins, allowing for subsequent pull-down and mass-spectrometry based identification of protein targets. This approach has been successfully used by other groups to identify the proteome of difficult-to-fractionate organelles, as well as specific regions of the cell that are not spatially confined (Kim et al., 2016; Mehus et al., 2016; Roux et al., 2018).

I wanted to design a system whereby I could specifically label proteins on and in the keratinocyte that are involved in the uptake and processing of melanosome phagosomes. The location of the BioID enzyme for these experiments is contingent on which model of melanosome transfer the researcher is testing. I first designed a system based on the exocytosis-phagocytosis model for technical reasons, but the BioId enzyme can be placed in different locations to test what proteins are present when keratinocytes are fed melanosome-containing packages derived from melanocytes, in the manner of the shedding phagocytosis model. The concept is that the BioID enzyme is positioned on the outside of the phagocytic target. As these targets are phagocytosed by the keratinocyte, proteins on the plasma membrane of the keratinocyte that encounter the phagocytic target are biotinylated. As the phagosomes mature, other proteins that participate in the maturation of the

phagosomes will also be biotinylated, as long as they are in the lumen of the phagosome, or have a luminal domain. One can then affinity purify biotinylated proteins from the sample using streptavidin beads, and perform mass spectrometry to identify the biotinylated proteins.

I was not able to successfully trouble-shoot and validate this system in keratinocytes. My progress is included in Appendix I. Although this experiment did not yield clearly interpretable results for me, the concept of this experimental design could be transferred to other phagocytic systems.

5.7 Conclusions

I have shown that keratinocytes are capable of phagocytosing beads of a similar size to melanosomes through a classical phagocytic pathway. This experiment does not provide evidence about what method the keratinocyte uses to internalize melanosomes, but does provide insight into the character of keratinocyte phagosomes. I also designed a novel method of assaying the proteome of phagosomes that contain biologically relevant targets. This method will require further troubleshooting and validating, but may be of interest to other researchers studying different phagocytic systems.

CHAPTER 6: FUTURE DIRECTIONS AND IMPLICATIONS

Melanosome transfer is an important process that facilitates the protection of keratinocyte DNA from ultraviolet radiation. It is also a process that relies on coordinated actions by two types of cells—melanocytes manufacture and deliver melanosomes, and keratinocytes internalize and store them. Previous work has implicated certain molecules as important for signaling from keratinocyte to melanocyte (discussed in section 1.10), and my thesis work indicates that the presence of melanocytes causes transcriptomic changes in the keratinocytes. Furthermore, my thesis has explored how communication between these cell types affects them both on a cellular level. In Chapter 2, I characterized the transcriptome of melanocytes and keratinocytes from recently harvested, healthy skin, in order to establish a baseline for transcriptomic experiments on cultured cells. In Chapter 3, I determined what keratinocyte genes changed expression levels when keratinocytes are grown with and without melanocytes. In Chapter 4, I studied the effect of ET-1 signaling on melanocyte gene expression and found that sets of genes involved in cytoskeletal regulation and dendrite formation were upregulated when melanocytes were stimulated with ET-1. I also observed changes in the actin structure of melanocytes when stimulated with ET-1. In Chapter 5, I carried out experiments to characterize the phagosomal proteins of keratinocytes and proposed potential experiments for studying keratinocyte that are more biologically native. In this final chapter, I will discuss the findings of my work and evaluate their implications. Finally, I will suggest several immediate future directions for this work.

6.1 Keratinocyte and Melanocyte Transcriptomics

Melanocytes and keratinocytes reside together in the epidermis, with each melanocyte contacting multiple keratinocytes *in-situ*. Keratinocytes are known to secrete signaling factors that affect the melanocyte. In my doctoral work, I sought to understand the consequences of melanocyte-keratinocyte communication for each cell type, which I accomplished through transcriptional studies.

Prior to experimentally perturbing melanocytes and keratinocytes to reveal changes in their gene expression profiles, I first characterized the transcriptional profile of the two cell types in their native environment. There are several reasons why it was important to establish a reference transcriptome for melanocytes and keratinocytes *in situ*, and here I want to emphasize two arguments.

Firstly, the gene expression patterns of these cells could deviate from their original state over time when grown in culture. Secondly, the gene expression pattern of these cells do change due to the absence of the complementary cell type. The reference transcriptome was used to show that the genes of interest identified in cell culture experiments were expressed in the tissue environment and allowed for us to validate the *in situ* expression of multiple genes simultaneously without individually testing each one using immunofluorescence.

This data set provides a reference for assaying the *in-situ* transcription status of any gene of interest in basal keratinocytes, suprabasal keratinocytes, and melanocytes in epidermis of human neonatal foreskin. While these transcriptomes were a valuable reference for me in the work I have described here, they will also

serve as a resource for other researchers who are studying gene expression in melanocytes and keratinocytes.

In Chapter 3, I sought to understand the effects of melanocyte-keratinocyte communication on the keratinocyte. Previous work on melanocyte-keratinocyte communication has focused on the consequences of this intercellular signaling on the melanocyte. I found that a small but reproducible set of genes were upregulated in keratinocytes when they were cultured in melanocytes. Of particular interest was the gene NRCAM, a cell adhesion molecule. NRCAM is upregulated in keratinocytes when they are grown with melanocytes, and NRCAM is also expressed in melanocytes *in situ* (based on our transcriptomic data). The role of NRCAM in keratinocytes and melanocytes has not been previously studied to my knowledge. NRCAM is known to play a role in axon guidance and the adhesion of neural cells, and it is expressed in populations of both neurons and glia If NRCAM could be shown to play a similar role in guiding the dendritic appendages of melanocytes, it would be another example of the neuron-like features of melanocytes but at the molecular level, and be used as a clue to transform the understanding of melanocyte biology. In order to evaluate this, I propose expressing an shRNA against NRCAM in keratinocytes and melanocytes (both individually and paired together), growing melanocytes and keratinocytes in co-culture, and motoring the morphology of both melanocytes and keratinocytes. This is the first study that implicates NRCAM in melanocyte-keratinocyte interactions, and it will be interesting to see what further studies reveal.

In Chapter 4, I characterized the effect of ET-1—a specific molecule that keratinocytes use to signal to melanocytes—on melanocyte gene expression. I found a reproducible population of upregulated genes in melanocytes after treatment with ET-1, and analyzed the Gene Ontology (GO) pathways that were represented in those upregulated genes. Pathways involved in cytoskeletal regulation were well represented. This finding is mechanistically plausible, as melanocytes change their morphology after ET-1 stimulation, and the cytoskeleton is ultimately responsible for the shape a cell takes. However, this is not an observation that had been previously reported. I examined the F-actin arrangement in melanocytes with and without ET-1 stimulation and observed an increase in punctate F-actin following ET-1 stimulation. I also observed an increase in punctate F-actin in co-cultured melanocytes.

The function of this punctate actin in the cell is not clear. However, previous studies have identified similar puncta in neurons at the sites where dendritic spines will later emerge (citations). It is possible that in melanocytes, these actin puncta represent sites where cellular extensions will emerge from. However, proving this speculation will require further examination. I propose visualizing the actin cytoskeleton of living melanocytes before and after treatment with ET-1 over a period of 48 hours. If indeed the actin puncta in melanocytes mark sites where dendritic extensions or spines will occur, such morphological changes would be revealed by this experiment.

The transcriptomic experiments identified particular actin-regulators that are upregulated in melanocytes in response to ET-1. I confirmed that one of these proteins, MAP2, is expressed in melanocytes *in situ* and *in vitro*. MAP2 binds to actin

as well as microtubules and is involved in coordinating the cytoskeleton during neurite formation (Dehmelt and Halpain, 2005). MAP2 had previously been identified as being expressed in the majority of melanocytic nevi and primary melanomas, but not expressed in malignant melanoma. Researchers found that MAP2 functions as a tumor suppressor for melanoma *in vivo* using a mouse model of melanoma. On a cellular level, they also found that expression of MAP2 induced dendritogenesis in a melanoma cell line that does not normally express the gene (Song et al., 2010). My work is the first time MAP2 has been studied in healthy melanocytes. It is also the first time that MAP2 expression has been linked to ET-1 signaling from keratinocytes. Taken together with the work of Song et al., I propose a model where keratinocytes express ET-1, which melanocytes receive as a signal that upregulates the expression of MAP2. The increased expression of MAP2 leads to dendritogenesis and regulated growth of melanocytes.

To validate the role of cytoskeletal machineries in healthy melanocyte morphogenesis, I suggest knocking down MAP2 in melanocytes and monitoring their morphology in co-culture. A comparison of the gross cell morphology, including the number of extensions, in MAP2 knockdown and control cells would be both simple and informative. To better understand the specific role of MAP2, one could knockdown MAP2 in melanocytes, treat the cells with ET-1, and observe the actin and/or microtubule cytoskeleton over time, which may provide insights and clues for identifying upstream and downstream pathways in which MAP2 is involved.

In addition to pathways of cytoskeletal genes being upregulated in melanocytes treated with ET-1, genes involved in neuronal growth and morphology

were upregulated. One of these genes was NGFR, which has been previously implicated in keratinocyte-melanocyte signaling. The finding that ET-1 stimulation of melanocytes leads to increased expression of NGFR is novel and reveals a node in the crosstalk between these two signaling pathways.

6.2 Studies of the Keratinocyte Phagosome

In Chapter 5, I characterized the proteomic content of keratinocyte phagosomes by incubating primary keratinocytes with polystyrene beads, fractionating out the bead-containing phagosomes from the cells and using mass spectrometry to analyze the proteins present. Through this analysis, I found that when keratinocytes phagocytose beads, they do so in a manner that is similar to other phagocytic cells, such as macrophages. Known phagocytic and lysosomal proteins were present on the phagosomes.

My original intention when designing this experiment was to use it as a control for understanding the baseline phagocytosis of keratinocytes that internalizing a generic material before moving on to studying keratinocytes phagocytosing more specific substrates and characterizing those proteomes. I built tools to study keratinocyte phagocytosis of melanocyte-derived materials by proximity labeling. I designed fusion proteins of BioID2, a non-specific biotin ligase, to localize BioID to melanocores. Although these tools require more validation, they constitute a novel method of studying the internal protein contents of phagosomes that contain specific biological targets, as opposed to latex beads. They can also be applied to characterizing the phagosomal contents of other phagocytic systems, as BioID2 can be fused to surface proteins of other phagocytic substrates including pathogens.

This tool has the potential to answer several interesting questions well beyond melanosome transfer. For example, not all phagocytic targets end up in identical compartments; some pathogens are phagocytosed but do not end up in a terminally degradative compartment, such as in the case of Mycobacterium tuberculosis, which stalls the fusion of phagosomes with lysosomes and resides in an arrested phagosome for a prolonged period (Sundaramurthy et al., 2017). Here, the technique of proximity labeling could be used to characterize the differences in protein content between phagosomes containing pathogens that do or do not escape lysosomes.

6.3 Conclusions

In this thesis, I have made contributions to our understanding of cell-cell communication between melanocytes and keratinocytes. I have uncovered gene expression changes in melanocytes by ET-1 signaling from keratinocytes. This increased understanding of the biology of healthy melanocytes can be used to improve our understanding of what goes awry in the transformation from melanocyte to melanoma cell. Dysregulation of cell-cell communication is characteristic of oncogenesis. Understanding homeostatic intercellular communication is essential to studying disease states. I have pointed to a possible role for MAP2 in melanoma cell progression, but there is more work to be done to characterize the potential roles of the genes I have identified in melanoma.

I have also shown how a co-culture of primary cells from healthy epidermal tissue is an excellent system for studying cell-cell communication. This system has the versatility of being conducive to live-cell imaging, transcriptomic and proteomic

experiments. Both melanocytes and keratinocytes can be sorted out of the system for analysis, and it is possible to express transgenes selectively in either cell type, as I have illustrated. This experimental system allows us to make new insights into both basic biology and disease states.

CHAPTER 7: MATERIALS AND METHODS

Isolation of Melanocytes and Keratinocytes

Foreskins of male neonates removed as a product of elective circumcision were collected by physicians at New York Presbyterian Hospital. The specimens were placed in CO2 Independent Medium (Thermo Fisher) supplemented with penicillin, streptomycin and amphotericin B (Anti-Anti, Gibco) at 4°C. Samples were collected within 48 hours of the procedure, and processed as follows. Subcutaneous tissue was removed and the samples were cleanly cut into approximately 3 mm by 3 mm squares. These pieces were incubated for 15-18 hours in 2 mL of 10 mg/mL dispase II (Sigma-Aldrich). The samples were then incubated at 37°C for 10 minutes. At this point, the epidermis was carefully separated from the dermis with a scalpel. The dermis was discarded, and the epidermis was minced finely and incubated in 2 ml of 0.5% trypsin (Gibco) for 5 minutes at 37°C. This sample was gently triturated 80 times, and 8 ml of Soybean Trypsin Inhibitor (STI) (Life Technologies) was added to deactivate the trypsin. Samples were centrifuged at 200 x g for 4 minutes, and then resuspended in 10 ml HBSS (-CaCl2 and -MgCl2). Samples were centrifuged and washed in HBSS three more times, and finally resuspended in melanocyte growth media or keratinocyte growth media (described below).

Culturing of Melanocytes and Keratinocytes

Melanocytes were cultured in Medium 254 supplemented with HMGS-2 (Gibco) and Anti-Anti at 37°C with 5% CO_2. Cells were used at below six passages for all experiments, and were always passaged below 80% confluency. When

melanocytes were frozen it was in 95% FBS with 5% DMSO. When passaged, melanocytes were incubated with 0.05% trypsin for between 30 seconds and 1 minute at room temperature, at which point trypsin was deactivated with STI.

Keratinocytes were cultured in Epilife (Gibco) medium supplemented with HKGS (Gibco) and Anti-Anti (Gibco). Cells were used at below six passages for all experiments, and were always passaged at below 80% confluency. When keratinocytes were frozen it was in 95% growth medium with 5% glycerol. At each passaging, cells were incubated with 0.05% trypsin for 1 minute at room temperature. This trypsin was discarded, and fresh trypsin was added for 3-5 minutes at 37°C, just until cells detached from the dish. Trypsin was deactivated with STI.

Proteomics of Isolated Keratinocyte Phagosomes

$6x10^5$ keratinocytes were seeded in three 15-cm dishes per replicate. When cells were confluent, the media was supplemented with calcium to a concentration of 1.06 mM for 72 hours. After 72 hours, the cells were incubated with media containing 1 μm Polybead® Carboxylate Blue Dyed Microspheres at a 1:50 dilution for 1 hour (Polysciences). For a non-internalization control, cells were incubated with 0.1% sodium azide for 30 minutes prior to incubation with beads. The cells were incubated with media containing latex beads and 0.1% sodium azide on ice in a 4°C room. After one hour, the plates were washed in HBSS and then trypsinized at 37°C for approximately 4minutes. The trypsin was deactivated with soybean trypsin inhibitor and cell pellets were centrifuged and resuspended in cold HBSS. Cells were pelleted again and then resuspended in 1.5 mL Homogenization Buffer

supplemented with protease inhibitors (cOmplete Mini EDTA-free, Millipore) (see buffer table below). Cells were homogenized by nitrogen cavitation at 900 PSI for 15 minutes. After cavitation, nuclei were pelleted by centrifugation at 900 x g for 5 minutes, and the post-nuclear supernatant (PNS) was used and nuclei were discarded.

The PNS was mixed with an equal volume of 68% sucrose supplemented with protease and phosphatase inhibitors. In an ultraclear ultracentrifuge tube (Beckman), a sucrose gradient was poured as follows from the bottom up: 68% w/v sucrose, sample, 35% w/v sucrose, 25% w/v sucrose, 10% w/v sucrose. 10% sucrose was added to equilibrate the weight of the tubes, and then samples were ultracentrifuged for 1 hour at 72,300 x g at 4°C (Beckman Coulter SW 41 Ti rotor).

After centrifugation, a blue band corresponding to the latex bead containing phagosomes was visible between the 10% and 25% sucrose layers. This band was removed with a transfer pipette and placed in a new ultracentrifuge tube, which was then filled with 4°C PBS. The samples were ultracentrifuged for 15 minutes at 28,400 x g at 4°C, and the supernatant removed. Samples were stored at °C. Samples were thawed and resuspended in 20 µL of LDS loading buffer and loaded onto a 4-12% gel (Thermo Fisher) and ran at 2000 V for 7minutes until the sample had traveled 12 mM into the gel. The gel was washed three times in water and stained in PageBlue stain (Thermo Fisher) for 1 hour. The gel was destained in water and transported to the Proteomics Resource Center for subsequent processing.

Mass Spectrometry

The gel band was excised and digested using trypsin (Promega) and Endopeptidase Lys-C (Wako). Extracted peptides were analyzed by LC-MS/MS (EasyLC 1200, Thermo Scientific) coupled to a Fusion Lumos (Thermo Scientific) operated in high/high mode. Peptides were separated by reversed phase (50cm EasySprayer, Thermo Scientific) using a gradient increasing from 2% B to 45% B in 115 or 220 minutes. MS data were queried against Uniprots Human databased using both Proteome Discoverer 1.4 (Thermo Fischer) /Mascot 2.4 (Matrix Science) and MaxQuant v/1.6.0.13. Cysteines were treated as fully carbamidomethylated and oxidation of methionine's and protein N-terminal acetylation were allowed as variable modifications. Matched peptides were filtered using <1% FDR (Percolator (Spivak et al., 2009)).

Preparation of Tissue for Flow Cytometry

Tissue specimens were prepared following an abbreviated protocol to reduce the time from tissue excision to RNA sequencing. The sample was dissected as described above, and then treated with Dispase II for five minutes at 37°C. The samples were minced, and treated with trypsin for 4 minutes, and triturated 80 times to form a single cell suspension. The rest of the sample preparation was the same as for all flow cytometry samples, and is described below

Flow Cytometry Sample Preparation

Cells were trypsinized, the trypsin deactivated with STI, and cells were passed through a blue cap filter to make a single cell suspension. Cells were

subsequently kept on ice. Cells were washed three times in FACS Buffer (1 mg/mL BSA, 25 mM HEPES, 5 mM EDTA). After the last wash was removed from the cell pellet, cells were resuspended in FACS buffer containing pretitered antibodies (see table below). Cells were incubated with antibodies on ice in the dark for 25 minutes, and gently flicked every 5 minutes. Antibodies are shown in Table 12. At this point, cells were washed three times with FACS buffer, and finally resuspended in FACS buffer containing DAPI. Cells were sorted on a BD FACSAria using an 85 µL nozzle. A maximum of 4,000 cells per sample were sorted into collection tubes containing 100 µL XB from the PicoPure RNA Isolation Kit (Thermo Fisher). RNA samples were processed using the PicoPure RNA Isolation Kit in accordance with the provided protocol.

Table 12 FACS Antibodies

ANTIBODY	Dye	SOURCE		SPECIES
Alpha 6-Integrin	**PE**	**Abcam**	**GoH3**	**Rat**
CD11c	**PerCP-eFluor 710**	**eBioscience**	**46-0116-42**	**Mouse**
C-Kit	**APC**	**ThermoFisher**	**CD11705**	**Mouse**

RNA Sequencing

RNA libraries were prepared using the SMARTer Universal Low Input RNA kit (Takara Bio), and were sequenced on an Illumina NextSeq 500 system, using paired-end reads of 75 base pairs, for the intact epidermis experiment, and single-end reads for all other experiments. Reads were subjected to quality control using FastQC (Babraham Institute), visualized by MultiQC.(Ewels et al., 2016), trimmed using BBduk (Joint Genome Institute), and were aligned and counted using Salmon (Patro et al., 2017). Fifferential expression analysis performed with DeSeq2 (Love et

al., 2014). P-value threshold of ≤ 0.05 was used, and log_2Fold Change ≥ 0.9 or ≤ -0.09. Gene Ontology analysis was performed using the ToppGene suite (http://toppgene.cchmc.org).

Preparation of Tissue for Immunofluorescence

Foreskin samples were trimmed of subcutaneous tissue and placed in 4% paraformaldehyde overnight at 4°C. The next day, the tissue was moved to 15% sucrose in PBS. Once the sample sank to the bottom of the 15% sucrose solution, it was placed in 30% sucrose in PBS. When the sample sank to the bottom of the 30% sucrose, it was cut into slices, arranged in a cryomold in O.C.T. Compound (Tissue-Tek), and frozen on a metal plate in a bed of dry ice.

Immunofluorescence of Cells

Cells grown in a 10 mM well MatTek dish were rinsed with PBS and fixed with 4% PFA for 10 minutes. Cells were washed three times with PBS and permeabilized with 0.1% Triton-X 100, then blocked in a buffer containing 2.5% Donkey Serum, 2.5% Goat Serum, 1% BSA, 0.1% Triton X-100. Cells were incubated with primary antibody in blocking buffer (dilutions described in a table below) overnight at 4°C. Cells were washed 3 times for 5 minutes in PBS, and incubated with secondary antibody diluted in blocking buffer for 1hour at room temperature. Cells were washed three times again, incubated with Hoechst 33342 (Life Technologies) at a 1:1000 dilution for 1 minute, washed once more, and mounted under a cover glass in ProLong Gold Antifade Mountant (Thermo Fisher). Specified samples were treated with Alexa Fluor 488 Phalloidin at a 1:40 dilution for 20 minutes. All analysis was performed using Image J. Quantification of MAP2 intensity was performed by

drawing a region of interest (ROI) within the cell and measuring the fluorescence mean intensities within that region. Three cells were selected at random from each condition, and the means of the intracellular fluorescence mean intensities were compared by a paired t-test.

Confocal Microscopy

Confocal microscopy was performed on an FV3000 microscope (Olympus) with a UPLXAPO60XO 60X immersion oil objective (NA of 1.42). The microscope has 2 multialkali PMTs. Images were obtained using CellSense software (Olympus).

Epifluorescence Microscopy

Epifluorescence imaging was performed on an on an Upright BX61WI microscope (Olympus) with a UMPlan FL 60× 1.0 NA water dipping objective (Olympus), an Orca Flash 4.0 digital CMOS camera (Hamamatsu) using MetaMorph image acquisition software (Molecular Devices). Samples stained with Alexa 488 or Alex 594 were acquired using GFP and mCherry filter sets, respectively. Hoechst and rhodamine phalloidin (Molecular Probes) staining was imaged using a broad CFP filter set and mCherry filter set, respectively.

Quantification of Bead Internalization

All analysis was performed in ImageJ. For sparse cells, I used made a mask around cells using thresholding to outline the cells as seen on the Phalloidin channel. I then applied this mask to the channel that contained the bead images. Removed beads that were outside of cell selection area, and found maxima in order to find the number of beads per cell.

For the dense cell condition, I used thresholding to identify nuclei on the Hoechst channel. I separated overlapping nuclei, and counted the number of nuclei using the “count particles” function. I then found maxima in order to identify the number of beads.

Immunofluorescence of Tissue Cryosections

5 to 10 micron slices of tissue pieces embedded in Optimum Cutting Temperature (OCT) were made on a cryostat. Tissue slices were placed on glass slides and stored at -20°C. At the time of immunofluorescence, slides were warmed to room temperature, and washed three times in a Coplin jar containing PBS. A hydrophobic pen (Abcam) was used to draw a circle around each sample. Subsequent incubations were performed in a bubble of liquid placed within the hydrophobic circle. The tissue was washed three times with PBS and permeabilized with 0.1% Triton-X 100, then blocked in a buffer containing 2.5% Donkey Serum, 2.5% Goat Serum, 1% BSA, 0.1% Triton X-100. The sample was incubated with primary antibody in blocking buffer (dilutions described in a table below) overnight at 4°C. Samples were washed 3 times for 5 minutes in PBS, and incubated with secondary antibody diluted in blocking buffer for one hour at room temperature. Secondary antibodies against mouse IgG, rat IgG, or rabbit IgG conjugated to Alexa Fluor 488 or 594 (Molecular Probes) were used at a 1:1,000 dilution. Samples were washed three times again, incubated with Hoechst 33342 at a 1:1000 dilution for 1 minute, washed once more, and mounted under a cover glass in ProLong Gold Antifade Mountant (ThermoFisher).

Table 13 Immunofluorescence Antibodies

ANTIBODY	CONCENTRATION	SOURCE		SPECIES
NGFR	**1:500**	**Abcam**	**ab245134**	**Mouse**
NRCAM	**1:100**	**Abcam**	**ab186247**	**Mouse**
TRP1	**1:200**	**Abcam**	**TA99**	**Mouse**
C-Kit	**1:100**	**ThermoFisher**	**CD11705**	**Mouse**
MAP2	**1:500**	**Abcam**	**ab32454**	**Rabbit**

Virus Production

Low-passage HEK293T cells were using polyethyleneimine. Plasmids were co-transfected in a 5:5:1 ratio of lentiviral plasmid to NI- GagPol plasmid (provided by Bieniasz lab) to VSV-G plasmid. Virus was made as a high-titer stock and frozen at -80°C for future use. High-titer virus stock was made by combining the lentivirus containing media of 24 h (and 48 h and/or 72 h, as needed) post transfection from several 150-mm dishes (transfected with 88 µg of total DNA/dish). Viral supernatants were concentrated using the Lenti-X reagent and concentration protocol (Clontech) and resuspend in HBSS at a 100x concentration.

Lentiviral Transduction

At the time of infection, 200-600 µL of concentrated lentivirus was added to the growth media of the cells of interest. Cultures were incubated with the virus for 4 – 17hrs, and then media was replaced.

Translating Ribosome Affinity Purification

Melanocytes or keratinocytes were transduced with 600 ul of concentrated virus for expression of GFP-L10. Cells were expanded, and then plated for experimental conditions. For all experiments, keratinocytes or Hela cells were plated

at 10-fold higher density than melanocytes. All experimental conditions were grown in Epilife media in a 10 cm dish. When co-cultured cells reached confluency, the media was changed to Epilife media supplemented to 1.06 mM $CaCl^2$. Cells were cultured in the higher calcium media for 72 hours, at which point the media was replaced with the same media containing cycloheximide at 100 µg/mL for 15 minutes. Cells were washed three times with PBS containing 100 µg/mL cycloheximide, which was then replaced with a lysis buffer containing cycloheximide, protease-inhibitor and RNase-inhibitors (composition below). Plates were incubated on ice for 10 minutes, and then cells were scraped off the dish and collected in a tube and lysed by gentle trituration. These cell lysates were centrifuged at 2,000 x g for 10 minutes, and the supernatant collected and mixed with 1/9 parts DHPC (Avanti Polar Lipids). Samples were centrifuged at 20,000 x g for 10 minutes, and supernatants were once more transferred to a new tube. At this point they were mixed with 200 µL of anti-GFP resin (provided by the Walz Lab) and incubated at 4°C for 18 hours. After 18 hours, the samples were centrifuged at 1000 x g for 1 minute and the supernatant was discarded. The samples were washed four times in a high salt buffer (composition below). After the final wash, the wash buffer was removed and the samples were warmed to room temperature. The beads were suspended in 100 µL lysis buffer from the Absolutely RNA Nanoprep kit (Agilent). At this point, samples were stored at -80°C.

Samples stored at -80°C were warmed to room temperature, and were processed using the Absolutely RNA Nanoprep kit in accordance with the protocol.

After elution, RNA samples were delivered to the Rockefeller Genomics Resource Center and evaluated for RNA quality and concentration.

Buffer Compositions:

Cell-Lysis Buffer

20 mM HEPES KOH
150 mMKCl
10 mM MgCl2
1% (vol/vol) NP40
In RNase-free water

High Salt Buffer

20mM HEPES KOH
350 mM KCl
10mM MgCl2
1% (vol/vol) NP40)

Construction of pGS28, BioID-M-Ink Expression Plasmid

Note: All PCR for cloning was done with Platinum™ PCR SuperMix High Fidelity (Thermo Fisher Scientific) according to manufacturer's protocols. PCR products were gel purified and conjugated using NEBuilder® HiFi DNA Assembly Cloning Kit (New England BioLabs).

The BioID2 containing plasmid was a gift from Dr. Elias Coutavas, and amplified with *5'- gaagttctgttccaggggttcaagaacctgatctggctgaaggaggtgg -3'* and *5'- agatccacgcggaacgcttcttctcaggctgaactcgccgc* -3' and cloned into the pEF-BOS GST M-INK plasmid, obtained from the Riken Plasmid Databank. The backbone was

amplified with *5'- gttccgcgtggatctgatgataatgacgagtctg -3' and 5' cccctggaacagaacttccagatccgattttgg -3'. BioID-M-Ink was then amplified with 5'- ttcacacaggaaacagtattcatggctagcatgactggtggacagcaaat -3'* and *5'- cgcgaggcagatcgtcacacagctgccccactctctttgag* -3' and cloned into pGEX vector (gift of Dr. Joan Pulupa), amplified with *5'- cgatctgcctcgcgcgtttcgg -3'* and *5'- gaatactgtttcctgtgtgaaattgttatccgctcacaattcc* -3' .

Purification of M-Ink-BioID

pGS28 (described above) was transformed into BL32-pLys RIL- competent cells (Stratagene). Expression was induced with 0.5 mM isopropyl *β*-D-1-thiogalactopyranoside (IPTG, Sigma) and cells were grown for 18 hours at 18°C. Cells were spun at 6,000 x g for 10 min at 4 °C and the pellet was frozen overnight before lysis (Sorvall SLA-1500). The pellet was resuspended in 50 mM D-PBS (Gibco), 150 mM NaCl with benzonase (at 25 U/mL, Millipore) and r Lysozyme (at 12 U/mL, Novagen) and 1x cOmplete protease inhibitors (Roche). The resuspended pellet was passed through a high pressure homogenizer (Avestin EmuliFlex-C3, ATA Scientific) for lysis. The supernatant was added to Glutathione Sepharose 4B (Sigma) and nutated at 4C for 1 hour. This supernatant was then loaded on a column (Qiagen) and washed 3x with 50 mM Tris pH8, 150 mM NaCl, 20 mM imidazole. The protein was then eluted with 5 mM glutathione in 50 mM Tris–HCl in 500 uL fractions. The concentration of protein was estimated by OD and the highest fractions were pooled and buffer exchanged and concentrated on Amicon Ultra Centrifugal Filter (10KD cutoff, Millipore). Samples were stored in aliquots of 10 mg

in 50 mM TRIS pH, 150 mM NaCl, and 10% glycerol. Purification was confirmed by running the protein on a 4-12% Tris-Glycine gel (Novex) and performing a Coomassie (Figure 30, PageBlue, Thermo Scientific).

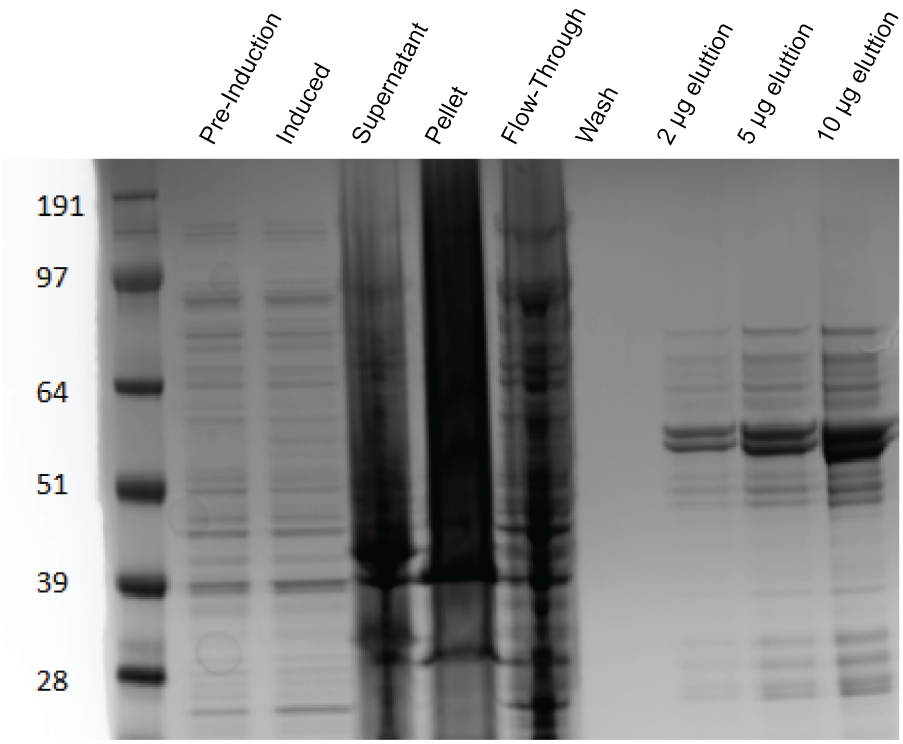

Figure 30 Coomassie-Stained Gel of Purification of BioID-M-Ink.

The predominant band in a Coomassie-stained gel shows purified BioID-M-Ink as a predominant band.

Streptavidin Blot

Cells were lysed in LDS Loading Buffer (Thermo Fisher), boiled for 10 minutes, and loaded on a 4-12% Bis-Tris gel (Thermo Fisher), and separated at 200

V for 30 minutes in MOPS running buffer (Thermo Fisher). Proteins were then transferred onto nitrocellulose membranes using the iBlot system (Invitrogen). The membranes were blocked in BSA blocking buffer (described below) for 30 minutes, and agitated in streptavidin-HRP (Pierce High Sensitivity Streptavidin-HRP, Thermo Fisher) at a 1:40,000 dilution in BSA bocking for 40 minutes at room temperature. The membranes were washed twice in PBS, and once in ABS blocking buffer for 5 minutes. They were washed three more times in PBS. Chemiluminescence substrates (ECL Prime, Amersham or West Pico or West Femto, Pierce) were used for visualization.

BSA blocking buffer
1% bovine serum albumin
0.2% (w/v) Triton X-100

ABS blocking buffer
10% (v/v) FBS
1% (w/v) Triton X-100

Melanocore Preparation and Labeling

MNT-1 melanoma cells were grown for 10 days to produce melanocore conditioned media. The supernatants were centrifuged to remove any floating cells. The supernatant was run through a 300,000 PES molecular weight cut-off Vivaspin concentrator column (Thermo Fisher), until the media volume had reduced to 3.2% of its original volume. The concentration was calculated by reading the absorbance at 340 nm, and calculated using the following calculation:

$Absorbance_{340} = (1.8546 \times concentration) - 0.0422$

Samples were stored in 5.86 ml aliquots. To label each aliquot, 2 aliquots of BioID-M-Ink were incubated with the melanocores overnight at 4°C. The melanocores were washed with 4 mLs of PBs and run through a Vivaspin column until less than 1 mL of liquid remained.

BioID Melanocore Treatment

10 cm dishes of keratinocytes were incubated with 5 mM ATP, 50 mM biotin and BioID-M-Ink labeled melanocores for 19 hours at 37°C. The cells were washed twice with PBS, and 540 microliters of lysis buffer were added to each dish, and the cells scraped to harvest. The lysed cells were collected, and 120 ul of 20% Triton X-100 was added to each sample. The lysates were sonicated for two sessions with 60 pulses each using a Branson Sonifier 250 at a 30% duty cycle and an output level of 4. 2.52 ml of prechilled lysis buffer was added to each sample, and the samples sonified for one more session. Samples were centrifuge for 10 minutes at 16,500 x g at 4°C, and the supernatants taken and split into three. 100 microliters of magnetic streptavidin beads (Dynabeads, Thermo Fisher) were added to each tube of supernatant from the previous step, and the samples incubated on a rotator overnight at 4°C. Cells were washed with Wash Buffer 1 twice, and then with Wash Buffer 2 and Wash Buffer 3. The samples were resuspend in 1 ml 60 mM Tris-HCL. Then this supernatant was removed, and the dry beads were delivered to the Proteomics Resource Center.

Lysis Buffer

Tris cl pH (7.4) 50 mM
NaCl 500 mM
SDS 0.20%

Wash Buffer 1

SDS (w/v) 2%

Wash Buffer 2

Deoxycholic acid 0.10%

Triton x-100 1%

EDTA 1 mM

NaCl 500 mM

HEPES 50 mM

Wash Buffer 3

Deoxycholic acid 0.50%

Triton X-100 0.50%

EDTA 1 mM

LiCl 250 mM

Tris Cl (pH 7.4) 10mM

Appendix I: Description of BioID Based Keratinocyte Phagocytosis Experiments

In order to coat melanocores with the BioID2 enzyme, I created a fusion protein of BioID2 to M-Ink. M-Ink is a peptide that has been characterized to have affinity for melanocores when purified and added to permeabilized cells or to isolated melanocores (Ishida et al., 2017). It binds to the pigment-covered melanin fibrils, not to the membrane of the melanosome. I cloned the BioID2-M-Ink fusion gene and purified this fusion protein. Next, I validated that this fusion protein is still able to label melanocores (Figure 31C), by permeabilizing melanocytes and incubating with purified BioID-M-Ink, and performing immunofluorescence with an anti-T7 antibody, which binds to the T7 tag present on the BioID-M-Ink fusion protein. I also confirmed both *in vitro* and *in vivo* that the BioID-M-Ink fusion protein retains biotinylation activity (Figure 31A-B).

I purified melanocores secreted by the MNT-1 cell line, a melanoma cell line that secretes generous amounts of membrane-less melanocores into the cell media (Correia et al., 2018). I then incubated the melanocores with BioID-M-Ink overnight at 4 degrees Celcius, washed off unbound BioID-M-Ink from the melanocores, and added the BioID-M-Ink labeled melanocores to primary keratinocytes with ATP. After allowing the keratinocytes to internalize these labeled melanocores, I washed off extraneous melanocores and pulled down biotinylated proteins with streptavidin beads, and sent these samples for LC-MS analysis. In addition to the condition where keratinocytes were fed BioID-M-Ink melanosomes, I also two control conditions—one where keratinocytes were incubated with non-bound M-Ink-BioID,

and another where the cells were treated with no BioID enzyme. The results of the proteomic analysis were not conclusive. It was not clear if the proteins being biotinylated were specific to the endosomal/phagosomal system, or if there was non-specific biotinylation occurring.

I performed GO analysis on proteins that were enriched in the BioID-M-Ink melanocore treated sample compared to the BioID-M-Ink alone treated sample. I considered proteins to be enriched if the $\log_2$Fold change was greater than 1.9. GO analysis of the cellular components in which the proteins present were found did identify “organelle envelop” and “vesicle lumen” in the top twenty cellular components. However, also represented were cellular components that I would not expect to be present if the biotinylation was specific to the lumen of an organelle. Specifically, actin cytoskeletal proteins were present, as well as ribosomal proteins.

Further analysis is necessary to validate the specificity of this experiment. One method of validation is to use fluorescently-labeled streptavidin to visualize the localization of the biotinylated proteins. I could co-label these samples with antibodies against known phagosomal and endosomal proteins to determine if biotinylation is occurring in these compartments. A potential issue with this experiment is that the pH of the acidifying phagolysosome may reduce the efficiency of biotinylation. Because I was particularly interested in receptor proteins that would be present in early phagosomes and would be recycled back to the plasma membrane, this did not originally discourage me from trying this experiment, but it is possible that even these early compartments are not amenable to BioID activity.

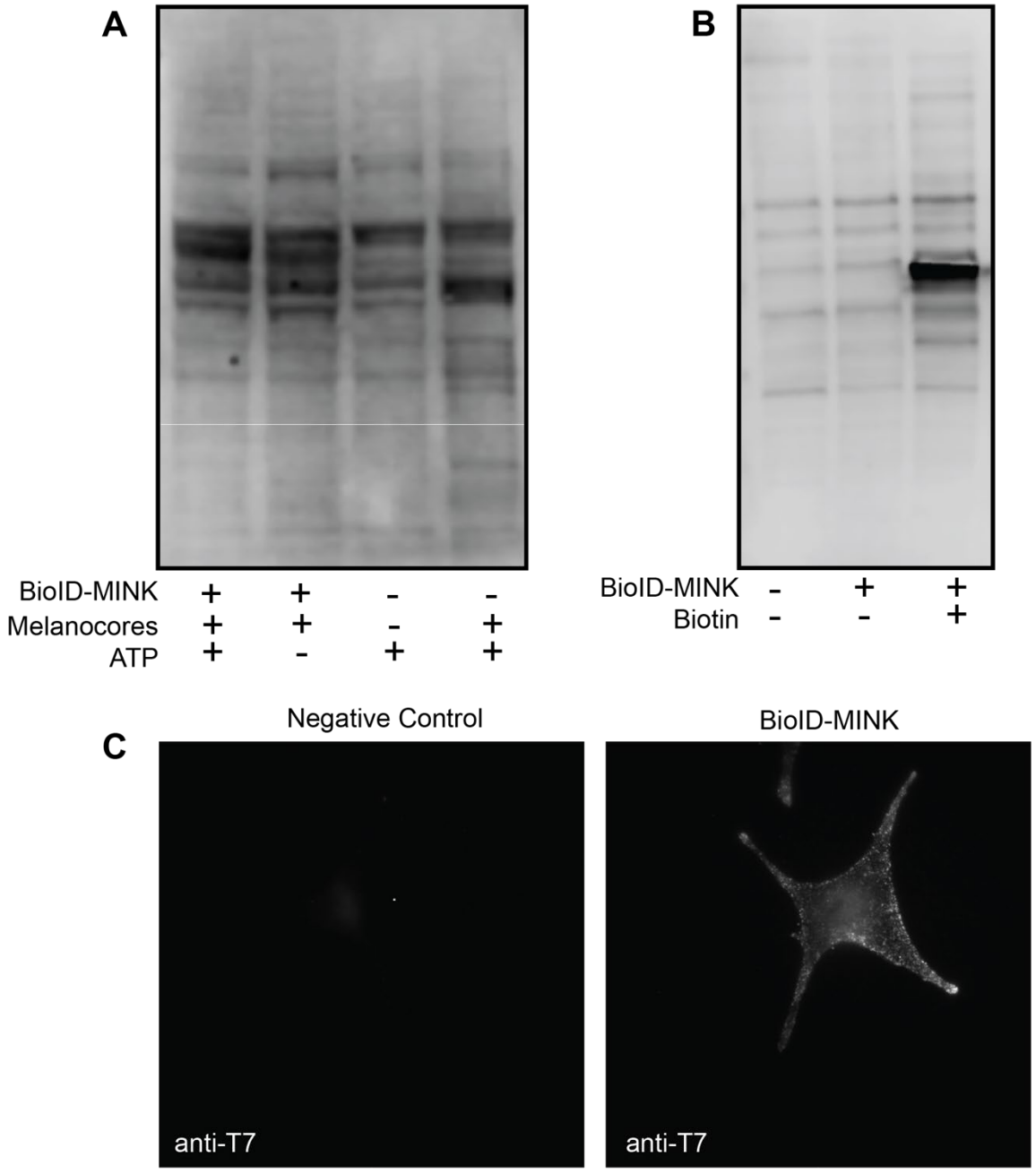

Figure 31 Testing the Biotinylation Efficacy and Binding Ability of BioID-M-Ink

A) Keratinocytes were treated with BioID-M-Ink labeled melanocores with or without 5 mM ATP, or free BioID-M-Ink for 19 hours. Cells were lysed and run on a SDS-PAGE gel and blotted with Streptavidin-HRP. B) Hap1 cell lysates were treated with purified BioID-M-Ink with or without biotin for 2 hours at 37 C. C) Melanocytes were fixed, permeabilized and either treated with BioID-M-Ink or not. Both samples were then treated with an anti-T7 antibody.

Table 14 GO Analysis of BioID-M-Ink Pulldown

ID	Name	p-value	q-value FDR B&Y	Hit Count in Query List	Hit Count in Genome
GO:0030055	cell-substrate junction	1.19E-38	7.96E-35	81	435
GO:0005925	focal adhesion	1.02E-37	3.41E-34	79	424
GO:0070161	anchoring junction	7.39E-35	1.65E-31	109	880
GO:1990904	ribonucleoprotein complex	6.53E-29	1.09E-25	93	768
GO:0099080	supramolecular complex	5.43E-28	7.28E-25	154	1895
GO:0099513	polymeric cytoskeletal fiber	1.16E-24	1.30E-21	120	1357
GO:0099512	supramolecular fiber	1.33E-22	1.27E-19	127	1572
GO:0099081	supramolecular polymer	2.08E-22	1.74E-19	127	1580
GO:0015629	actin cytoskeleton	2.97E-21	2.21E-18	85	837
GO:0031967	organelle envelope	1.21E-20	7.36E-18	110	1316
GO:0031975	envelope	1.21E-20	7.36E-18	110	1316
GO:0005739	mitochondrion	4.11E-19	2.30E-16	135	1897
GO:0043209	myelin sheath	2.23E-18	1.15E-15	38	207
GO:0005840	ribosome	2.90E-18	1.39E-15	43	269
GO:0044391	ribosomal subunit	3.73E-18	1.66E-15	38	210
GO:0031983	vesicle lumen	8.94E-18	3.74E-15	47	330

GO:0101002	ficolin-1-rich granule	1.86E-17	7.34E-15	35	185
GO:0034774	secretory granule lumen	2.29E-17	8.52E-15	46	324
GO:0060205	cytoplasmic vesicle lumen	3.73E-17	1.31E-14	46	328
GO:0030141	secretory granule	5.62E-17	1.88E-14	81	905

REFERENCES

Adameyko, I., Lallemend, F., Aquino, J.B., Pereira, J.A., Topilko, P., Muller, T., Fritz, N., Beljajeva, A., Mochii, M., Liste, I.*, et al.* (2009). Schwann cell precursors from nerve innervation are a cellular origin of melanocytes in skin. Cell *139*, 366-379.

Anderson, C.L., Shen, L., Eicher, D.M., Wewers, M.D., and Gill, J.K. (1990). Phagocytosis mediated by three distinct Fc gamma receptor classes on human leukocytes. J Exp Med *171*, 1333-1345.

Ando, H., Niki, Y., Ito, M., Akiyama, K., Matsui, M.S., Yarosh, D.B., and Ichihashi, M. (2012). Melanosomes are transferred from melanocytes to keratinocytes through the processes of packaging, release, uptake, and dispersion. J Invest Dermatol *132*, 1222-1229.

Baranov, M.V., Kumar, M., Sacanna, S., Thutupalli, S., and van den Bogaart, G. (2020). Modulation of Immune Responses by Particle Size and Shape. Front Immunol *11*, 607945.

Belote, R.L., and Simon, S.M. (2020). Ca2+ transients in melanocyte dendrites and dendritic spine-like structures evoked by cell-to-cell signaling. J Cell Biol *219*.

Berson, J.F., Harper, D.C., Tenza, D., Raposo, G., and Marks, M.S. (2001). Pmel17 initiates premelanosome morphogenesis within multivesicular bodies. Mol Biol Cell *12*, 3451-3464.

Bhawan, J., Whren, K., Panova, I., and Yaar, M. (2005). Keratin 16 expression in epidermal melanocytes of normal human skin. Am J Dermatopathol *27*, 476-481.

Bhawan, J., Whren, K., Panova, I., and Yaar, M. (2010). Keratin 16 expression in epidermal melanocytes. Br J Dermatol *162*, 218; author reply 218-219.

Bissig, C., Rochin, L., and van Niel, G. (2016). PMEL Amyloid Fibril Formation: The Bright Steps of Pigmentation. Int J Mol Sci *17*.

Bohm, S.K., Kong, W., Bromme, D., Smeekens, S.P., Anderson, D.C., Connolly, A., Kahn, M., Nelken, N.A., Coughlin, S.R., Payan, D.G.*, et al.* (1996). Molecular cloning, expression and potential functions of the human proteinase-activated receptor-2. Biochem J *314 (Pt 3)*, 1009-1016.

Boissy, R.E. (2003). Melanosome transfer to and translocation in the keratinocyte. Exp Dermatol *12 Suppl 2*, 5-12.

Brenner, M., and Hearing, V.J. (2008). The protective role of melanin against UV damage in human skin. Photochem Photobiol *84*, 539-549.

Brummendorf, T., and Rathjen, F.G. (1996). Structure/function relationships of axon-associated adhesion receptors of the immunoglobulin superfamily. Curr Opin Neurobiol *6*, 584-593.

Cardinali, G., Ceccarelli, S., Kovacs, D., Aspite, N., Lotti, L.V., Torrisi, M.R., and Picardo, M. (2005). Keratinocyte growth factor promotes melanosome transfer to keratinocytes. J Invest Dermatol *125*, 1190-1199.

Chekeni, F.B., and Ravichandran, K.S. (2011). The role of nucleotides in apoptotic cell clearance: implications for disease pathogenesis. J Mol Med (Berl) *89*, 13-22.

Chemes, H. (1986). The phagocytic function of Sertoli cells: a morphological, biochemical, and endocrinological study of lysosomes and acid phosphatase localization in the rat testis. Endocrinology *119*, 1673-1681.

Cichorek, M., Wachulska, M., Stasiewicz, A., and Tyminska, A. (2013). Skin melanocytes: biology and development. Postepy Dermatol Alergol *30*, 30-41.

Cohen, S., and Levi-Montalcini, R. (1956). A Nerve Growth-Stimulating Factor Isolated from Snake Venom. Proc Natl Acad Sci U S A *42*, 571-574.

Correia, M.S., Moreiras, H., Pereira, F.J.C., Neto, M.V., Festas, T.C., Tarafder, A.K., Ramalho, J.S., Seabra, M.C., and Barral, D.C. (2018). Melanin Transferred to Keratinocytes Resides in Nondegradative Endocytic Compartments. J Invest Dermatol *138*, 637-646.

Costin, G.E., and Hearing, V.J. (2007). Human skin pigmentation: melanocytes modulate skin color in response to stress. FASEB J *21*, 976-994.

Cramer, S.F., and Fesyuk, A. (2012). On the development of neurocutaneous units--implications for the histogenesis of congenital, acquired, and dysplastic nevi. Am J Dermatopathol *34*, 60-81.

D'Orazio, J., Jarrett, S., Amaro-Ortiz, A., and Scott, T. (2013). UV radiation and the skin. Int J Mol Sci *14*, 12222-12248.

De Fabo, E.C. (2005). Arctic stratospheric ozone depletion and increased UVB radiation: potential impacts to human health. Int J Circumpolar Health *64*, 509-522.

Desjardins, M., Huber, L.A., Parton, R.G., and Griffiths, G. (1994). Biogenesis of phagolysosomes proceeds through a sequential series of interactions with the endocytic apparatus. J Cell Biol *124*, 677-688.

Duclos, S., Diez, R., Garin, J., Papadopoulou, B., Descoteaux, A., Stenmark, H., and Desjardins, M. (2000). Rab5 regulates the kiss and run fusion between phagosomes and endosomes and the acquisition of phagosome leishmanicidal properties in RAW 264.7 macrophages. J Cell Sci *113 Pt 19*, 3531-3541.

Fitzpatrick, T.B., and Breathnach, A.S. (1963). [the Epidermal Melanin Unit System]. Dermatol Wochenschr *147*, 481-489.

Flannagan, R.S., Jaumouille, V., and Grinstein, S. (2012). The cell biology of phagocytosis. Annu Rev Pathol *7*, 61-98.

Frantz, C., Stewart, K.M., and Weaver, V.M. (2010). The extracellular matrix at a glance. J Cell Sci *123*, 4195-4200.

Fuchs, E. (1995). Keratins and the skin. Annu Rev Cell Dev Biol *11*, 123-153.

Fuchs, E. (2016). Epithelial Skin Biology: Three Decades of Developmental Biology, a Hundred Questions Answered and a Thousand New Ones to Address. Curr Top Dev Biol *116*, 357-374.

Fuchs, E., and Green, H. (1980). Changes in keratin gene expression during terminal differentiation of the keratinocyte. Cell *19*, 1033-1042.

Giordano, F., Simoes, S., and Raposo, G. (2011). The ocular albinism type 1 (OA1) GPCR is ubiquitinated and its traffic requires endosomal sorting complex responsible for transport (ESCRT) function. Proc Natl Acad Sci U S A *108*, 11906-11911.

Guo, M., Hartlova, A., Dill, B.D., Prescott, A.R., Gierlinski, M., and Trost, M. (2015). High-resolution quantitative proteome analysis reveals substantial differences between phagosomes of RAW 264.7 and bone marrow derived macrophages. Proteomics *15*, 3169-3174.

Hanayama, R., Tanaka, M., Miwa, K., Shinohara, A., Iwamatsu, A., and Nagata, S. (2002). Identification of a factor that links apoptotic cells to phagocytes. Nature *417*, 182-187.

Haney, C.A., Sahenk, Z., Li, C., Lemmon, V.P., Roder, J., and Trapp, B.D. (1999). Heterophilic binding of L1 on unmyelinated sensory axons mediates Schwann cell adhesion and is required for axonal survival. J Cell Biol *146*, 1173-1184.

Haniffa, M., Collin, M., and Ginhoux, F. (2013). Ontogeny and functional specialization of dendritic cells in human and mouse. Adv Immunol *120*, 1-49.

Hara, M., Yaar, M., and Gilchrest, B.A. (1995). Endothelin-1 of keratinocyte origin is a mediator of melanocyte dendricity. J Invest Dermatol *105*, 744-748.

Hearing, V.J., and Tsukamoto, K. (1991). Enzymatic control of pigmentation in mammals. FASEB J *5*, 2902-2909.

Heiman, M., Kulicke, R., Fenster, R.J., Greengard, P., and Heintz, N. (2014). Cell type-specific mRNA purification by translating ribosome affinity purification (TRAP). Nat Protoc *9*, 1282-1291.

Hines, M.D., and Allen-Hoffmann, B.L. (1996). Keratinocyte growth factor inhibits cross-linked envelope formation and nucleosomal fragmentation in cultured human keratinocytes. J Biol Chem *271*, 6245-6251.

Hoashi, T., Watabe, H., Muller, J., Yamaguchi, Y., Vieira, W.D., and Hearing, V.J. (2005). MART-1 is required for the function of the melanosomal matrix protein PMEL17/GP100 and the maturation of melanosomes. J Biol Chem *280*, 14006-14016.

Hoath, S.B., and Leahy, D.G. (2003). The organization of human epidermis: functional epidermal units and phi proportionality. J Invest Dermatol *121*, 1440-1446.

Hori, Y., Toda, K., Pathak, M.A., Clark, W.H., Jr., and Fitzpatrick, T.B. (1968). A fine-structure study of the human epidermal melanosome complex and its acid phosphatase activity. J Ultrastruct Res *25*, 109-120.

Imokawa, G., Yada, Y., and Miyagishi, M. (1992). Endothelins secreted from human keratinocytes are intrinsic mitogens for human melanocytes. J Biol Chem *267*, 24675-24680.

Iozzo, R.V. (2005). Basement membrane proteoglycans: from cellar to ceiling. Nat Rev Mol Cell Biol *6*, 646-656.

Ishida, M., Marubashi, S., and Fukuda, M. (2017). M-INK, a novel tool for visualizing melanosomes and melanocores. J Biochem *161*, 323-326.

Ishihara, H., Connolly, A.J., Zeng, D., Kahn, M.L., Zheng, Y.W., Timmons, C., Tram, T., and Coughlin, S.R. (1997). Protease-activated receptor 3 is a second thrombin receptor in humans. Nature *386*, 502-506.

Kadmon, G., and Altevogt, P. (1997). The cell adhesion molecule L1: species- and cell-type-dependent multiple binding mechanisms. Differentiation *61*, 143-150.

Kaidbey, K.H., Agin, P.P., Sayre, R.M., and Kligman, A.M. (1979). Photoprotection by melanin--a comparison of black and Caucasian skin. J Am Acad Dermatol *1*, 249-260.

Kevany, B.M., and Palczewski, K. (2010). Phagocytosis of retinal rod and cone photoreceptors. Physiology (Bethesda) *25*, 8-15.

Kim, D.I., Jensen, S.C., Noble, K.A., Kc, B., Roux, K.H., Motamedchaboki, K., and Roux, K.J. (2016). An improved smaller biotin ligase for BioID proximity labeling. Mol Biol Cell *27*, 1188-1196.

Kim, T., Echeagaray, O.H., Wang, B.J., Casillas, A., Broughton, K.M., Kim, B.H., and Sussman, M.A. (2018). In situ transcriptome characteristics are lost following culture adaptation of adult cardiac stem cells. Sci Rep *8*, 12060.

Kobayashi, N., Karisola, P., Pena-Cruz, V., Dorfman, D.M., Jinushi, M., Umetsu, S.E., Butte, M.J., Nagumo, H., Chernova, I., Zhu, B.*, et al.* (2007). TIM-1 and TIM-4 glycoproteins bind phosphatidylserine and mediate uptake of apoptotic cells. Immunity *27*, 927-940.

Kripke, M.L. (1988). Impact of ozone depletion on skin cancers. J Dermatol Surg Oncol *14*, 853-857.

Love, M.I., Huber, W., and Anders, S. (2014). Moderated estimation of fold change and dispersion for RNA-seq data with DESeq2. Genome Biol *15*, 550.

Madison, K.C. (2003). Barrier function of the skin: "la raison d'etre" of the epidermis. J Invest Dermatol *121*, 231-241.

Maness, P.F., and Schachner, M. (2007). Neural recognition molecules of the immunoglobulin superfamily: signaling transducers of axon guidance and neuronal migration. Nat Neurosci *10*, 19-26.

Marchese, C., Rubin, J., Ron, D., Faggioni, A., Torrisi, M.R., Messina, A., Frati, L., and Aaronson, S.A. (1990). Human keratinocyte growth factor activity on proliferation and differentiation of human keratinocytes: differentiation response distinguishes KGF from EGF family. J Cell Physiol *144*, 326-332.

Markovic, S.N., Erickson, L.A., Rao, R.D., Weenig, R.H., Pockaj, B.A., Bardia, A., Vachon, C.M., Schild, S.E., McWilliams, R.R., Hand, J.L.*, et al.* (2007). Malignant

melanoma in the 21st century, part 1: epidemiology, risk factors, screening, prevention, and diagnosis. Mayo Clin Proc *82*, 364-380.

Marks, M.S., and Seabra, M.C. (2001). The melanosome: membrane dynamics in black and white. Nat Rev Mol Cell Biol *2*, 738-748.

Mehus, A.A., Anderson, R.H., and Roux, K.J. (2016). BioID Identification of Lamin-Associated Proteins. Methods Enzymol *569*, 3-22.

Melak, M., Plessner, M., and Grosse, R. (2017). Actin visualization at a glance. J Cell Sci *130*, 525-530.

Mesa, K.R., Rompolas, P., Zito, G., Myung, P., Sun, T.Y., Brown, S., Gonzalez, D.G., Blagoev, K.B., Haberman, A.M., and Greco, V. (2015). Niche-induced cell death and epithelial phagocytosis regulate hair follicle stem cell pool. Nature *522*, 94-97.

Metral, E., Bechetoille, N., Demarne, F., Rachidi, W., and Damour, O. (2017). alpha6 Integrin (alpha6(high))/Transferrin Receptor (CD71)(low) Keratinocyte Stem Cells Are More Potent for Generating Reconstructed Skin Epidermis Than Rapid Adherent Cells. Int J Mol Sci *18*.

Mohan, R., and John, A. (2015). Microtubule-associated proteins as direct crosslinkers of actin filaments and microtubules. IUBMB Life *67*, 395-403.

Molino, M., Barnathan, E.S., Numerof, R., Clark, J., Dreyer, M., Cumashi, A., Hoxie, J.A., Schechter, N., Woolkalis, M., and Brass, L.F. (1997). Interactions of mast cell tryptase with thrombin receptors and PAR-2. J Biol Chem *272*, 4043-4049.

Monks, J., Rosner, D., Geske, F.J., Lehman, L., Hanson, L., Neville, M.C., and Fadok, V.A. (2005). Epithelial cells as phagocytes: apoptotic epithelial cells are engulfed by mammary alveolar epithelial cells and repress inflammatory mediator release. Cell Death Differ *12*, 107-114.

Murase, D., Hachiya, A., Takano, K., Hicks, R., Visscher, M.O., Kitahara, T., Hase, T., Takema, Y., and Yoshimori, T. (2013). Autophagy has a significant role in determining skin color by regulating melanosome degradation in keratinocytes. J Invest Dermatol *133*, 2416-2424.

Nakanishi, Y., and Shiratsuchi, A. (2004). Phagocytic removal of apoptotic spermatogenic cells by Sertoli cells: mechanisms and consequences. Biol Pharm Bull *27*, 13-16.

Newton, R.A., Cook, A.L., Roberts, D.W., Leonard, J.H., and Sturm, R.A. (2007). Post-transcriptional regulation of melanin biosynthetic enzymes by cAMP and resveratrol in human melanocytes. J Invest Dermatol *127*, 2216-2227.

Nystedt, S., Emilsson, K., Wahlestedt, C., and Sundelin, J. (1994). Molecular cloning of a potential proteinase activated receptor. Proc Natl Acad Sci U S A *91*, 9208-9212.

Nystedt, S., Larsson, A.K., Aberg, H., and Sundelin, J. (1995). The mouse proteinase-activated receptor-2 cDNA and gene. Molecular cloning and functional expression. J Biol Chem *270*, 5950-5955.

Patro, R., Duggal, G., Love, M.I., Irizarry, R.A., and Kingsford, C. (2017). Salmon provides fast and bias-aware quantification of transcript expression. Nat Methods *14*, 417-419.

Peacocke, M., Yaar, M., Mansur, C.P., Chao, M.V., and Gilchrest, B.A. (1988). Induction of nerve growth factor receptors on cultured human melanocytes. Proceedings of the National Academy of Sciences of the United States of America *85*, 5282-5286.

Proksch, E., Brandner, J.M., and Jensen, J.M. (2008). The skin: an indispensable barrier. Exp Dermatol *17*, 1063-1072.

Rabinovitch, M. (1995). Professional and non-professional phagocytes: an introduction. Trends Cell Biol *5*, 85-87.

Ramot, Y., Gaspar, E., Dendorfer, A., Langbein, L., and Paus, R. (2009). The 'melanocyte-keratin' mystery revisited: neither normal human epidermal nor hair follicle melanocytes express keratin 16 or keratin 6 in situ. Br J Dermatol *161*, 933-938.

Rasmussen, J.P., Sack, G.S., Martin, S.M., and Sagasti, A. (2015). Vertebrate epidermal cells are broad-specificity phagocytes that clear sensory axon debris. J Neurosci *35*, 559-570.

Roux, K.J., Kim, D.I., Burke, B., and May, D.G. (2018). BioID: A Screen for Protein-Protein Interactions. Curr Protoc Protein Sci *91*, 19 23 11-19 23 15.

Santulli, R.J., Derian, C.K., Darrow, A.L., Tomko, K.A., Eckardt, A.J., Seiberg, M., Scarborough, R.M., and Andrade-Gordon, P. (1995). Evidence for the presence of a protease-activated receptor distinct from the thrombin receptor in human keratinocytes. Proc Natl Acad Sci U S A *92*, 9151-9155.

Scott, G., Deng, A., Rodriguez-Burford, C., Seiberg, M., Han, R., Babiarz, L., Grizzle, W., Bell, W., and Pentland, A. (2001). Protease-activated receptor 2, a receptor involved in melanosome transfer, is upregulated in human skin by ultraviolet irradiation. J Invest Dermatol *117*, 1412-1420.

Scott, G., Leopardi, S., Printup, S., and Madden, B.C. (2002). Filopodia are conduits for melanosome transfer to keratinocytes. J Cell Sci *115*, 1441-1451.

Segre, J.A. (2006). Epidermal barrier formation and recovery in skin disorders. J Clin Invest *116*, 1150-1158.

Seiberg, M., Paine, C., Sharlow, E., Andrade-Gordon, P., Costanzo, M., Eisinger, M., and Shapiro, S.S. (2000). The protease-activated receptor 2 regulates pigmentation via keratinocyte-melanocyte interactions. Exp Cell Res *254*, 25-32.

Shannon, P., Markiel, A., Ozier, O., Baliga, N.S., Wang, J.T., Ramage, D., Amin, N., Schwikowski, B., and Ideker, T. (2003). Cytoscape: a software environment for integrated models of biomolecular interaction networks. Genome Res *13*, 2498-2504.

Sharlow, E.R., Paine, C.S., Babiarz, L., Eisinger, M., Shapiro, S., and Seiberg, M. (2000). The protease-activated receptor-2 upregulates keratinocyte phagocytosis. J Cell Sci *113 (Pt 17)*, 3093-3101.

Simpson, R.J. (2010). Disruption of cultured cells by nitrogen cavitation. Cold Spring Harb Protoc *2010*, pdb prot5513.

Song, Z., He, C.D., Sun, C., Xu, Y., Jin, X., Zhang, Y., Xiao, T., Wang, Y., Lu, P., Jiang, Y.*, et al.* (2010). Increased expression of MAP2 inhibits melanoma cell proliferation, invasion and tumor growth in vitro and in vivo. Exp Dermatol *19*, 958-964.

Spivak, M., Weston, J., Bottou, L., Kall, L., and Noble, W.S. (2009). Improvements to the percolator algorithm for Peptide identification from shotgun proteomics data sets. J Proteome Res *8*, 3737-3745.

Statello, L., Guo, C.J., Chen, L.L., and Huarte, M. (2021). Gene regulation by long non-coding RNAs and its biological functions. Nat Rev Mol Cell Biol *22*, 96-118.

Szabo, G., Gerald, A.B., Pathak, M.A., and Fitzpatrick, T.B. (1969). Racial differences in the fate of melanosomes in human epidermis. Nature *222*, 1081-1082.

Szklarczyk, D., Gable, A.L., Lyon, D., Junge, A., Wyder, S., Huerta-Cepas, J., Simonovic, M., Doncheva, N.T., Morris, J.H., Bork, P.*, et al.* (2019). STRING v11: protein-protein association networks with increased coverage, supporting functional discovery in genome-wide experimental datasets. Nucleic Acids Res *47*, D607-D613.

Tadokoro, R., Murai, H., Sakai, K.I., Okui, T., Yokota, Y., and Takahashi, Y. (2016). Melanosome transfer to keratinocyte in the chicken embryonic skin is mediated by vesicle release associated with Rho-regulated membrane blebbing. Sci Rep *6*, 38277.

Tadokoro, T., Kobayashi, N., Zmudzka, B.Z., Ito, S., Wakamatsu, K., Yamaguchi, Y., Korossy, K.S., Miller, S.A., Beer, J.Z., and Hearing, V.J. (2003). UV-induced DNA damage and melanin content in human skin differing in racial/ethnic origin. FASEB J *17*, 1177-1179.

Tarafder, A.K., Bolasco, G., Correia, M.S., Pereira, F.J.C., Iannone, L., Hume, A.N., Kirkpatrick, N., Picardo, M., Torrisi, M.R., Rodrigues, I.P.*, et al.* (2014). Rab11b mediates melanin transfer between donor melanocytes and acceptor keratinocytes via coupled exo/endocytosis. J Invest Dermatol *134*, 1056-1066.

Tsubaki, M. (1993). Fourier-transform infrared study of azide binding to the Fea3-CuB binuclear site of bovine heart cytochrome c oxidase: new evidence for a redox-linked conformational change at the binuclear site. Biochemistry *32*, 174-182.

Tsuboi, R., Sato, C., Kurita, Y., Ron, D., Rubin, J.S., and Ogawa, H. (1993). Keratinocyte growth factor (FGF-7) stimulates migration and plasminogen activator activity of normal human keratinocytes. J Invest Dermatol *101*, 49-53.

Tykocki, N.R., and Watts, S.W. (2010). The interdependence of endothelin-1 and calcium: a review. Clin Sci (Lond) *119*, 361-372.

Vu, T.K., Hung, D.T., Wheaton, V.I., and Coughlin, S.R. (1991). Molecular cloning of a functional thrombin receptor reveals a novel proteolytic mechanism of receptor activation. Cell *64*, 1057-1068.

Wickstead, B., and Gull, K. (2011). The evolution of the cytoskeleton. J Cell Biol *194*, 513-525.

Willemsen, M., Luiten, R.M., and Teunissen, M.B.M. (2020). Instant isolation of highly purified human melanocytes from freshly prepared epidermal cell suspensions. Pigment Cell Melanoma Res *33*, 763-766.

Wolff, K., and Honigsmann, H. (1971). Permeability of the epidermis and the phagocytic activity of keratinocytes. Ultrastructural studies with thorotrast as a marker. J Ultrastruct Res *36*, 176-190.

Wolff, K., and Konrad, K. (1972). Phagocytosis of latex beads by epidermal keratinocytes in vivo. J Ultrastruct Res *39*, 262-280.

Wu, X., and Hammer, J.A. (2014). Melanosome transfer: it is best to give and receive. Curr Opin Cell Biol *29*, 1-7.

Wu, X.S., Masedunskas, A., Weigert, R., Copeland, N.G., Jenkins, N.A., and Hammer, J.A. (2012). Melanoregulin regulates a shedding mechanism that drives melanosome transfer from melanocytes to keratinocytes. Proc Natl Acad Sci U S A *109*, E2101-2109.

Xu, W.F., Andersen, H., Whitmore, T.E., Presnell, S.R., Yee, D.P., Ching, A., Gilbert, T., Davie, E.W., and Foster, D.C. (1998). Cloning and characterization of human protease-activated receptor 4. Proc Natl Acad Sci U S A *95*, 6642-6646.

Yaar, M., Grossman, K., Eller, M., and Gilchrest, B.A. (1991). Evidence for nerve growth factor-mediated paracrine effects in human epidermis. J Cell Biol *115*, 821-828.

Yada, Y., Higuchi, K., and Imokawa, G. (1991). Effects of endothelins on signal transduction and proliferation in human melanocytes. J Biol Chem *266*, 18352-18357.

Yates, R.M., Hermetter, A., and Russell, D.G. (2005). The kinetics of phagosome maturation as a function of phagosome/lysosome fusion and acquisition of hydrolytic activity. Traffic *6*, 413-420.